

INFORMATION TO USERS

This manuscript has been reproduced from the microfilm master. UMI films the text directly from the original or copy submitted. Thus, some thesis and dissertation copies are in typewriter face, while others may be from any type of computer printer.

The quality of this reproduction is dependent upon the quality of the copy submitted. Broken or indistinct print, colored or poor quality illustrations and photographs, print bleedthrough, substandard margins, and improper alignment can adversely affect reproduction.

In the unlikely event that the author did not send UMI a complete manuscript and there are missing pages, these will be noted. Also, if unauthorized copyright material had to be removed, a note will indicate the deletion.

Oversize materials (e.g., maps, drawings, charts) are reproduced by sectioning the original, beginning at the upper left-hand corner and continuing from left to right in equal sections with small overlaps.

Photographs included in the original manuscript have been reproduced xerographically in this copy. Higher quality 6" x 9" black and white photographic prints are available for any photographs or illustrations appearing in this copy for an additional charge. Contact UMI directly to order.

**Bell & Howell Information and Learning
300 North Zeeb Road, Ann Arbor, MI 48106-1346 USA
800-521-0600**

UMI[®]

A NUMERICAL SIMULATION
OF THE YOUNG STELLAR OUTFLOW
DG TAURI B

by
Kevin Arthur Douglas

Submitted in partial fulfillment of the
requirements for the degree of
Master of Science in Astronomy

Department of Astronomy and Physics
Saint Mary's University
Halifax, Nova Scotia
B3H 3C3

©2000 by Kevin A. Douglas

Submitted March 2000



National Library
of Canada

Bibliothèque nationale
du Canada

Acquisitions and
Bibliographic Services

Acquisitions et
services bibliographiques

395 Wellington Street
Ottawa ON K1A 0N4
Canada

395, rue Wellington
Ottawa ON K1A 0N4
Canada

Your file *Votre référence*

Our file *Notre référence*

The author has granted a non-exclusive licence allowing the National Library of Canada to reproduce, loan, distribute or sell copies of this thesis in microform, paper or electronic formats.

L'auteur a accordé une licence non exclusive permettant à la Bibliothèque nationale du Canada de reproduire, prêter, distribuer ou vendre des copies de cette thèse sous la forme de microfiche/film, de reproduction sur papier ou sur format électronique.

The author retains ownership of the copyright in this thesis. Neither the thesis nor substantial extracts from it may be printed or otherwise reproduced without the author's permission.

L'auteur conserve la propriété du droit d'auteur qui protège cette thèse. Ni la thèse ni des extraits substantiels de celle-ci ne doivent être imprimés ou autrement reproduits sans son autorisation.

0-612-56707-9

Canada

Contents

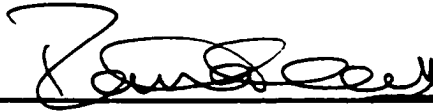
Certificate of Examination	v
Abstract	vi
Acknowledgements	vii
List of Figures	ix
List of Tables	x
1 INTRODUCTION	1
1.1 Early Observations and Theory	1
1.2 Current Observations	4
1.2.1 Optical Studies of Young Stellar Outflows	5
1.2.2 Near Infrared Studies of Young Stellar Outflows	7
1.2.3 Radio and Far Infrared Studies of Young Stellar Outflows	8
1.3 Current Theory—Improvements on Earlier Ideas	10
1.3.1 Constraints on Model Types	14
1.3.2 Cooling in the Jet—Realistic Nonadiabaticity	18
1.3.3 Time-Dependence in the Jet—Variability	21
1.3.4 Higher Dimensions—Breaking Symmetries	23

1.4	DG Tauri B—A Case Study	24
2	METHODOLOGY	34
2.1	The Numerical Code: ZEUS3D	34
2.1.1	Current Capabilities	35
2.2	Necessary Additions to the ZEUS3D Code	36
2.2.1	Variable Jet Velocity	36
2.2.2	Radiative Cooling in the Jet	37
2.2.3	Tracing Optical and Molecular Emission	42
2.3	Modelling of DG Tau B with ZEUS3D	44
2.3.1	Preliminary Modelling Constraints	44
2.3.2	Parameter Search for the DG Tau B Young Stellar Outflow	46
3	RESULTS	49
3.1	General Characteristics of the Simulations	49
3.1.1	Simulations Without Cooling Or Variability—Simulation A	50
3.1.2	Addition Of Cooling—Simulation B	50
3.1.3	Addition Of Variability (No Cooling)—Simulation C	52
3.1.4	Cooling And Variability—Simulation D	54
3.2	Creation Of Emission Maps	59
3.3	Comparison To DG Tau B	61

3.3.1	Kinematical Features of the Outflow	62
3.3.2	Emission Features in the Outflow	66
3.4	Conclusion And Suggestions For Further Refinement	70
	Appendix	75
	References	113

Certificate of Examination

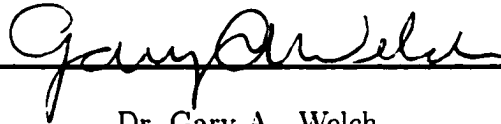
Saint Mary's University
Department of Astronomy and Physics



Dr. David A. Clarke
Associate Professor
Department of Astronomy and Physics
Saint Mary's University
(Co-supervisor)



Dr. George F. Mitchell
Professor
Department of Astronomy and Physics
Saint Mary's University
(Co-supervisor)



Dr. Gary A. Welch
Associate Professor
Department of Astronomy and Physics
Saint Mary's University



Dr. Chris Loken
Associate Professor
Department of Astronomy and Physics
Saint Mary's University



Dr. R. N. Henriksen
Professor
Department of Physics and Astronomy
Queen's University
(External Reader)

Abstract

A NUMERICAL SIMULATION OF THE YOUNG STELLAR OUTFLOW DG TAURI B

Kevin Douglas

Submitted March 2000

A series of axisymmetric, radiatively cooling variable jets was modeled with the ZEUS3D hydrodynamic code, revealing features commonly seen in outflows from Young Stellar Objects. The jet known as DG Tau B, discovered in 1983 by Mundt and Fried, was used to determine the parameters for the jet to be modeled. A molecular outflow surrounding the jet is also modeled in the simulations. New subroutines were written and implemented in order to model DG Tau B, believed to be a radiatively cooling jet possibly undergoing variability in jet velocity. Comparison to the observations in optical and radio wavelengths of DG Tau B shows a notable correspondence to the morphological and emission features in the atomic and molecular components of the simulated outflow.

Acknowledgements

Many thanks must be given to the faculty and staff in the Department of Astronomy and Physics at Saint Mary's University for their friendship and for providing a positive academic environment. Thanks goes to David Clarke for all his advice with his ZEUS3D code and other matters besides. I thank George Mitchell for his supervision and for the opportunity to study the fascinating field of stellar outflows. To the other professors, David Turner, Gary Welch, Malcolm Butler, David Guenther, and Mike West, I thank each of you for your own unique contribution to my learning. Thanks must also be given to Elfrie Waters, David Lane and Shawn Mitchell for support with things as far-ranging as disk quotas to fax etiquette. I must also thank Rachid Ouyed for many helpful discussions since his arrival in Halifax as a post-doctoral fellow.

Thanks to the grad students who were around during the years this thesis was being put together, especially to my friend and roommate, René Tanaja, thanks for a year of successful co-habitation. We didn't play as much cribbage as I wished we did but we got along better than most roomies I've known. To Steve Shorlin, I thank you for your constant humour and good cheer these past few years. Life was never dull when you were around. Thanks to Beverly Miskolczi and Gary Gidney for putting up with the music downstairs. Thanks to Yi Gong for always having a smile on his face. To Juan Ramon Sanchez-Velaz, *Gracias a todos, amigo*. To Andreea Font, thank you for interesting discussions and opinions on all types of topics.

Thanks to Hema & Rowan Douglas for being the source of my inspiration. If ever a piece of scientific literature could also be a love letter, it's this thesis.

Since the beginning of this research I have become a husband and a father, and the rewards that go with that exceed anything this research has given me. Thank you for being patient and understanding while I slaved away at school.

Additional thanks goes to the following: Steve Hackett, Django Bates, Christian Vander, Bill Bruford, Mike Keneally, Ian Anderson, Annie Haslam, Tony Banks, John Goodsall, Mike Ratledge, Anthony Phillips, Tony Levin, Keith Emerson, Tatsuya Yoshida of Ruins, Percy Jones, Dagmar Krause, Robert Fripp, Dave Stewart, Chris Norman, the Shulmans, and most of all Frank Zappa. Music is the best.

List of Figures

1.1	Picture of Young Stellar Outflow	3
1.2	Discovery image of DG Tau B	25
1.3	CO $J = 3 - 2$ map of DG Tau B	30
1.4	CO $J = 1 - 0$ map of DG Tau B	32
2.1	Cooling Rates For Hydrogen	38
2.2	Cooling Rates For Neutral Oxygen and Ionised Carbon	40
3.1	Densities for Simulations A and B	51
3.2	One-Dimensional Parameter Plots for Three Simulations	53
3.3	Densities for Simulations C and D4	54
3.4	Densities for Simualtion D	55
3.5	Predicted Neutral Oxygen Emission for Simulation D4	58
3.6	Predicted CO Emission for Model D3	60
3.7	Kinematic Images for Simulation D5	64
3.8	Emissivity Images for Simulation D5	65
3.9	Direct Comparison of Jet and Ambient Emissivities	68

List of Tables

1	Important Observational Data for DG Tau B (redshifted lobe)	47
2	Added Physics of the Simulations	49
3	Initial and Effective Parameters For Simulation D Runs	56

1. INTRODUCTION

The scenario involving outflows as an integral part of star formation has been evolving since the discovery of many Herbig-Haro objects (often denoted as “HH” followed by an identification number) in the late 1940s and early 1950s. A great deal of work has gone into creating the present picture of star formation, both phenomenologically and by simulations, and an extensive review of the observational and theoretical contributions is warranted. A brief history of the early work done on stellar outflows is given below, followed by a review of recent studies, and in particular the object DG Tauri B is discussed in detail.

1.1. Early Observations and Theory

The study of Herbig-Haro objects was begun in the middle of the twentieth century by George Herbig and Guillermo Haro. In 1950 Herbig reported that Burnham’s Nebula, discovered *c.* 1890, had a rather peculiar spectrum, exhibiting strong emission lines of [S II], [O II] and hydrogen (Herbig 1950). In the next few years he discovered many objects displaying similar spectral features, and observations by Haro around the same time led to the postulation by Ambartsumian (1954) that these “Herbig-Haro” objects, because of their proximity to emission-line stars, might be associated with the early stages of star formation. Indeed, the following years saw many suggestions based on observation that protostars were hidden within these Herbig-Haro objects. An embedded infrared source was discovered by Strom *et al.* (1974) very close to HH 100, which allowed theorists to propose models wherein Herbig-Haro objects are excited by a newly-forming star. The exact process by which this excitation takes place is now accepted to be the result of strongly cooling shocks

interacting with the environment surrounding the protostar (see also Reipurth & Heathcote, 1997 for other references).

Jets with proper motions exceeding 100 km s^{-1} were soon found to emanate from nebulae thought to contain newly forming stars. Carbon monoxide (CO) gas was detected around two diffuse galactic nebulae by Knapp *et al.* (1976), showing that CO emission with high-velocity components could prove a good indicator of star formation. Bipolar molecular outflows were first observed by Snell *et al.* (1980) when they discovered CO lobes around L1551 IRS 5. This led to suggestions that molecular gas and Herbig-Haro objects were intimately associated (Königl 1982). The same year Elias detected molecular hydrogen emission in several Herbig-Haro objects, requiring that at least part of the outflow have velocities not exceeding 50 km s^{-1} (Elias 1980). With observations dating from the 1950s of objects with multiple bowshocks suggesting episodic outflows with timescales on the orders of years (Herbig 1957), these results and others posed many challenges to theorists.

Early theoretical models were based on the assumption that stellar jets arise because of the accretion process occurring during stellar formation. Angular momentum must be removed somehow, since most evolved stars have low angular momenta. Non-analytic models had to be crude because of a lack of computing power, and analytic models had to be simplified in order to be solved. In 1978 two key papers came out which both suggested that shocks are essential to the excitation of Herbig-Haro objects. Schwartz (1978) proposed a model whereby the wind from a T Tauri star formed quasi-stationary shocks when interacting with small nearby cloudlets of gas. Furthermore, Böhm (1978) suggested that variable "running shocks" could be at work in addition to the stationary shocks of Schwartz. The realisation of the importance of shocks in stellar outflows helped greatly in the

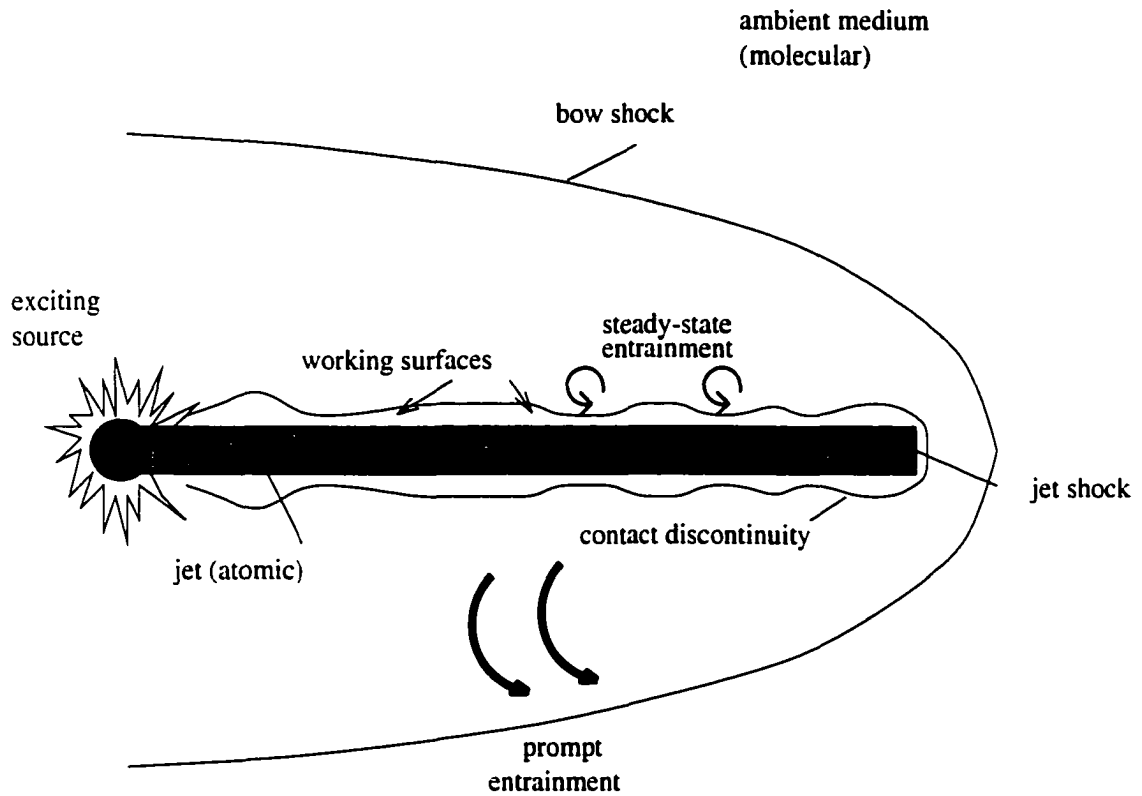


Fig. 1.1.— Illustration of a Young Stellar Outflow. Key components and entrainment sites are labelled.

advancement of the theory.

Figure 1.1 illustrates some of the major processes involved in the formation of a young stellar outflow. Whenever two supersonic fluids collide, with the collision speed exceeding the sound speed in both media, two shocks occur, one moving through each of the fluids. The shock moving through the ambient medium is called the bowshock, and it accelerates the material in the envelope. The shock sent back through the jet material is referred to as the jet shock, or Mach disk. The two-shock structure is separated by a contact discontinuity.

Improvements in computing power have allowed many unphysical assumptions, including adiabaticity, symmetry, and complete ionisation in the jet, to be relaxed. For example, analytic models based on the viscous Burgers equation (Kofman & Raga 1992) were insightful in explaining the appearance of knots (discontinuities) in the flow, but since they assumed zero pressure, their applications were limited and were eventually surpassed by hydrodynamic computer codes which could perform complicated nonlinear calculations with relatively little trouble (Hartigan & Raymond 1993).

1.2. Current Observations

Different parts of the electromagnetic spectrum help to probe various parts of stellar outflows. Observations indicate that there are molecular, atomic, and ionic components to outflows from Young Stellar Objects (Mundt *et al.* 1987, Bacciotti *et al.* 1995, Hartigan *et al.* 1996, Mitchell *et al.* 1997). Optically visible emission lines were the first indication of regions where star formation had been occurring. Infrared spectroscopy and imaging with radio telescopes furthered the knowledge of these outflows and allowed a more complete picture of the star-formation process to be ascertained. As more objects are discovered, it is possible to determine the average properties of outflows from Young Stellar Objects, which will be referred to as *Young Stellar Outflows* in this thesis. These widely observed features will be described briefly before a specific example, DG Tauri B, is discussed.

1.2.1. *Optical Studies of Young Stellar Outflows*

It is from optical observations that most of the features of Young Stellar Objects have been discovered. The nebulosities known as Herbig-Haro objects are often characterised as components of a stellar “jet” with a mostly linear chain of knotty structures emanating from a nearby young stellar object. Often a bow-shaped terminal feature is also seen (Reipurth & Heathcote 1992), presumably where the ejected material from the star meets the ambient medium. Plambeck & Snell revisited the L1551 region in 1995, observing narrow, partially-ionised jets within bipolar outflows of molecular emission. The knots in Herbig-Haro objects produce emission spectra with fairly low-excitation lines, the most prominent being $H\alpha$ at 6563 Å, the forbidden singly-ionised sulphur doublet — denoted $[S\text{II}]\lambda\lambda 6716,6731$, and $[O\text{I}]\lambda\lambda 6300,6363$ (Poetzl *et al.* 1992). The bow-shaped terminus, in contrast, exhibits a higher degree of ionisation and excitation than the chain of knots. In addition to the lines mentioned above, emission spectra observed at the jet/ambient interface include transitions from neutral atoms such as $[C\text{I}]$ and $[N\text{I}]$, and from ions of very many elements such as $[O\text{II}]$, $[O\text{III}]$, $[N\text{II}]$, and $[Fe\text{II}]$ (Bacciotti *et al.* 1995).

The relatively low excitation along the jet further complicates the scenario of a high speed shock as the singular source for the Herbig-Haro objects’ morphology, and instabilities have been invoked to explain the nodular emission structures (Bacciotti *et al.* 1995 for example). While the low excitation presented problems for theorists, the low degree of ionisation in the jet was a key to solving an apparent discrepancy in the momentum and mass-loss rates when compared to the outflow rates for molecular outflows. The optical jets were initially thought to be nearly completely ionised and therefore appeared to lack sufficient mass to drive the molecular outflows, which was a popular idea for those trying to find a causal relation between the two

types of flow. By assuming an ion fraction of about 10%, it was possible to raise mass-loss rates in the optical jet to acceptable values (Masson & Chernin 1993, Raga & Cabrit 1993), the argument being that since most of the jet is neutral it is not easily detected.

Herbig-Haro objects associated with high-luminosity young stellar objects have been observed (eg. Poetzel *et al.* 1992), though the optical detection of most outflows is from observations of low-luminosity objects (of approximately solar luminosity). Many reasons could explain this result. First, obvious selection effects are the brightness of nebulae surrounding these high-luminosity pre-main sequence stars, which makes detection of the Herbig-Haro flow more difficult, and the greater number of low-luminosity stars overall. Evolutionary timescales also imply that the stars with higher luminosity will evolve faster, with a shorter freefall time, giving less time for the outflow to be visible. The visibility of these high-luminosity Herbig-Haro flows is also diminished by the finding that many young stellar objects with high luminosities are detected as embedded infrared sources, not as optical T Tauri stars. One might argue that stars with very high luminosities may be too powerful to form Herbig-Haro objects as readily as low-mass young stellar objects. The mass loss rates for high-luminosity stars are only 2-3 times greater than for typical low-luminosity outflows, which seems to imply that outflows are quite possible. A more telling possibility is that the outflow properties, whether for low- or high-mass stars, may depend more on the luminosity contribution from the accretion disk, rather than from the star itself (Poetzel *et al.* 1992). Since the accretion disk contributes a significantly lower fraction of the total stellar luminosity in the case of high-mass protostars, the ejection of accreted matter into emission nebulae such as Herbig-Haro objects may be less likely to occur.

1.2.2. Near Infrared Studies of Young Stellar Outflows

At near-infrared wavelengths, observations are possible for the most abundant molecule in the universe, namely molecular hydrogen. For example, the $v = 1-0 S(1)$ rovibrational (rotational and vibrational) transition of H_2 at a wavelength of $2.121 \mu\text{m}$ is excited by low-velocity shocks in stellar outflows. Typical velocities are $30-50 \text{ km s}^{-1}$, which is considerably less than the $\sim 200 \text{ km s}^{-1}$ outflow velocities that would dissociate the molecules. Nevertheless, oblique shocks in bowshock wings have lower velocities than the forward jet velocity, and may give rise to the collisional excitation of molecular hydrogen by shocks (see Hartigan *et al.* 1996). In fact, the interface between the collimated stellar jet and the molecular environment has been observed in H_2 for many young stellar outflows (Davis *et al.* 1994, Davis & Smith 1995, Schwartz *et al.* 1995, Hartigan *et al.* 1996). These observations show that molecules are definitely present close to the interior of the jet, perhaps entrained by turbulence from the jet as it passes through the ambient medium. The processes related to the entrainment of molecular gas will be discussed later.

In addition to the observations of shock-excited molecular hydrogen at the jet-medium interface, H_2 counterparts to $H\alpha$ and $[S \text{ II}]$ are found inside the jet where knots of emission (Herbig-Haro objects) move away from the jet source. H_2 emission in Herbig-Haro objects was first observed by Elias (1980), and since then a strong spatial correlation between H_2 and $[S \text{ II}]$ emission has been found for many objects. This implies that either the entrainment of molecular hydrogen drives it straight into the jet, or that the molecular hydrogen gets there some other way, whether by forming on dust grains behind the shock surface, or by having been present already and managing not to be dissociated. Neither of the last two mechanisms is believed to be possible given the conditions created by the jet, but they cannot be

completely discounted. Certainly the shocks do not all travel with the same speed as that inferred from proper motion studies. The best way to explain this observation could be a jet which has episodes of outflow since many working surfaces allow the possibility of H_2 to be swept up more than once because of previous entrainment by earlier working surfaces.

Besides the above-mentioned rovibrational transition, higher-excitation states of H_2 at infrared wavelengths have been discovered (same references as above) in some outflows. Line ratios have been used to infer excitation temperatures, as well as to explain what types of shocks produce the different emission lines. Atomic hydrogen is also observable at infrared wavelengths at $2.166 \mu\text{m}$ for the $Br\gamma$ ($n=4-3$) transition. As well, photometry of embedded infrared sources is possible for some objects in the J , H , K , and L bands, though many forming stars have only weak emission and are not easily detected.

1.2.3. Radio and Far Infrared Studies of Young Stellar Outflows

The rotational transitions of the carbon monoxide (CO) molecule, observable at millimetric and sub-millimetric wavelengths, continue to be the most frequently studied lines in the investigation of molecular outflows around protostars. The $J=1-0$, $2-1$, and $3-2$ transitions are observed at wavelengths of 2.6 mm, 1.3 mm, and 0.87 mm respectively, for the most commonly occurring isotope of CO, that is $^{12}\text{C}^{16}\text{O}$. Experience has shown that the emission at this wavelength is optically thick because of the high abundance of CO in molecular clouds, so observations of different isotopes such as ^{13}CO or C^{18}O are often made to probe further into the cloud, as well as to determine important physical properties. Better resolution is

becoming available for observations of CO and other molecules emitting at radio and far infrared wavelengths, as interferometric techniques allow smaller regions of a protostar to be studied in much better detail. Also, improvements in spectroscopic techniques have made radial velocity studies a very powerful tool in determining the structure of an outflow. Some other important molecules which emit radiation in the radio/far infrared spectrum, and which have been observed around protostars are CS, CN, OH, as well as other more complex molecules. It should be noted that these radio-wavelength outflows usually surround the optical emission whenever the two are observed for the same object. This has led to the very reasonable suggestion that molecular outflows are actually driven by the jet, though it is also possible that a second wind powers the outer molecular gas, possibly from an accretion disk around the protostar.

As well as these molecular transitions, one can also detect the presence of a protostar by continuum radio emission from ions that come from the partially ionised jet (Martin 1996). A model has been proposed whereby these ions could be flung out by a wind, possibly driven by the presence of an accretion disk, threaded by a magnetic field (Pudritz & Norman 1986). This is supported by an apparent correlation between the momentum rate and the centimetre continuum luminosity of molecular outflows (Anglada 1995). The radio emission is unaffected by dust and is often useful in detecting the exciting source of the outflow. Good angular resolution sometimes shows a radio jet, and information on collimation scales can be obtained.

Ions may be flung out by magnetic field lines (the possible presence of magnetic fields will be discussed later) which are coupled to the accretion disk of the protostar. These ions will also drive out neutral atoms through ion-neutral collisions, and this collisional drag heats the gas via ambipolar diffusion. The gas reaches temperatures

$T \sim 10^4$ K and allows the emission of thermal bremsstrahlung, or free-free radiation. Models by Martin (1996) show that the electron density must be high ($n_e \sim 10^7$ to 10^{12} cm^{-3}) at distances of about 1 AU from the star. At distances greater than 10 AU it is found that $n_e \sim 10^4$ cm^{-3} . This result shows the high densities present in the vicinity of the protostar.

1.3. Current Theory—Improvements on Earlier Ideas

It was not immediately assumed that molecular outflows could be driven by the same stellar jets which created the shocks in their optical counterparts, especially since the outflow speeds and degrees of collimation were so different for the two types of flow. A second, wide-angle wind has also been proposed as a means of sweeping out the molecular material surrounding the protostar. This slower wind could arise from an accretion disk and give rise to the less-collimated, lower-velocity molecular outflows. Shu *et al.* (1991) explained the molecular outflow phenomenon as “a natural and fundamental consequence of the accretion of mass from a centrifugally supported disk to a rapidly rotating protostar.” While strengthening the link between bipolar outflows and star formation, no direct physical connection to phenomena such as Herbig-Haro objects or jets is implied, leaving the possibility of independent yet coeval origins for stellar jets and molecular outflows. That is, the molecular outflows are not driven by the jet but rather the outer wide-angle disk wind. Models by Frank and Mellema (1994, 1996a) produce highly collimated stellar jets by assuming the presence of a dense envelope of material surrounding the protostar. Clearly it is desirable to produce a model which successfully produces both these highly-collimated stellar jets as well as the less-collimated molecular outflows.

Efforts to link the phenomena of bipolar optical jets and molecular outflows date back many years (Königl 1982), and over time the model has gained strength from this early work. A unified model suggesting a common origin for molecular and optical outflows has been put forth by Raga *et al.* (1993). In this unified picture, a single high-velocity, collimated wind is the driving force for an envelope of slower material. A highly collimated outflow may be the primary way that a young star loses its angular momentum gained from accreting material from a circumstellar disk (Hartigan & Raymond 1993), while also sweeping out the material surrounding the object. This outer material is entrained by the fast stellar wind and is set into motion by viscous coupling (Raga & Cabrit 1993). The leading bowshock intercepts and ejects sideways the ambient material it encounters as the jet ploughs through the surroundings. A series of working surfaces evinces a more-evolved outflow, but in order to entrain a sufficient amount of environmental gas, the leading working surface should excite a bowshock within the ambient medium. This process has come to be known as prompt entrainment, as the material is pushed ahead and sideways by the jet at its head, forming a shroud of ambient material around the jet behind the bowshock. A second process called steady-state entrainment has the ambient gas swept up along the boundary of a jet, as a result of turbulent mixing through Kelvin-Helmholtz instabilities. Both processes are believed to occur in stellar outflows (Chernin *et al.* 1994), but which process dominates will be discussed below.

Observationally the entrainment process appears to take place on a scale about 20 times larger than the jet diameter (Chernin *et al.* 1994), so a bowshock with a much larger cross-section is a very favourable mechanism for disturbing gas further from the jet axis, especially since bow-shaped terminal features are readily seen in

many Herbig-Haro objects. Subsequent working surfaces behind the leading head of the jet give rise to “internal working surfaces” (see Figure 1.1) that can explain the knotty structures forming the linear chain of Herbig-Haro objects (Raga & Cabrit 1993). The strong velocity gradient between the intercepted environmental gas and the pre-shock material leads to the formation of a turbulent mixing layer along the jet axis (giving rise to the sites of “steady-state” entrainment in Figure 1.1) confined by the ram pressures of the two fluids. This layer will be subject to Kelvin-Helmholtz instabilities as a result of the change in velocity across the beam/environment boundary (Raga 1995). Close to the head of the bowshock this layer will be approximately adiabatic, but away from the axis, balance between turbulent dissipation and radiative cooling leads to the formation of a mixing layer that is nearly isothermal with a temperature $\sim 10^4\text{K}$. A low-pressure cavity forms behind the high-pressure bowshock (Raga & Cabrit 1993). A turbulent wake is formed after the leading bowshock passes through a region of the ambient medium, and the mixing layer loses its inner support. The material ejected sideways by the leading shock undergoes a re-expansion and fills in the cavity. As well, material through which the bowshock passed can also fill this cavity. The entrainment mechanisms serve to explain an apparent “acceleration” away from the outflow source that has been observed for some objects (Raga & Cabrit 1993), wherein the outflowing gas seems to be moving faster as it moves away from the protostellar object. The reasoning is that the gas observed close to the protostar is entrained less vigorously than the material closer to the bowshock (assuming a steady flow), so the velocities of the swept-up ambient material along the jet appear to be increasing away from the source. In this way bowshocks could explain the features governed by entrainment of ambient gas.

One might argue against the unified stellar jet/molecular outflow model because the high-velocity jet heats the jet/ambient interface to temperatures that should dissociate most molecules. Raga *et al.* (1995) have found that indeed the molecular environment undergoes dissociation in the stagnation region of the leading bowshock (the region between bow shock and jet shock in Figure 1.1), but in the weaker bowshock wings the dissociation is not as severe. The wings of the bowshock make up most of the cross-sectional area of the bowshock and so the partial dissociation does not affect so much molecular material that one can discount the unified model.

A stronger argument against the unified model was the claim that the optical jet could not have the required momentum rate to drive the molecular outflow, but this discrepancy was partially explained when it was found that the jet was mostly neutral, through the discovery of extremely-high velocity H α in some objects, and also from observations by Bacciotti *et al.* (1995). It was found that the $\sim 10\%$ ion fraction along most of the jet seriously underestimated the amount of gas flowing outward. In fact, the ion fractions for the species in the jet are often as low as 2% (Hartigan *et al.* 1996), and are believed to be remnants of the heating and excitation in the initial acceleration rather than obeying collisional and thermal equilibrium arguments (Bacciotti *et al.* 1995). In other words, the ion fractions do not significantly change with weak temperature variations or internal shocks. Still, some features of jets and molecular outflows could not be explained in a unified model until more sophisticated simulations were performed. Improvements in computational work will be described in detail below.

1.3.1. Constraints on Model Types

Naturally, for any model which seeks to explain the properties of outflows from newly-forming stars, whether the flows are ionic, atomic, or molecular, there are constraints on these models which come from observational studies of the Young Stellar Outflows. Though there is no canonical HH object which typifies all others, the morphology described above—that of a linear chain of emission knots with a bow-shaped terminal end—should be reproducible by any model seeking to explain the origin of these objects. Clearly the type of protostellar object must have some effect on the nature of the outflow. It would make sense that young stellar objects with a higher luminosity (often referred to as Herbig Be or Ae stars) would produce stronger jets, and good correlations have been found between a source's bolometric luminosity and its outflow momentum flux (Chandler *et al.* 1996). The difficulty in observing Herbig-Haro jets from more massive protostars has been attributed in part to the shorter timescales expected for these faster-evolving stars (Poetzel *et al.* 1992).

T Tauri stars, the low-luminosity sources of many Young Stellar Outflows, are often classified as Class I or Class II objects, depending on their spectra. Class I objects are thought to have more circumstellar material in their vicinity, since they exhibit stronger emission lines, suggesting they are younger than Class II objects. Class 0 sources are deeply-embedded sources often referred to as embedded infrared sources. These Class 0 objects are generally much more powerful and violent than Class I objects (André 1997), and indeed have been observed to propel their own molecular outflows (Ward-Thompson *et al.* 1995). It is important to differentiate between the classes of protostars since each has its own set of parameters (Chandler *et al.* 1996). Indeed Frank & Mellema (1996a) caution that their models of outflows

from an object with a dense circum-protostellar envelope may be more applicable to Class 0 objects than to the more studied Class I objects. The environment in which the stellar outflow is found is obviously another constraint that numerical simulations must take into account in some manner. The surrounding material may have an effect on the degrees of collimation and entrainment occurring in the outflow (Hartigan *et al.* 1996; Plambeck and Snell 1995), which are two other very important model constraints.

Certainly some outflows lack the classical bipolar morphology because the protostar is found right at the end of a very dense molecular cloud which obscures, or perhaps quenches, one of the two outflows. A 3-dimensional study by de Gouveia Dal Pino *et al.* (1996) shows that the interaction of a cooling jet with a non-homogeneous ambient medium can result in a collimated, knotty structure. Different sections of the propagating jet may undergo compression or expansion, depending on the density and pressure gradient across the jet-ambient boundary.

The amount of collimation in the jet, briefly mentioned above, seems intimately coupled to the environmental constraints. The behaviour of the propagating jet appears to be strongly influenced by its surroundings. A stratified ambient medium such as that in the models of de Gouveia Dal Pino *et al.* (1996), or Mellema & Frank's (1997) aspherical circum-protostellar density distribution (first studied by Frank & Mellema 1996a), are two non-uniform environments which have been successful in increasing the effectiveness of the collimation process. Perhaps more favourable is the role of a magnetic field in collimating the jet, a mechanism suggested by Blandford & Rees (1974), Chan & Henriksen (1980), and Achterberg *et al.* (1983), among others. A magnetic field threaded through the accretion disk of the protostar provides a very naturally-occurring mechanism by which the outflowing gas can be

focussed at large distances. Magnetohydrodynamic models of Young Stellar Outflows have been proposed (Pudritz & Norman 1986; Todo *et al.* 1992) and the strength of the magnetic field appears to affect the morphology of the outflow (Frank *et al.* 1997) significantly, with stronger fields being more effective in collimating jets than those models with weak or no magnetic fields. Chan & Henriksen (1980) also report that a pinching of the jet can arise from either the magnetic field or external pressure, possibly giving rise to the observed Herbig-Haro knots. Hartigan & Raymond (1993) report that if magnetic fields are to be important in the collimation of the jet at the bowshock, the magnetic pressure must be comparable to the ram pressure. However, weaker magnetic fields, with pressure comparable to the *thermal* jet pressure, can affect collimation away from the bowshock (Clarke *et al.* 1986). Hartigan & Raymond (1993) also find that a strong magnetic field tends to cause velocity perturbations to dissipate more quickly, providing some extra stability against the disruption of the flow. Large opening angles for some objects (Chandler *et al.* 1996) suggest collimation may not be efficient in all protostars, but a wandering jet (Raga 1995, for example) may also give rise to these larger opening angles. A distinction must be made between the opening angles of molecular outflows and atomic jets, since the molecular material enshrouds the jet and is always much less collimated.

Another important constraint on models of Young Stellar Outflows is the distribution of momentum along the jet. Since molecular outflows are driven by radiatively cooling shocks in the “prompt entrainment model,” kinetic energy is dissipated away faster than if there were no cooling, while the total momentum of the jet + ambient gas remains conserved. Chernin and Masson (1995) studied the CO emission of six outflows and found peaks in the momentum distribution which were near the centre of the outflow, with minima near both the star and the end of

the flow. The molecular emission was studied because the atomic component of the total momentum is an order of magnitude lower than that of the molecular material (Chernin & Masson 1995). This result, that of a momentum-driven outflow with a momentum peak approximately halfway between the outflow source and its terminus, called into question many of the leading stellar outflow models. Steady-state jet models and wide-angle wind models produce momentum peaks near the end of the flow, while jet/bowshock models display momentum peaks at the position of the central star. The suggested remedy to this problem was to invoke variability in the jets, which will be discussed in a section below.

Models which seek to reproduce the observed momentum distribution should also consider the process by which the momentum is transferred. This involves the concept of entrainment, which was introduced earlier. Chernin *et al.* (1994) calculated models which showed that prompt entrainment by a bowshock is the dominant process in stellar outflows, especially for outflows with Mach numbers exceeding $M = 10$. An observation of the young outflow RNO 15-FIR by Davis *et al.* (1997) shows the dominance of prompt entrainment over turbulence. The turbulent entrainment occurring along the sides of jets, referred to as steady-state entrainment, is only significant for low Mach number flows with $M < 6$ (Chernin *et al.* 1994). As stated above, however, the momentum peak occurs in the middle of the jet, so a single bowshock entraining molecular material only at the jet head is too simplistic a model, and multiple working surfaces within the jet have been proposed (Raga & Cabrit 1993, Raga 1995 for example).

It may seem that with all the possible variations, modelling a young stellar outflow gives little physical insight into any one object. Still, tests of models using different parameters such as jet velocity and density can allow predictions to be

made for objects with properties similar to the computer model. A synergistic relationship exists, wherein theoretical and observational searches complement each other in an effort to piece together the puzzle of star formation.

1.3.2. *Cooling in the Jet—Realistic Nonadiabaticity*

Hydrodynamical models of jets in which radiative losses can be neglected are termed adiabatic models. Extragalactic jets are thought to be adiabatic since the dynamic evolutionary timescale is shorter than the timescale for which significant energy loss from radiative cooling occurs (Stone & Norman 1993a). They can usually be characterised in models by only two parameters, the Mach number M , which is the ratio of the jet speed to the jet sound speed, and the ratio of jet-to-ambient density, η . This is in contrast to the case of protostellar jets, in which a third parameter, χ , defined as the ratio of the cooling length scale to the radius of the jet (Stone & Norman 1993a), is often used in modelling these types of jets. As well, the density ratios are usually greater than unity for protostellar jets, while extragalactic jets are underdense with respect to their surrounding environment.

A brief general description of adiabatic jets here precedes a summary of the progress toward more realistic cooling functions that will explain better the dynamics of stellar jets. Adiabatic jets flow supersonically through the ambient medium without suffering any radiative losses. The high-velocity gas in the *beam*, defined as the jet material behind the jet head, is decelerated at a working surface near the jet head (Blandford & Rees 1974). The gas becomes shocked, and a cocoon of this shocked beam material surrounds the jet. Separated from this shocked jet gas by a contact discontinuity is ambient material shocked by the bow shock. Ambient

gas that traverses the bowshock forms a shroud of shock-heated gas around the cocoon of beam material. The velocity and density of the jet will determine how prominent these features are, since a diffuse, fast-moving jet will form a broad cocoon of beam gas while a denser jet will plough through the ambient medium without accumulating nearly as much material around it (Norman *et al.* 1983).

The above picture is somewhat simplistic, and basic models are successful in producing the features described by adiabatic jets. However, in modelling a realistic young stellar outflow, many modifications need to be made. Before discussing the need for a more thorough treatment of cooling, it must first be noted that protostars occupy an environment quite unlike that of most other astronomical objects. They are often embedded deep within molecular clouds, and this fact must be considered when modelling an outflow. As will be discussed later, a molecular ambient medium has serious implications for the behaviour of the jets, in both the thermal and chemical dynamics of the outflow.

The realisation that radiative cooling plays an important role in the formation and propagation of protostellar jets has prompted theorists to add significant changes to the adiabatic picture in order to model these outflows more properly. Early models (Blondin *et al.* 1990) modelled very dense jets ($\eta \gg 1$) with the argument that such jets behave nearly isothermally, while underdense jets are chiefly adiabatic in nature. An important result found by Blondin *et al.* is that radiative cooling reduces the thermal pressure and removes entropy in the working surface, causing less waste material to be swept up, thus making the shroud surrounding the cocoon considerably smaller than for adiabatic jets. The decrease in thermal pressure also causes the cocoon to be narrower since it is the pressure inside the beam that serves to inflate the cocoon. In addition, a dense, dynamically unstable shell of gas forms

at the working surface as a result of the cooling, since the ambient gas that comes in contact with the bowshock is compressed towards the cocoon. Other properties of cooling jets that differ from adiabatic jets encountered by Blondin *et al.* include the decreased production of internal beam shocks and a decline in the strength of these shocks as the cooling gets stronger. However as the cooling increases the degree of collimation increases, since the decline in thermal energy and pressure does not allow the bowshock to expand outward and compression along the jet is less prevalent. These effects seem to be what is expected for denser jets with a higher value of η , so the numerical model proved its ability to confirm and predict some features of stellar outflows.

Modelling of cooling jets has evolved considerably since the beginning of this decade. Blondin *et al.* (1990) assumed their jet was completely ionised, which is now known to be untrue. The fact that most of the jet is only partially ionised has motivated a more thorough investigation of the cooling in terms of the chemical composition of the protostellar environment. This treatment of cooling jets using “microphysics” was a major step in modelling jets that behaved more like the outflows observed around newly-forming stars. Early models began with hydrogen as the only material present, but even that assumption forced theorists to consider the ionisation and recombination rates of hydrogen in their models (Stone & Norman 1993a & 1993b). Models and observational data (Bacciotti *et al.* 1995) both showed that the ionisation fraction of the material in the jet remains approximately constant along its extent, but keeping track of the state of ionisation is still instructive when investigating shock regions, for example. Using an empirical cooling function for hydrogen that was dependent on temperature greatly improved the treatment of cooling in the jets (Stone & Norman 1993a).

Expansions on this model soon followed, with the processes of ionisation expanded to include collisions and the recombination rates considering both radiative and dielectronic contributions. Other processes such as charge exchange and free-free emission have also been adapted for the cooling of hydrogen. More importantly, additional elements have been included in numerical simulations so that the environment around protostars is modelled more realistically (Bacciotti *et al.* 1995; Raga *et al.* 1997). Other atoms known to have appreciable cosmic abundances include carbon, nitrogen, oxygen, neon, and sulphur. Helium, although quite abundant, is inert and does not readily contribute to cooling by ionisation or recombination. Contributions to the cooling from molecular species are not as well-studied yet, and efforts to model such cooling in molecular outflows has not been done in as much detail. Still, cooling curves and tables are valuable assets to theoretical studies of radiative processes around newly-forming stars. More will be said about cooling tables in the next chapter.

1.3.3. Time-Dependence in the Jet—Variability

As mentioned previously, a stellar jet which is variable in velocity or direction can be used to explain some of the features seen in observations of young stellar outflows. The linear chain of knots seen in many Herbig-Haro jets hints at an episodic mechanism that causes an ejection of matter from the region of the protostar at some regular interval on the order of tens of years. A succession of shock waves passing through the ambient medium can create a series of working surfaces within the jet, which are the sites of emission corresponding to the knots seen in Herbig-Haro objects. These “pulsed jets” provide regions inside the jet where momentum transfer takes place, giving rise to the momentum peaks exhibited along

the outflow, as observed by Chernin & Masson (1995). Hartigan & Raymond (1993) produced models that showed the velocity perturbations from a stellar jet evolving into a chain of shock-heated knots moving quickly away from the source. Similarly, Stone & Norman (1993b) continued on previous work by allowing their jet velocity to vary sinusoidally at the inlet, producing pulses which quickly steepened to shocks. Also, in the same year, Falle & Raga (1993) successfully produced a chain of knots with a jet which varied in velocity. The classic two-shock structure is produced in all three of these models. The physical mechanism by which these pulses arise is still under debate and is not within the scope of this thesis.

For some Herbig-Haro flows, the chain of knots deviates from a straight line. While a colinear series of emission knots is explained satisfactorily by a jet with velocity variations, directional variability may be used to explain the misalignment of these knots. This will result in a shock that wanders off the axis, creating wider lobes and opening angles (Chernin & Masson 1995). A combination of the two variable components may have further consequences, according to models by Raga (1995). Variability in both velocity and direction seems to break the jet beam up into a series of independent “bullets” with individual bowshocks. The variability also appears to increase the efficiency of the coupling between the jet and the ambient medium: a large number of internal working surfaces in the jet provides more surface area with which the environmental gas can come into contact, shocking whatever material may be entrained along the jet boundaries in turbulent mixing layers (Raga 1995).

1.3.4. Higher Dimensions—Breaking Symmetries

With improvements in computing power, it has recently become possible for simulations to be run disregarding any symmetries that oversimplify the problem at hand. In the case of outflows, using three dimensional grids introduces new modes of instability that are suppressed by the imposition of axisymmetry or slab symmetry (see Stone & Norman 1994 for example), giving a more realistic model of the jet's behaviour. It seems unrealistic to expect the jet to remain in a plane for its entire path. A specific model is discussed below, but many other three-dimensional models exist which explore the dynamics of young stellar outflows in greater detail than is possible within the limits of one- and two-dimensional models (Chernin *et al.* 1994 for example).

As has just been discussed, directional variability is one way of producing emission knots which do not fall on the axis of the flow. In two-dimensional models the jet is still confined to a plane and cannot reproduce all the observable characteristics. However, allowing the jet to precess freely in three-dimensional models has provided a new means for numerical simulations to investigate young stellar outflows. The importance of precessing jets is seen in models by Cliffe *et al.* (1995, 1996), which have morphologies and momentum distributions matching the properties of some observed outflows better than models from straight jets or wind-blown bubbles. Two-dimensional axisymmetric simulations will suppress higher-order instability modes which are more efficient in entraining ambient material. When these modes are able to act on the environment, they allow internal shocks to expand the leading bow shock.

Observational evidence of precessing jets has also been reported. Gueth *et al.*

(1996) find limb-brightened cavities in the molecular outflow L 1157, possibly created by large bowshocks from a precessing jet. The precession itself is thought to be quite small, so the size of the bowshock is more important than the wandering tendency of the primary, collimated jet. The global bowshock described above seems a likely explanation for the large opening angle and seemingly very large bowshock.

As can be seen clearly, the modelling of young stellar outflows is a very challenging theoretical problem. Many factors need to be considered, and eventually assumptions need to be made which might compromise in some way the physical insight desired from the models while making other aspects of the model more understandable. The price of computing high-resolution models with full dimensionality may be too expensive, requiring perhaps a sacrifice of one in exchange for the other. Still, the progress made in recent years in computing power has greatly enhanced the ability to simulate astrophysical phenomena, including outflows from newly-forming stars.

1.4. DG Tauri B—A Case Study

For the purposes of this thesis, the object named DG Tauri B was chosen as a modelling target. The source also has also been classified as HH 159 (Reipurth 1994), but the more common name DG Tau B will be used throughout this thesis. Observations of DG Tau B at both optical and radio wavelengths have shown remarkable structure, and infrared studies have also contributed to the understanding of this object in the context of star formation. A brief history of the observations of this fascinating object will illustrate the motive behind the project described herein.

First mentioned in a letter titled “Jets From Young Stars”, the outflow DG Tau

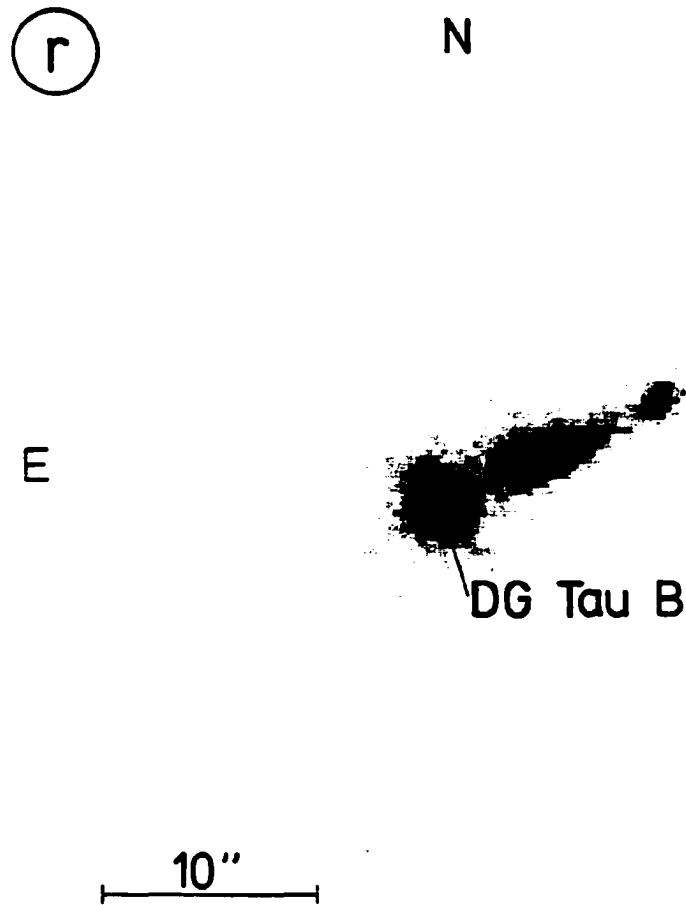


Fig. 1.2.— Discovery image of DG Tau B. Taken from Mundt & Fried (1983). Courtesy R. Mundt.

B was described by Mundt and Fried (1983) as a jet-like emission nebula, $47''$ south and $28''$ west of the star DG Tauri. They observed the outflow using an $H\alpha$ filter, and an r-filter ($\lambda_c = 6560 \text{ \AA}$, $\Delta\lambda = 800 \text{ \AA}$), which allowed observations of $[O\text{I}]$ and $[S\text{II}]$ emission. What they saw was a series of approximately equally spaced emission knots (see Figure 1.2). They claimed the eastern bright spot of their Figure 4 was a faint red star with V magnitude of ≈ 20.5 , which at a distance of 150 pc

and an estimated reddening of $A_V = 6 \pm 1$, implied an absolute visual magnitude of $M_V = 9 \pm 1$, a reasonable estimate for a T Tauri star. This identification of an exciting “star” was later called into question, as is discussed below. The optical chain was measured to be 4×10^{16} cm long, with an opening angle of $\leq 5^\circ$, suggesting a well-collimated jet. In fact for the five jets discussed in Mundt and Fried’s paper, collimation must have occurred on scales less than 3×10^{15} cm, or roughly 0.001 pc (200 AU). They claimed that DG Tau B was not a bipolar outflow like others in their sample, yet the geometry of the jets observed gave more evidence that regions of star formation do not possess spherical symmetry, a result known from molecular studies at longer wavelengths. Vrba *et al.* (1985) measured *JHKL* photometric magnitudes of four jet nebulosities including DG Tau B, with the conclusion that the Herbig-Haro jet sources observed were pre-main-sequence (pre-MS) low-mass stars. The total visual extinction derived for DG Tau B was 6.6, in agreement with Mundt & Fried (1983). No *J*-band photometry for DG Tau B was possible since no signal was detected. Nevertheless, the claim that DG Tau B was a pre-MS star with a single jet emanating from it was given strength by the work of Vrba *et al.* (1985).

The search for the definitive position of the exciting star in the DG Tau B jet continued with $95 \mu\text{m}$ far-infrared observations by Cohen *et al.* (1985). In their $95 \mu\text{m}$ observation of DG Tau, extended emission from DG Tau B was also detected, and an upper limit of 50 K was imposed on the colour temperature based on the fact that no emission from DG Tau B was seen at $47 \mu\text{m}$ (Cohen *et al.* 1985). This far-infrared emission extended nearly orthogonally to the optical jet of DG Tau B, but the peak infrared emission coincided with the position of the visible jet.

This picture of a single outflow from DG Tau B was challenged in by Jones & Cohen (1986), who observed DG Tau B spectroscopically and showed it to be bipolar

with a very weak blueshifted lobe. Seven knots were identified, three of which were blueshifted, the remaining four describing the jet seen by Mundt and Fried. The exciting star was believed to lie between the two knots denoted A and E, the two largest nodular structures, based on the radial velocity and emission differences between the eastern and western extents, as well as the excess red continuum in this region. Although no dark cloud is readily seen around DG Tau B, it is currently identified as a young stellar system with a bipolar outflow. The bipolarity of DG Tau B was confirmed by Mundt *et al.* (1987), with the heliocentric radial velocities of the jet found to be -100 km s^{-1} for the blueshifted lobe and 60 km s^{-1} for the more pronounced redshifted lobe. Other important physical quantities for DG Tau B have been measured and will be presented in another section.

Further studies of DG Tau B were performed in the 1990's in order to understand the emission and structure of the jet better. At optical wavelengths, observers studied the jet width and degree of collimation along the redshifted jet of DG Tau B (Mundt *et al.* 1991), as well as its proper motion (Eislöffel & Mundt 1995). This work is further expanded with long-slit spectroscopic observations by Eislöffel & Mundt (1998) wherein they find that the ratio of working surface velocity (called the pattern velocity in their paper) to jet velocity (referred to as the flow velocity), ζ , varies from one working surface to another. Some knots travel with the same speed as the jet, yet others have velocities around 50% of the flow speed. While the variation in the radial velocities of the knots is quite small, $\leq 10\%$, the tangential velocities determined from proper motion studies differ by a factor of two and are the main reason for the varying values of ζ . They interpret this range of values for ζ as a source of difficulties for models which use internal shocks resulting from variations in velocity to explain the observed knots. An irregular variation in

the velocity may, however, be successful in reproducing jets with different outflow velocities. Surely the addition of directional variability would also have the effect of creating different radial and tangential velocities for the knots of dense gas in the outflow. Directional variability would be useful in modeling an outflow with knots that are away from the jet axis, but the high linearity of the DG Tau B jet suggests that directional variability is not needed in simulations of this particular object.

Detailed CCD images of the $H\alpha$ and $[S\text{II}]$ emission, plus an I -band image, showed a dramatic difference between the ionised, atomic, and continuous emission coming from DG Tau B (Mundt *et al.* 1991). The opposite lobes of the outflow show very different degrees of excitation and ionisation, and some of the knots seen at low resolution by Jones & Cohen (1986) are found to consist of two components, increasing the total number of knots to about 10, seven of which are in the redshifted lobe, and the position of the exciting pre-MS star is now taken to be knot E of Jones and Cohen's nomenclature. An interesting result from Mundt *et al.* (1991) is that the opening angle of the jet decreases from about 5° close to the source (between $5''$ and $30''$) to zero at further distances. The faint blueshifted counterjet, though not as reliably measured, opens at about 17° . The collimation of the jet is more pronounced at distances about 1000 AU from the protostar than at closer distances, suggesting a large-scale mechanism for collimation rather than a local mechanism. Asymmetries between the two jets are probably caused chiefly by the environment around DG Tau B, not by factors such as optical extinction between the source and earth.

In addition to the wealth of information ascertained from optical studies, infrared- and radio-wavelength observations greatly contributed to the understanding of young stellar outflows. DG Tau B, being one of many Herbig-Haro jets of great

interest, was observed at these lower frequencies to probe other components of its complex morphology. As discussed above, H₂ emission is common from Herbig-Haro objects, particularly those with low excitation. If one observes emission from molecular hydrogen in a stellar outflow, it is collisional excitation in shock waves that produces the rovibrational lines. Again, evidence of molecular and atomic gas with similar morphologies can give credence to the unified model for stellar jets and molecular outflows. Schwartz *et al.* (1995) performed infrared spectroscopy on seven Herbig-Haro objects, including DG Tau B. Though only weak H₂ emission was detected near “knot A” (Jones & Cohen 1986), the association of any molecular gas with a region where atomic and ionised species are also known to exist presents a challenge to the models. Clearly the shock structure of these outflows must produce both low- and high-velocity shocks. In other words, bowshocks are favoured since the range of velocities in a bowshock results in a range of excitation conditions. Schwartz *et al.* were also able to compute the K magnitude of DG Tau B from continuum emission in their spectra, and compared their result to the photometry done by Vrba *et al.*, finding very good agreement with $K = 11.7$ while Vrba *et al.* (1985) found $K = 11.5$.

At radio wavelengths, thermal bremsstrahlung and CO observations of DG Tau B have shown details unseen in the optical and infrared regimes. DG Tau B was one of two sources observed at $\lambda = 3.5$ cm by Rodriguez *et al.* (1995). The peak intensity of DG Tau B at 3.5 cm, identified as the exciting source, was detected $\approx 1''$ from the position of the optical centre, but the position angle is almost exactly that of the redshifted jet. The derived FWHM of the radio source is less than half an arcsecond, implying that the scales being probed are approximately that of the base of the collimated jet, only tens of astronomical units in size. The fair agreement in

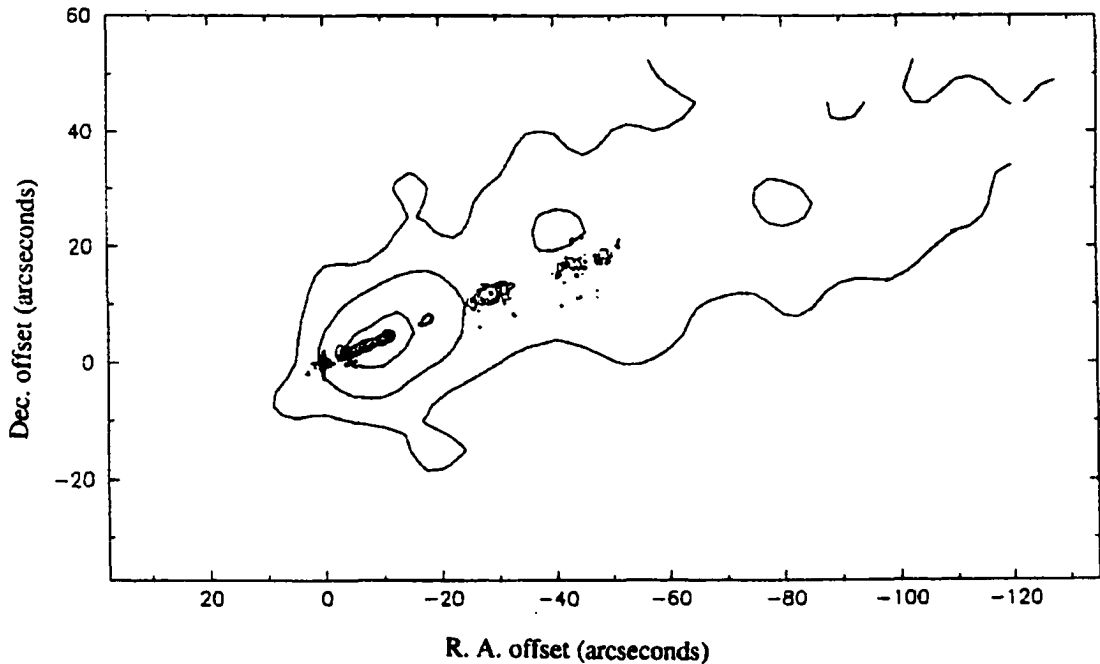


Fig. 1.3.— CO $J = 3 - 2$ map of DG Tau B, superimposed on [S II] image of Mundt. Courtesy G. Mitchell

both position and jet widths between the optical and radio emission supports this argument.

The agreement between the optical and radio structures of DG Tau B is even more prevalent when comparing the CO molecular emission to the optical jet. A molecular outflow associated with DG Tau B has been observed by Mitchell *et al.* (1994) in the $J = 3 - 2$ and $J = 2 - 1$ rotational states and Mitchell *et al.* (1997, hereinafter MSM97) for the $J = 1 - 0$ state. The coexistence of molecular outflows and optical jets has long been expected but observational evidence is not always possible for many objects, because of extinction or low densities. As Figure 1.3 illustrates, the $J = 3 - 2$ map (Mitchell *et al.* 1994) of CO emission shows an

extended lobe of molecular gas surrounding the redshifted, northwest-bound optical jet (seen best by the deconvolved [S II] image of Mundt *et al.* 1991). The CO gas in Figure 1.3 extends more than twice as far as the optical emission. Spectra were obtained for five positions along this molecular outflow for the $J = 2 - 1$ line of CO, and the isotope ^{13}CO , which allowed the calculation of key physical parameters such as optical depth, excitation temperature, mass, and momentum. It was found that the momentum transport rates of the jet and the molecular outflow were in very good agreement, suggesting that the stellar jet may indeed drive the molecular outflow.

The further work with CO $J = 1 - 0$ observations reported in MSM97 showed an even closer association between the knots in the jet and the structure of the molecular gas. A high-resolution, 4" map acquired using the OVRO at 2.6 mm shows the molecular outflow in much greater detail than the 14" map from $J = 3 - 2$ data (see Figure 1.4). The redshifted molecular gas extends westward from DG Tau B, in a fairly narrow beam for the first 1000 AU, where the width does not exceed 500 AU. Then between 1000 AU and 1800 AU, the outflow broadens in successive "jumps" to a width of about 900 AU, before splitting into two separate ridges for the next ~ 4000 AU. The width of the molecular outflow broadens to approximately 4200 AU. As seen in Figure 1.4, when this remarkable CO structure is superimposed on the optical [S II] jet imaged by Mundt *et al.* (1991) the knots in the redshifted lobe seem to coincide with the sites of broadening in the molecular gas. This apparent interaction between the atomic and molecular species allows an investigation of the effects of entrainment by the jet as it shocks the surrounding ambient medium. In addition to the amazing structure seen in the redshifted lobe, Mitchell *et al.* (1997) claim that the blueshifted velocities do not evince an outflow, but possibly a

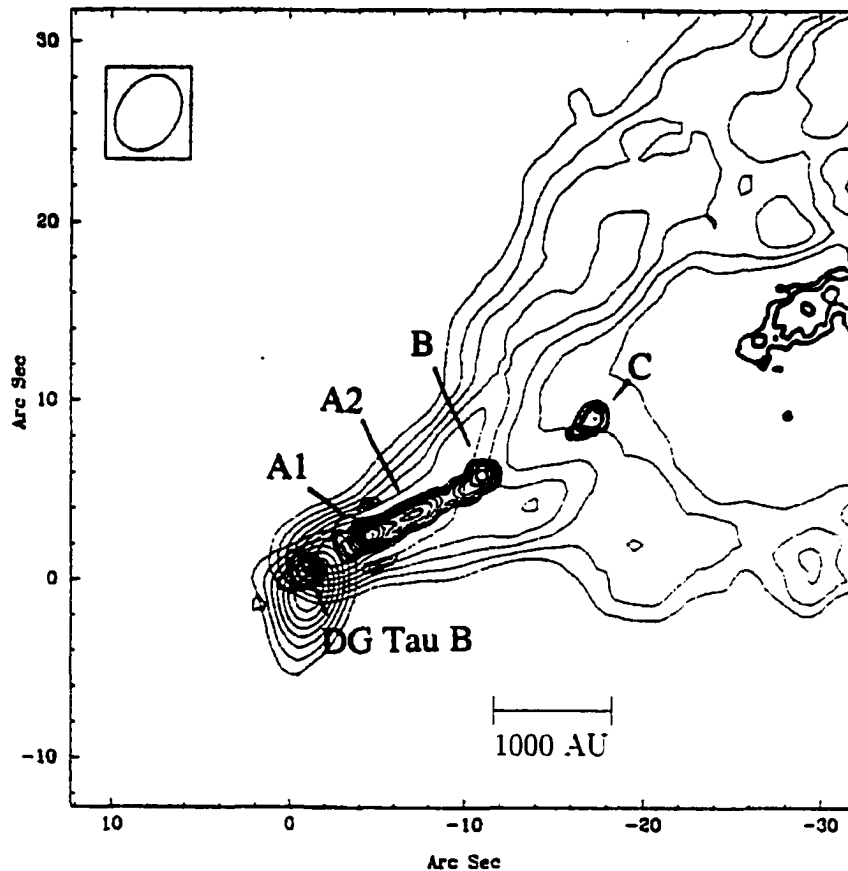


Fig. 1.4.— CO $J = 1 - 0$ map of DG Tau B, superimposed on [S II] image of Mundt. Courtesy G. Mitchell

molecular core or clump surrounding DG Tau B, which could explain its faintness at other wavelengths. The correspondence between the ambient molecular gas and the knots in the DG Tau B jet provides a challenge to the modelling of young stellar outflows: *Can a stellar jet produce the emission features observed in the DG Tau B outflow?* Many of the important derived physical parameters of DG Tau B will be discussed in the next chapter.

Even more recently, observations of DG Tau B have been made with the Hubble Space Telescope (Stapelfeldt *et al.* 1997). Krist (1998) also included DG Tau B in a search for circumstellar disks with the Hubble Space Telescope. The first Hubble image shows a compact, diffuse bipolar nebula, which may be evidence of a circumstellar envelope surrounding the exciting star and possibly a disk, though no star is directly visible. Images of DG Tau B and other young stellar outflows can be seen on the World Wide Web at <http://opposite.stsci.edu/pubinfo/pr/1999/05/index.html>. This discovery can give more insight to the ways in which stellar jets are launched, how they are collimated, and their effect on the surrounding environment.

2. METHODOLOGY

2.1. The Numerical Code: ZEUS3D

ZEUS3D is a FORTRAN computer code maintained by D. A. Clarke which solves the following magnetohydrodynamic equations in three possible geometries.

$$\frac{\partial \rho}{\partial t} + \nabla \cdot (\rho \mathbf{v}) = 0 \quad (2.1)$$

$$\frac{\partial \mathbf{S}}{\partial t} + \nabla \cdot (\mathbf{S} \mathbf{v}) = -\nabla(p_1 + p_2) - \rho \nabla \Phi + \mathbf{J} \times \mathbf{B} \quad (2.2)$$

$$\frac{\partial e_1}{\partial t} + \nabla \cdot (e_1 \mathbf{v}) = -p_1 \nabla \cdot \mathbf{v} \quad (2.3)$$

$$\frac{\partial e_2}{\partial t} + \nabla \cdot (e_2 \mathbf{v}) = -p_2 \nabla \cdot \mathbf{v} \quad (2.4)$$

$$\frac{\partial \mathbf{B}}{\partial t} = \nabla \times (\mathbf{v} \times \mathbf{B}) \quad (2.5)$$

where ρ is the density of the fluid, \mathbf{v} is the velocity of the fluid, \mathbf{S} is the momentum density vector (also written as $\rho \mathbf{v}$), p is the fluid pressure, Φ is the gravitational potential, \mathbf{J} and \mathbf{B} are the current density and magnetic field, respectively, and e is the energy density. Since two separate fluids are used in these models, the pressures and energy densities of each fluid are subscripted to identify each medium separately. Densities are not separated in this way, but simple expressions in terms of pressure or energy density can be derived if such delineation is desired.

Modifications to the above equations were implemented, which include the exclusion of magnetic field terms and the inclusion of a radiative energy loss term. These changes will be discussed below in more detail.

2.1.1. *Current Capabilities*

ZEUS3D (Clarke 1996) is a computer program which solves the difference equations of non-relativistic magnetohydrodynamics, based on equations 2.1-2.5. A second-order monotonic upwinded time-centred interpolation scheme is used on a staggered mesh to perform explicit numerical solutions of the equations describing the behaviour of the fluid. ZEUS3D operates using natural or dimensionless units, so any physical quantities extracted from the simulations must be converted to real physical units by way of scaling factors. A feature of ZEUS3D that makes it ideal for the study of outflows is the ability of the code to trace the dynamics of two separate fluids, such as an ambient molecular medium being disrupted by a supersonic atomic jet.

The major thrust of the research described in this thesis is the incorporation of cooling rates for *several* atomic species into the ZEUS3D code, to enable the modelling of stellar outflows. The primary use of the code has been to model extragalactic jets, in which cooling does not contribute significantly (Raga 1995). The modelling of extragalactic jets using ZEUS3D has been accomplished numerous times (Clarke *et al.* 1997, Casey 1996, to name only two) in efforts to simulate the behaviour of these powerful outflows. The cooling performed by Stone & Norman (1993a, 1993b, 1994) for stellar objects, discussed above, was performed for only one element, namely hydrogen, and an extension to a larger number of species is desirable. In this work, neutral and partially-ionised carbon and oxygen species were considered in addition to hydrogen, though a self-consistent coupling of cooling with fractional abundance was not implemented as it was in the one-element case of Stone & Norman (1993a).

It is possible to perform simulations with ZEUS3D using one, two, or three dimensions, using Cartesian, cylindrical, or spherical coordinate systems as desired. The preferred geometry for a two-dimensional simulation of a young stellar outflow is cylindrical coordinates, since a bipolar morphology is strongly favoured over a spherical distribution of matter.

2.2. Necessary Additions to the ZEUS3D Code

The new physics necessitated by the observations of DG Tau B are described below. Each addition of physics is accompanied by new modules for the ZEUS3D program, including new subroutines as well as minor changes to existing routines to allow for the inclusion of these subroutines. The physics is outlined below, while the subroutines are described in the appendix.

2.2.1. Variable Jet Velocity

The linear system of knots seen in the DG Tau B outflow may imply the outflow is episodic, so a variable flow must be used in the modelling. Only variations in velocity are needed since directional variability is forbidden by the imposed cylindrically symmetric geometry. To establish this variable flow, a sinusoidally varying inlet velocity, similar to that in Stone & Norman (1993b) with the form

$$v_{inlet} = v_o(1 + \phi \sin \omega t) \quad (2.6)$$

was used. Here, ϕ represents the amplitude of the velocity variations and ω determines the frequency of the pulses. Because not all jets exhibit knots that are equal distances apart, an extra term can be added to make the amplitude variable

in time with a frequency different than that of the jet. So, if we assume that $\phi(t) = \phi(1 + \cos \theta t)$, then equation 2.6 becomes

$$v_{inlet} = v_o[1 + \phi(1 + \cos \theta t) \sin \omega t] \quad (2.7)$$

This prescription allows for a jet with a variable velocity that is episodic, but which does not necessarily eject pulses of jet material with similar velocities. Thus, irregular knot spacings and differing knot velocities can be produced by such a prescription. This is only one possible form for a variable amplitude, with no physical mechanism behind it. Thus we do not implement such a prescription in the code.

2.2.2. Radiative Cooling in the Jet

In equations 2.3 and 2.4 above, the energy equation has only one process by which energy is expended in the outflow, namely by the work done by the jet gas as it expands. Radiative cooling is not represented, so an additional term is introduced (for the atomic jet only) to characterise the cooling rate in the outflow:

$$\frac{\partial e_1}{\partial t} + \nabla \cdot (e_1 \mathbf{v}) = -p_1 \nabla \cdot \mathbf{v} - L \quad (2.8)$$

Cooling manifests itself as the term L in the energy equation. The cooling rate L (from the collisional excitation of atoms) can be expressed as the contribution of cooling from the many components in the outflowing gas:

$$L = \sum_i n_e n_i \Lambda_i(n_e, T) \quad (2.9)$$

In this expanded form i represents each ionic or atomic species, n_e is the electron density, n_i is the number density of species i , and Λ_i is a volume cooling rate for each

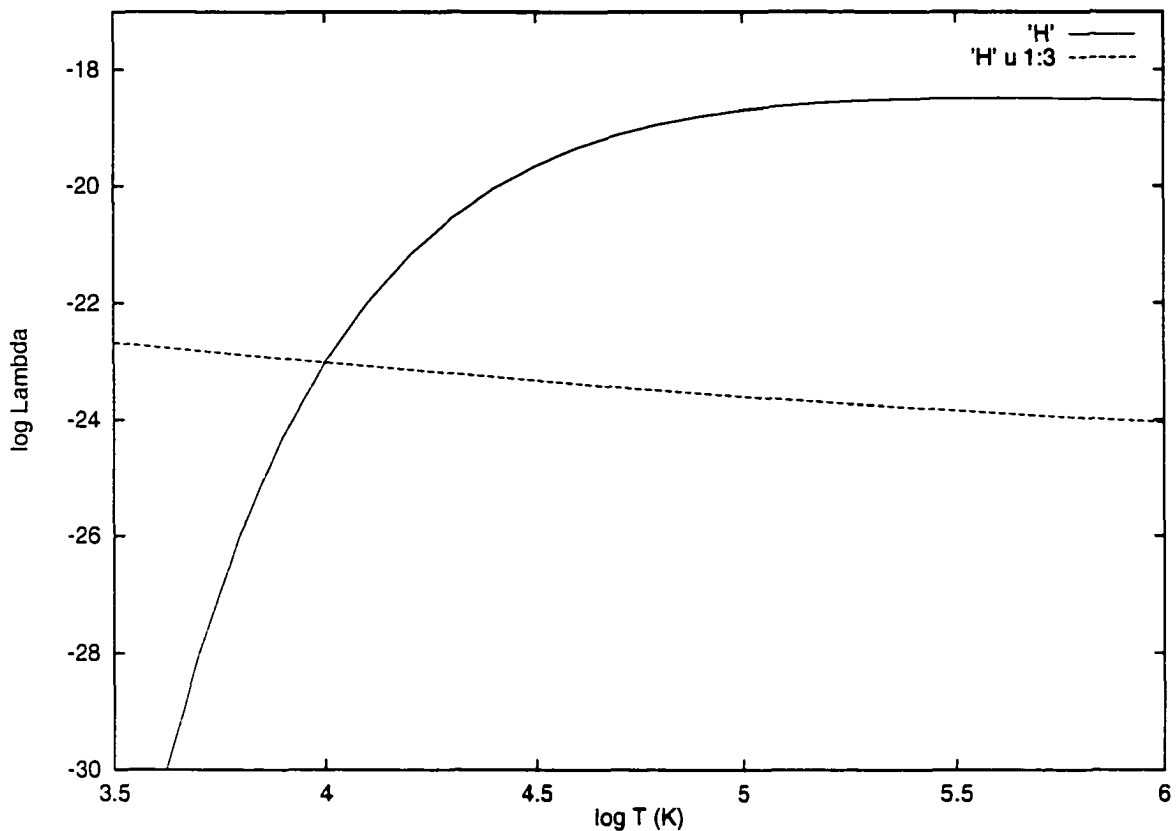


Fig. 2.1.— Radiative Cooling Rates for Hydrogen. Λ is measured in units of $\text{erg s}^{-1} \text{cm}^3$. The solid line is for neutral hydrogen.

of the individual species. As seen in the above expression, Λ_i is dependent on n_e and on the temperature of the gas, so the code must be able to calculate all these values for several species in order to model the cooling realistically. This form of L is not the only one in use but it is quite commonly used (Bacciotti *et al.* 1995), and given cooling rates for certain species, the problem of modelling stellar jets with cooling is made much easier. Analytic expressions for atomic and molecular coolants are another common tool for the implementation of radiative cooling into a numerical simulation.

The subroutines written to simulate the cooling in DG Tau B utilise recently

published cooling tables (Raga *et al.* 1997) which tabulate values for Λ_i , the volume cooling rate, for temperatures in the range $100 K \leq T \leq 10^6 K$ and for electron densities satisfying $1 \text{ cm}^{-3} \leq n_e \leq 10^6 \text{ cm}^{-3}$. Tables for 14 species, for four elements (H, C, O, Ne) with various degrees of ionisation, are published. From this set of 14 species, cooling rates for H I, H II, C I, C II, C III, O I, O II, and O III were taken to be used in the modelling of DG Tau B. Neon species and highly-ionised carbon and oxygen were not included because of their lower abundances. These eight tables are found in the appendix as part of the subroutines added to ZEUS3D. Figures 2.1 and 2.2 show cooling rates for some of the species thought to be important in radiative cooling processes in the interstellar medium. It appears that hydrogen will be the dominant radiative coolant because of its abundance. Still, inclusion of the other species may allow us to trace the sites of cooling for each of these species.

As well, certain assumptions regarding the abundance of each of these species had to be made. The atomic abundances of hydrogen, carbon and oxygen were taken to be 0.999, 3.3×10^{-4} and 6.6×10^{-4} as used in Raga *et al.* (1997). The degree of ionisation for each element is apt to change under the conditions in stellar jets where shocks are heating gas and dissociating molecules. The finding that along most of the jet beam the ionisation fraction remains constant (Bacciotti *et al.* 1995, Stone & Norman 1993a) prompted the use of a *constant* ionisation fraction at all grid points where the jet is present, an assumption that is unrealistic but can be rectified in subsequent refinements of the code. For hydrogen a 10% ionisation fraction is assumed. For carbon we assumed 7% and a 1% ionisation fraction was used for oxygen. These values were calculated using Table 5 of Arnaud and Rothenflug (1985), assuming a $\sim 13000 K$ protostellar environment at the site of ejection. To simplify things further the abundance ratios of C II to C III and of O II to O III were

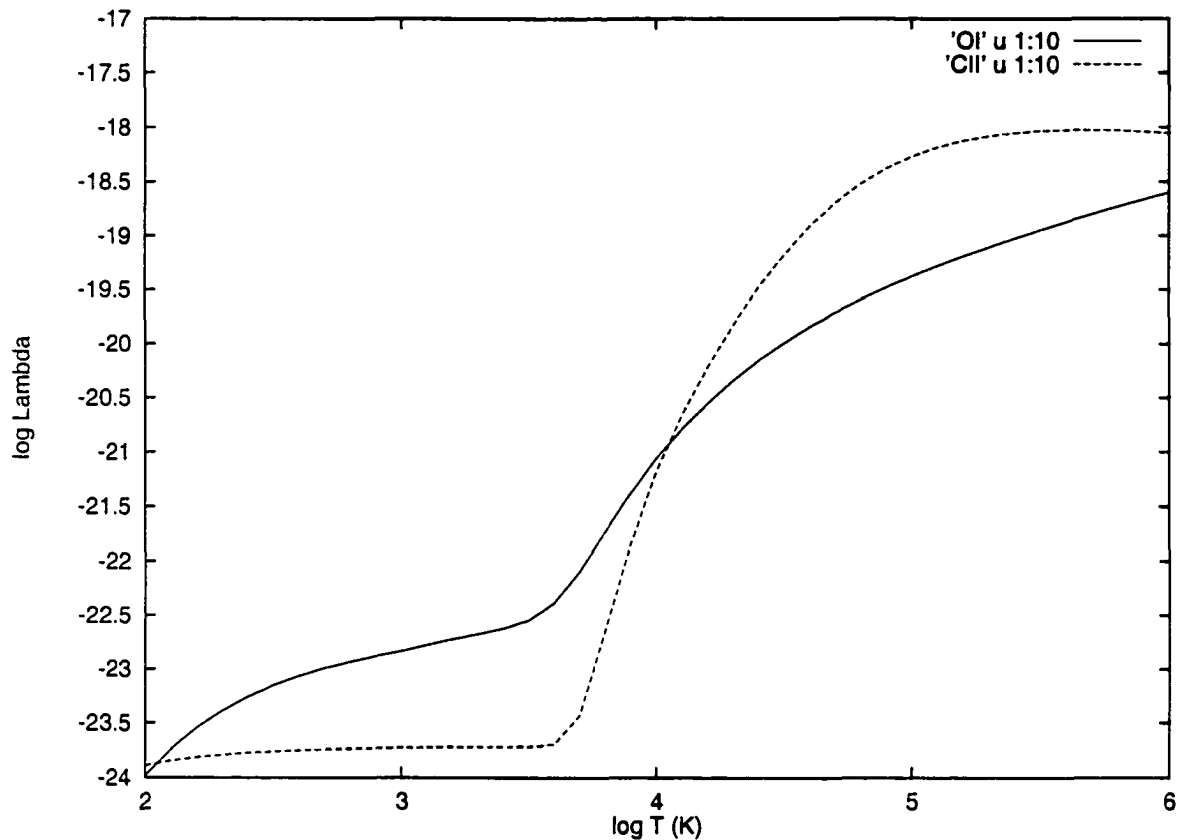


Fig. 2.2.— Radiative Cooling Rates for Neutral O and Singly-Ionised C, at a density of $n = 10^4 \text{ cm}^{-3}$. The solid line represents the oxygen species.

kept constant at 10^3 . With these approximations, this treatment of atomic cooling is not fully self-consistent, as no calculation of ionization states is performed.

Since the cooling rate is a function of temperature and therefore of the specific internal energy, the energy equation must be solved by implicit techniques. In other words, the values of the energy for the next timestep in the model must be found using iterative procedures, not simply using explicit difference methods. This further complicates the cooling subroutine since the cooling function is recalculated upon each iteration, requiring significantly more calculations to arrive at an acceptable energy loss in each timestep. The subroutines written to incorporate the cooling

function make use of secant-method root solvers in the iterative process as well as an interpolation scheme to find the volume cooling rates from the tables of Raga *et al.* (1997).

An attempt was made to use the newly-written subroutines to reproduce the models of Stone & Norman (1993a, 1993b). These models were some of the first to incorporate hydrogen cooling into models of stellar jets. We sought only a qualitative match to the earlier models, since differences in the codes prevented a complete reconstruction of the simulations. The grid size used by Stone & Norman greatly exceeded the capabilities of the computing power at hand, for example. Other notable differences that were recognised included the use of different symmetries. Stone & Norman used Cartesian coordinates, while in the present models axisymmetry was used. The neutral hydrogen cooling rates used in the two models do not differ significantly, despite the fact that the earlier cooling rates were simple fits to a curve; a discrepancy between the *ionised* hydrogen cooling rates was noted, which would affect the energy loss from collisional excitation of HII differently in each simulation for certain temperatures. The simulations of Stone and Norman were able to monitor the ionisation fraction, while in the current models this treatment is not considered. With these differences between the codes, it was still possible to verify that the programs written for ZEUS3D produced cooling jets that behaved generally the same way as the earlier ones. It was verified that the interpolation routines were working properly for the cooling rate tables, and that the program was scaling between physical units and dimensionless ZEUS3D quantities in the right manner.

2.2.3. Tracing Optical and Molecular Emission

As the observations of DG Tau B in [S II] and rotational CO emission show the most prominent features of the outflow, it is desirable to model the emission expected from these species. The coolants for which cooling rates are calculated in our simulations may have their emission modelled quite easily, given the assumption that the emission from these species is proportional to the amount of energy lost by the jet from radiative cooling. Since S II is not a dominant coolant, it is not included in the simulations of Raga *et al.* (1997), nor is it implemented here. Fortunately, it has been found that another forbidden emission line, [O I], is a reliable tracer of [S II] emission in both HH objects and in T Tauri Stars (Smith *et al.* 1997b, Cabrit *et al.* 1990, Edwards *et al.* 1987 and references therein). Cooling caused by neutral oxygen is included in our simulations and thus can be used as a “surrogate” species which allows the prediction of emission from singly-ionised sulphur.

The prediction of emission from rotational lines of CO must be approached in a different manner, since there is no atomic species whose emission correlates well with the molecular gas distribution in the vicinity of forming stars. Temperature-dependent cooling functions for CO rotational lines are calculated by Neufeld & Kaufman (1993) and Neufeld *et al.* (1995) as part of a complex, four-parameter analytic representation of radiative cooling in molecular gas. Alternatively, Smith *et al.* (1997a) and Suttner *et al.* (1997) adopt an approximate analytic expression for CO emissivity derived by McKee *et al.* (1982).

For the purposes of this thesis, a scheme was devised to estimate the CO emission using a somewhat “brute-force” method. We are interested in the low-velocity CO gas giving rise to the lowest rotational transitions. A subroutine

was written which effectively rotates the two-dimensional grid about the jet axis and integrates through the resulting cylinder, summing the ambient energy density for cells within a specified velocity interval. This is very similar to observing an outflow along a given line of sight. The observed intensity along the line of sight is proportional to the column density of the ambient gas, so this method mimics the manner in which telescopic observations of CO are performed. The images of predicted atomic and molecular emission appear in the next chapter.

The decision to employ the ambient energy density as the quantity to trace the molecular outflow ensures that only the ambient gas is being traced, as opposed to the mass density. The ZEUS3D code calculates the total density of the cells in the simulation grid without discerning between the two fluids. It is not difficult to estimate what fraction of the cell density is from the ambient medium; indeed we perform a similar task as part of the atomic cooling. CO integrations are made by the summation of characteristic temperature values within the available radial velocity “channels,” and the resulting flux measurements are proportional to the column density of the source. The subroutine is an attempt to remain faithful to this practice, with the energy density being the quantity most closely related to the ambient gas temperature (of the variables that ZEUS3D is designed to store in the computer memory). Numerical simulations with ZEUS3D offer the tantalising opportunity to measure the densities *directly*, a luxury not enjoyed by the observational astronomer. It is envisioned that future versions of the subroutines written should allow for many possible prescriptions for the duty of creating molecular emissivity images.

The complete FORTRAN subroutines written to implement the variability, radiative cooling and emission predictions are found in the appendix.

2.3. Modelling of DG Tau B with ZEUS3D

Here we describe the programming and computing that was done to consider the DG Tau B outflow using the ZEUS3D code. Prior to the creation of any new subroutines, decisions regarding the geometry, symmetry, and inclusion or exclusion of certain terms in the magnetohydrodynamic equations are considered.

2.3.1. Preliminary Modelling Constraints

Based on the appearance of the DG Tau B jet and molecular outflow, certain assumptions can be made about the type of model that may reproduce the observed features. The linearity of the knotty sulphur emission peaks is an indication that the jet does not wander by an appreciable amount, suggesting that the need for three-dimensional calculations—as is the case for precessing jets—will not be a requirement. Thus a two-dimensional model using axisymmetric cylindrical coordinates is favoured. The differences in the velocities for each of the knots, and the fact that they are not equally spaced along the jet, suggest that a purely sinusoidal variation in velocity is not sufficient to reproduce the exact morphology of DG Tau B.

Also to be considered is whether to add the effects of magnetic fields. Observations of thermal radiation at radio wavelengths (Rodriguez *et al.* 1995, Martin 1996) has given evidence of a possible magnetic field constraining the paths of ions being flung from DG Tau B's exciting star. However, the strength of the magnetic field is not well known, and thus it is difficult to gauge the importance of a magnetic field for this source. Polarisation studies have shown that unlike other outflows, the global magnetic field around DG Tau B is not oriented parallel

to the direction of the outflow, but is nearly perpendicular to it (McGregor *et al.* 1994). Perhaps this indicates that the role of the magnetic field is not always an important agent in containing the ionised material that is ejected by a young stellar outflow. Because there is no compelling evidence that the magnetic field is dynamically important in DG Tau B, simulations for this thesis were constructed without magnetic fields.

Self-gravity is another physical entity that must be considered. The self-gravitational potential term in equation 2.2 is usually ignored in models of outflows, with the justification that the escape velocity associated with the protostar is much less than the velocity of the jet in these outflows. Additional physics relevant to DG Tau B is the inherent difference in the two fluids in the problem, since the ambient medium is assumed to be completely molecular, with adiabatic index $\gamma = \frac{7}{5}$. The jet is composed of atoms and ions, both of which are characterised by a fluid with adiabatic index $\gamma = \frac{5}{3}$. For these models, it was assumed that the ambient medium has a *constant* density throughout the region of modelling, prior to the introduction of the jet. Models with density gradients could provide more insight to the physical structure of the molecular medium, as will be discussed later.

When using cylindrical coordinates with symmetry in the (azimuthal) ϕ -direction, and with magnetic and self-gravitational terms ignored, equations 2.1 – 2.4 reduce to:

$$\frac{\partial \rho}{\partial t} + \frac{1}{r} \frac{\partial \rho u_r}{\partial r} + \frac{\partial \rho u_z}{\partial z} = 0 \quad (2.10)$$

$$\frac{\partial \rho u_r}{\partial t} + \frac{1}{r} \frac{\partial \rho u_r^2}{\partial r} + \frac{\partial \rho u_r u_z}{\partial z} = - \frac{\partial (p_1 + p_2)}{\partial r} \quad (2.11)$$

$$\frac{\partial \rho u_z}{\partial t} + \frac{1}{r} \frac{\partial \rho u_z u_r}{\partial r} + \frac{\partial \rho u_z^2}{\partial z} = - \frac{\partial (p_1 + p_2)}{\partial z} \quad (2.12)$$

$$\frac{\partial e_1}{\partial t} + \frac{1}{r} \frac{\partial e_1 u_r}{\partial r} + \frac{\partial e_1 u_z}{\partial z} = -p_1 \left(\frac{1}{r} \frac{\partial u_r}{\partial r} + \frac{\partial u_z}{\partial z} \right) - L \quad (2.13)$$

$$\frac{\partial e_2}{\partial t} + \frac{1}{r} \frac{\partial e_2 u_r}{\partial r} + \frac{\partial e_2 u_z}{\partial z} = -p_2 \left(\frac{1}{r} \frac{\partial u_r}{\partial r} + \frac{\partial u_z}{\partial z} \right) \quad (2.14)$$

2.3.2. Parameter Search for the DG Tau B Young Stellar Outflow

Extensive studies of Young Stellar Outflows including DG Tau B have been performed in order to ascertain the average values of important parameters which can be used to characterise these flows. Mundt and his collaborators have done much of the work with CCD observations of DG Tau B (Mundt *et al.* 1987, Mundt *et al.* 1991). More recent data from Eislöffel and Mundt (1995, 1998) have delineated much of the velocity information, not just for the jet but for each of the knots in both the redshifted lobe and the obscured blueshifted jet. The notable variation in the speeds of the knots, differing by a factor of about two, serves as a reminder that it is difficult to characterise these jets completely with only a small set of parameters.

Table 1 shows some key values (or upper limits) for properties of the redshifted lobe of the DG Tau B jet. Some parameters were calculated based on the observational data given in the literature, since values were not explicitly stated.

The Mach number in Table 1 was estimated from dynamical scales for the jet. The Mach number is by definition the jet speed divided by the sound speed for the jet. Assuming the temperature of gas near the forming star is a few $\times 10^4 K$, a sound speed of approximately 15 km s^{-1} is inferred. From observations, the flow velocity is no greater than 260 km s^{-1} , and thus

$$M \leq \frac{260}{\sqrt{\frac{\gamma k T}{\langle m \rangle}}} \quad (2.15)$$

Parameters for DG Tau B	
Quantity	Value
Distance	160 pc
Length	0.045 pc (9280 AU)
Width	~ 200 AU
n_e	$\leq 4000 \text{ cm}^{-3}$
$n_{\text{ambient,preshock}}$	$\sim 10^4 \text{ cm}^{-3}$
N_{knots}	7
Flow (Jet) Velocity	$\leq 260 \text{ km s}^{-1}$
Mach Number	~ 15
η	~ 3.0

Table 1: Observational Data For the Redshifted Lobe of DG Tau B. Data are taken from Mundt *et al.* 1991.

An average mass of $\langle m \rangle = 1.22m_p$ was used in this calculation to account for the heavier species, following Raga *et al.* (1997).

Mach numbers of 6 or less, which are more capable of steady-state entrainment along the jet boundary, may be more difficult to justify because of the physically unreasonable temperatures required to give a sufficiently high sound speed. Still, we investigate a region of parameter space including low Mach numbers, and find that cooling can raise the effective Mach number slightly.

The value for η , the ratio of jet density to ambient density, is found using

equation [4] from Mundt (1986)

$$\frac{\rho_j}{\rho_a} = \frac{v_{ws}^2}{(v_j - v_{ws})^2} \quad (2.16)$$

and the observation that some of the knots (working surfaces) of the DG Tau B jet move at about 60% to 65% of the flow speed (Eislöffel and Mundt 1995). In other words, $v_{ws} \simeq 0.6v_j$ so

$$\frac{\rho_j}{\rho_a} = \eta \simeq 2 - 3 \quad (2.17)$$

It is important to remember that the ζ parameter for DG Tau B varies by more than 50% between knots, so this method of determining η is at best an estimate that characterises only certain parts of the jet at the present epoch. For this reason a small parameter search was performed with different values of M and η instead of using just one value for each variable.

3. RESULTS

Table 2 summarises the simulations discussed in this chapter, leading to a model of DG Tau B.

Jet Simulation Types				
Simulation	Cooling	Variability	M	η
A	No	No	15	3
B	Yes	No	15	3
C	No	Yes	15	3
D	Yes	Yes	varied	varied

Table 2: List of Simulations Showing Added Physics.

3.1. General Characteristics of the Simulations

The simulations described in this chapter are all two-fluid, hydrodynamic (no **B** field) calculations in two dimensions. Each type of simulation outlined in Table 2 is reviewed below. Simulations were run with a grid of 240 equal-sized zones along the jet axis, covering a distance of 60 jet radii. Along the vertical axis, 120 zones covered a 30 jet-radius distance, with 30 of those zones within the first three jet radii. The remaining 90 zones are continuously staggered in size so that the uppermost zone is slightly larger than the lowermost one. For simulations with variable velocities, a constant amplitude of 0.20 was used ($\phi = 0.20$, independent of time). The pulse frequency ω had to be varied for each model since the number of knots scales with

M and η .

3.1.1. *Simulations Without Cooling Or Variability–Simulation A*

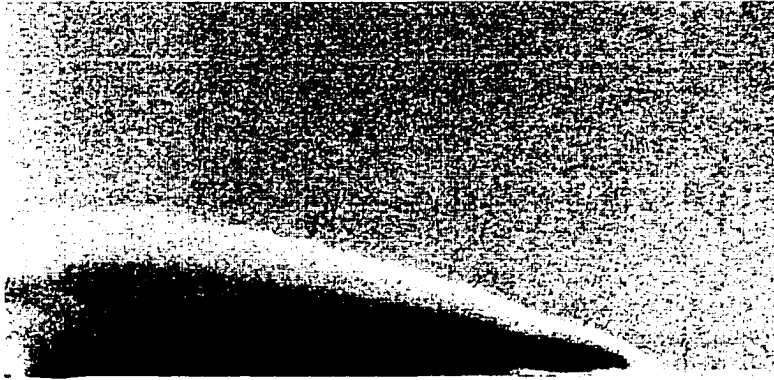
Simulation A was a simple monatomic ($\gamma = \frac{5}{3}$) jet flowing into a molecular ($\gamma = \frac{7}{5}$) ambient medium. No cooling or variability was included, as this simulation was to be used as a standard against which the progressively more complicated simulations were to be compared.

Figure 3.1a shows the density profile for the non-variable, non-cooling jet, with its smooth bow shock being the main feature visible. A high value of η gives a strong bow shock (vital for driving the CO gas) with a two-shock structure as seen by Stone and Norman (1993a, among many others). The pair of shocks is best visualised by the $\nabla \cdot \mathbf{v}$ plot of Figure 3.2a. The divergence of the velocity becomes negative in the presence of a shock, and the pair of shocks can be seen as two narrow “stalactites” centred near $x_i = 53$, the leading (right) one representing the bow shock and the spike to the immediate left being the jet shock. Slices of density and pressure along the jet axis in Figure 3.2a show enhancements in those parameters at the jet head. A relationship between Figure 3.1a and the density of 3.2a is not immediately visible, but a series of slices through the grid parallel to the jet axis would give results consistent with the greyscale image.

3.1.2. *Addition Of Cooling–Simulation B*

Figure 3.1b shows the density profile of a jet with cooling added, from Model B. Cooling has the effect of making the bow shock narrower, and a higher density is

a) Model A



b) Model B



Fig. 3.1.— Logarithmic Density Images for Simulations A and B. The cooling in Model B results in a narrower outflow that reaches further. The grid dimensions for all figures are 240×120 zones. The physical dimension in units of jet radius are 60×30 unless otherwise specified. Dark regions have low density; brighter regions are denser. The greyscale varies logarithmically with dimensionless ZEUS3D values ranging from 0.01 to 100.0, with the unperturbed ambient density at 1.0 for reference.

observed at the head of the jet, much like the plug of material seen by de Gouveia Dal Pino & Benz (1994) and by Masson & Chernin (1993), who also found the bow shock structure to be considerably narrower. These effects help give rise to a higher degree of collimation. Accordingly, cooling jets also go farther in the same amount of computing time, since mass flux must be conserved.

3.1.3. Addition Of Variability (No Cooling)-Simulation C

Figure 3.3a shows a density image of a simulation where the velocity of a non-cooling jet is varied at its origin. A chain of dense knots is observed along the jet axis, each one accompanied by a bow shock which increases the degree of entrainment occurring along the jet. In addition, the parabolic shape of the leading bow shock is distorted by the later inner shocks. With a Mach number of 15, we do not expect to see a high degree of steady-state entrainment along the sides of the jet (Chernin *et al.* 1994), since a majority of the entrainment occurs at the leading bow shock. However, a series of nested bow shocks such as those produced by a variable jet will certainly disrupt the ambient gas in a manner that could fall under the definition of steady-state entrainment given by Chernin *et al.* (1994). Interaction between the jet and the environment at the leading bow shock is seen in all of the simulations.

Figure 3.2b displays the density, pressure, and $\nabla \cdot \mathbf{v}$ for the simulated variable jet, and numerous differences with Figure 3.2a are immediately evident, all of which can be attributed to the variability of the velocity of the jet. The many peaks in density and pressure are coincident with the positions of the knots on the jet axis, and the velocity divergence also decreases at each working surface, though the spikes

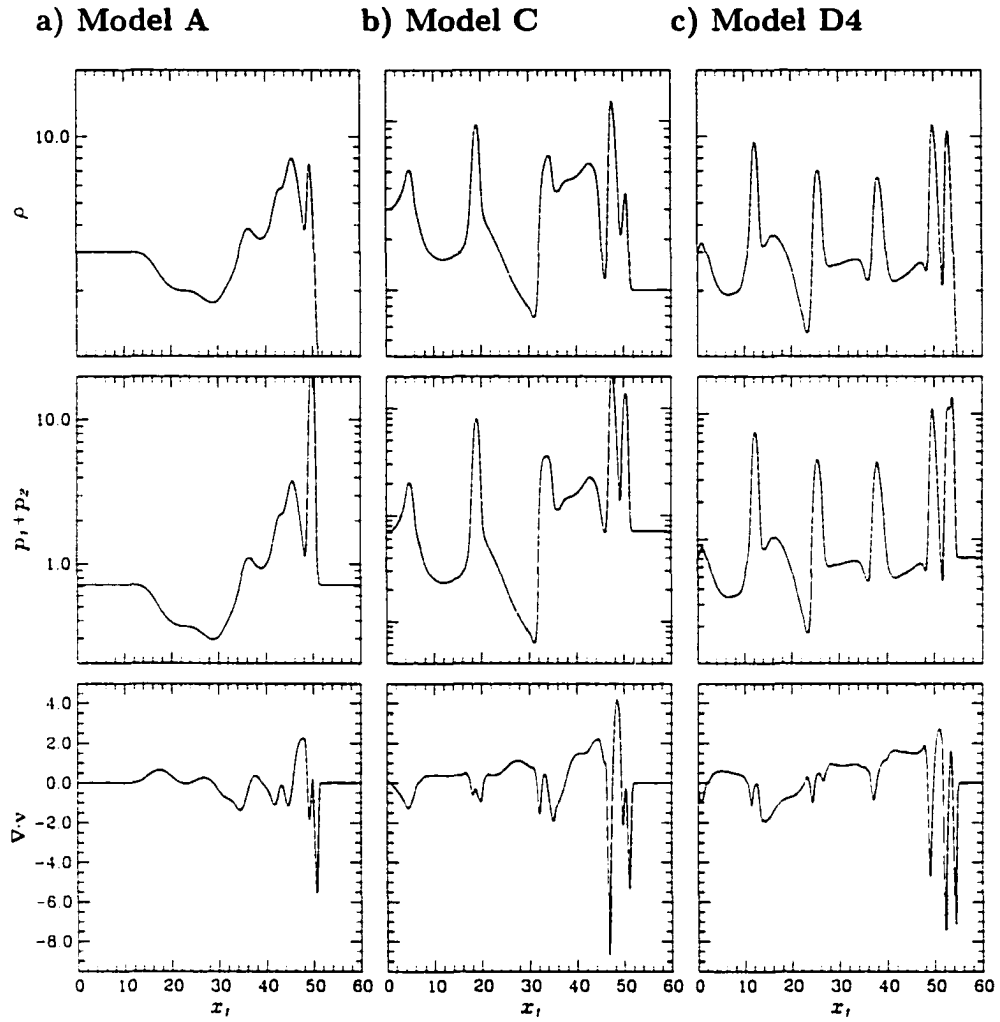


Fig. 3.2.— One-Dimensional Plots of Density, Jet Pressure and Velocity Divergence for Models A, C, and D4, along the jet axis. All are Mach 15 jets with $\eta = 3$.

are not always so narrow. At the jet head an interesting “triple-shock” feature is seen, which is interpreted as the first internal shock having caught up with the leading bow shock.

a) Model C



b) Model D4

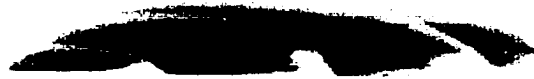


Fig. 3.3.— Logarithmic Density Images for Simulations C and D4. Again, the cooling model is narrower and has progressed further. The greyscale is the same as in Figure 3.1.

3.1.4. *Cooling And Variability—Simulation D*

Combined variable and cooling jets illustrate two important processes at work. Model D, which includes both cooling and variability, includes a number of simulations designed to investigate the effects of different initial conditions, and

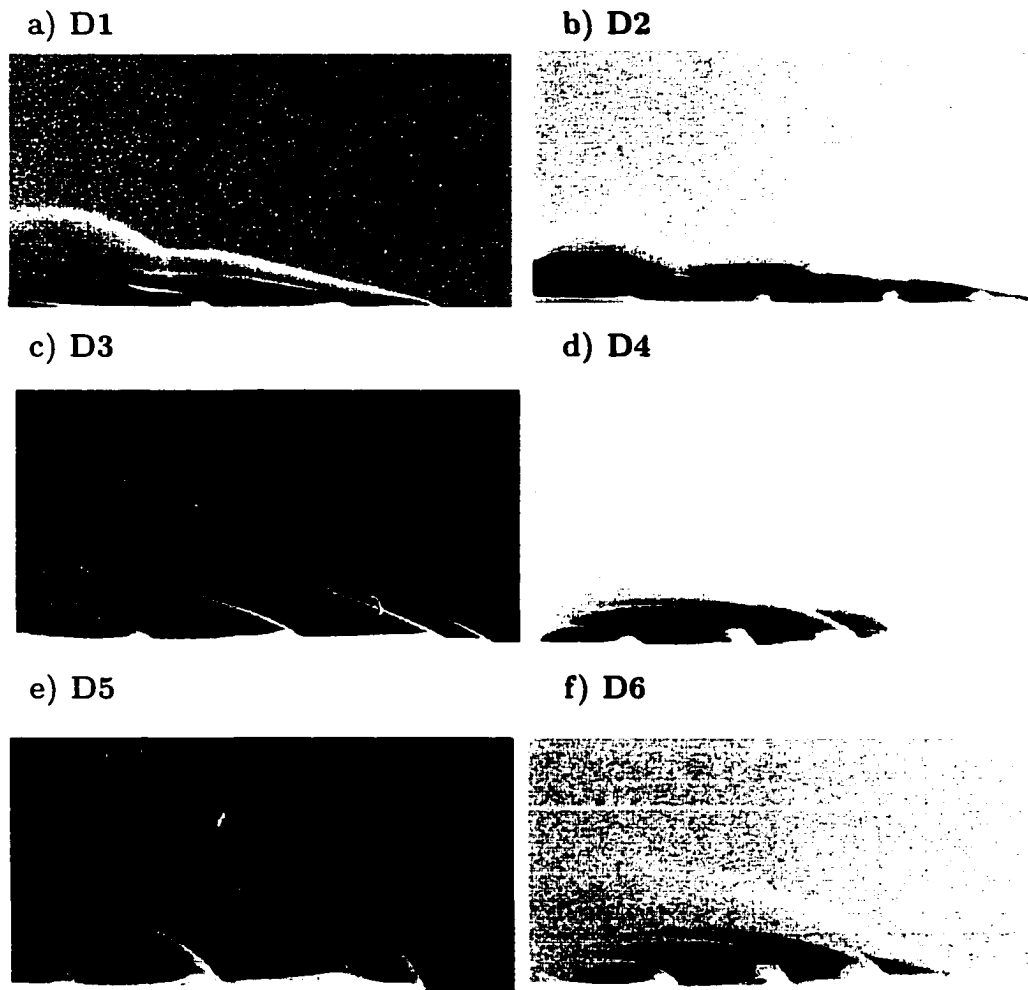


Fig. 3.4.— Logarithmic Density Images for Simulation D. Greyscale ranges are as given in Figure 3.1. Parameters are found in Table 3.

these separate cases are tabulated in Table 3. The Mach number and η were varied to study the effect of changing the initial conditions.

In a given simulation, the initial conditions are not preserved along the jet. Rather, the Mach number and density ratio will change as a result of the cooling

Initial (i) and Effective (s) Values of M and η				
Model	η_i	M_i	η_s	M_s
D1	0.5	5.0	5.1	18.4
D2	0.5	15.0	3.5	16.9
D3	3.0	5.0	25.0	12.2
D4	3.0	15.0	3.0	15.0
D5	10.0	5.0	20.0	6.0
D6	10.0	15.0	10.0	15.0

Table 3: Initial and Effective Parameters For Simulation D Runs

and dynamics occurring in the simulation. Table 3 shows how these parameters change along the jet axis. To arrive at the effective values η_s and M_s , averages were calculated at the end of the simulation (corresponding to the point where the physical length of the optical emission in DG Tau B is achieved) along the jet axis with the following prescriptions:

$$\eta_s = \frac{\langle \rho_{jet} \rangle}{\langle \rho_{ambient} \rangle} \quad (3.1)$$

$$M_s = \frac{\langle v_{jet} \rangle}{\langle c_{jet} \rangle} \quad (3.2)$$

where

$$c_{jet} = \sqrt{\frac{\gamma P_{jet}}{\rho_{jet}}} \quad (3.3)$$

is the jet sound speed. Twenty evenly-spaced points along the jet axis were chosen in determining the effective values for the variable cooling jets. A stright integration would include the peaks and possibly corrupt the data. In determining M_s , we

calculate an average jet velocity ($\langle v_{jet} \rangle$) which corresponds to the “flow” velocity in the work of Eislöffel & Mundt (1998). A ratio of M_s to M therefore gives the ratio of $\langle v_{jet} \rangle$ to $v_{jet,inlet}$. By comparing this flow velocity to the speed of individual knots, it was found that the knots generally tended to travel between 0.75 and 1.10 times the average jet speed. The sinusoidal variation (of about 10%) in the ejection velocity obviously had some effect on this result, but adopting a mean value of about 0.9 for ζ , the ratio of knot speed to jet speed, falls within the range of 0.5 to 1.0 which was found by Eislöffel and Mundt (1998).

Figure 3.4 shows density images of all six D simulations and the resulting shapes of the outflows. The effects of cooling appear to affect the ultimate morphology of some jets more than others, depending on their initial conditions. In Simulation D1, for example, the density ratio along the jet axis rose by a factor of ten, while the effective Mach number more than tripled. These variations in M and η can be explained by the effects of cooling in the models; models with a low initial Mach number have a higher temperature, which causes the fluid to cool rapidly. This fast cooling compresses the jet material and along the axis the fluid is able to flow out faster, as a result of the decrease in cross-sectional area and corresponding increase in pressure. Similarly, the compression of the fluid towards the jet axis will increase the effective value of η , the ratio of jet-to-ambient density. However, it appears that initially overdense jets are less susceptible to this dramatic increase in M and η . This may be attributable to the larger momentum that is present in a denser jet. This may be explained since a denser jet behaves more isothermally and is therefore more rigid than an underdense jet. The effective values of these two parameters stay essentially constant for models D4 and D6, while their Mach 5 counterparts undergo a mild increase in η and M . In summary, it appears that the low-density,

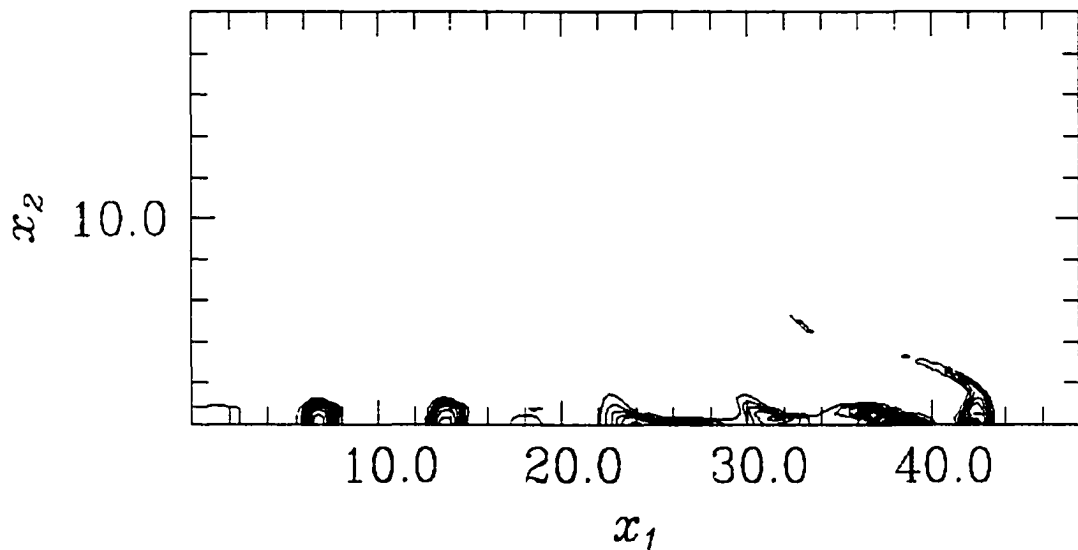


Fig. 3.5.— Two-Dimensional Contour Plot of Predicted Oxygen Emission for an early Simulation D4, with dimensions of 48×20 jet radii and different variability parameters.

low-Mach number jet is the most pliable and that the cooling of the fluid in this region of parameter space has the greatest change in its initial conditions. Similar Mach number jets with higher densities are less compressed into the jet axis, as are Mach 15 jets since the cooling is not as large.

3.2. Creation Of Emission Maps

Emission caused by several atomic species and molecular CO can be simulated using the arguments made in the previous chapter. A major *caveat* is that these are two-dimensional simulations and thus plain emissivity maps do not give a true representation of the total emission integrated along the lines of sight through the simulations, unless the angle of inclination for the object is zero.

For the simulations in which cooling was included, two-dimensional contour diagrams and pixelated greyscale images of the emission features were created in addition to those images created for the non-cooling jets. For illustrative purposes, the predicted [O I] emissivity contour diagram is shown in Figure 3.5 for Model D4, showing the chain of knots along the jet axis. As mentioned previously, the spatial correlation between [O I] and [S II] emission allows us to interpret the emission from neutral oxygen as a tracer of the sulphur emission seen in jets such as DG Tau B.

A greyscale image of predicted CO emission is seen in Figure 3.6, for model D3. The image shows the low-velocity ambient gas entrained by the working surfaces of the outflow. It is seen how bow shocks are able to disturb the gas to a considerable distance from the jet axis.

Observationally, CO images are obtained by limiting the range of velocities along the line of sight. In a cylindrically symmetric simulation in which the fluid is not rotating about the symmetry axis, such as those performed in this work, there are just two velocity components. These are the *axial* (v_1) and *radial* (v_2) components which are respectively parallel and perpendicular to the symmetry axis of the simulation. If one were to consider the calculation plane to be in the plane of the sky, then clearly v_1 will always be perpendicular to the line of sight, even after



Fig. 3.6.— Two-Dimensional Greyscale Image of Predicted CO Emission for Model D3. This image plots emissivity for molecular gas in the velocity range between 0.5 and 5.0 km s^{-1} , where low rotational energy states of CO can be excited.

rotating the simulation plane about the symmetry axis, and thus does not contribute to the CO emission.

On the other hand, spinning the simulation about its symmetry axis will bring v_2 along the line of sight in a non-uniform way. For example, near the periphery of the CO emission region, v_2 remains tangential to the line of sight, and thus in the simulations, should not contribute to the CO emission. Already we see a problem with the assumption of 2-D axisymmetry. In nature, the motion of the gas is fully

3-D and likely turbulent, and at the periphery of the CO emission region, there should be a sizable component of the velocity along the line of sight. Thus, 2-D axisymmetric simulations are apt to underestimate the brightness near the periphery of the CO emission region. Proceeding now to lines of sight through the jet axis, a component of v_2 will be parallel to the line of sight all the way through the emission region, rendering a high CO brightness in the centre of the CO emission region. However, post-shock dissociation of CO, which would tend to reduce the CO brightness, has not been accounted for in these simulations. Further, the true 3-D nature of the gas motion will tend to reduce the effective velocity component along lines of sight through the jet axis. Thus, these 2-D axisymmetric simulations are apt to overestimate the CO brightness in the interior of the CO emission region.

Taken together, these 2-D effects and the lack of CO dissociation will yield images more centre-brightened than they might be if the simulations were fully three dimensional, and included a broader suite of physics. This facet will become important when we attempt to make detailed comparisons of the simulations with DG Tau B in the next section.

3.3. Comparison To DG Tau B

Now that the main types of simulations have been described, an attempt to identify features in the observational images of DG Tau B with features seen in the simulations will be made. Pixelated greyscale images of the density, velocity divergence, and predicted $[\text{O I}]$ (acting as a surrogate for $[\text{S II}]$) and CO emission for Simulation D5 are shown in Figures 3.7 and 3.8. We compare these images with the optical and radio observations in an attempt to identify features in the model

that correspond to physical characteristics of the jet. Although the Mach number and density ratio in Simulation D5 are not the closest match to DG Tau B, the widely-spaced features of D5 offer an opportunity for comparisons not offered by the other jet simulations.

3.3.1. Kinematical Features of the Outflow

The success of creating an episodic outflow, with the generation of internal working surfaces and nested bow shocks, is the basis for the kinematical comparisons made between the simulations and DG Tau B. The internal dynamics of the cooling, variable jet gives rise to interesting features near the jet axis as well as far into the extended envelope of the leading bow shock.

A feature often seen in numerical simulations is the entrainment of the ambient gas into a region behind the leading bow shock. As the bow shock of a supersonic jet passes through the ambient gas, the ambient gas is accelerated toward the bow shock and largely away from the jet axis. We have described this mechanism as “prompt entrainment”. In addition, some of the ambient gas very close to the working surface of the jet is engulfed by the shocked jet material, and thereby carried away in a “steady-state entrainment” process.

Looking to Figure 3.7a, we see several clumps of high-density material along the jet. The clumps are sites where most of the cooling takes place, which the atomic emissivity image confirms. We identify these clumps with the knots of optical emission that are known as Herbig-Haro objects. The density profiles behind the bow shocks are also interesting, since the dense shocks are followed by a region of very low density before the ambient gas is entrained into this space. Looking back

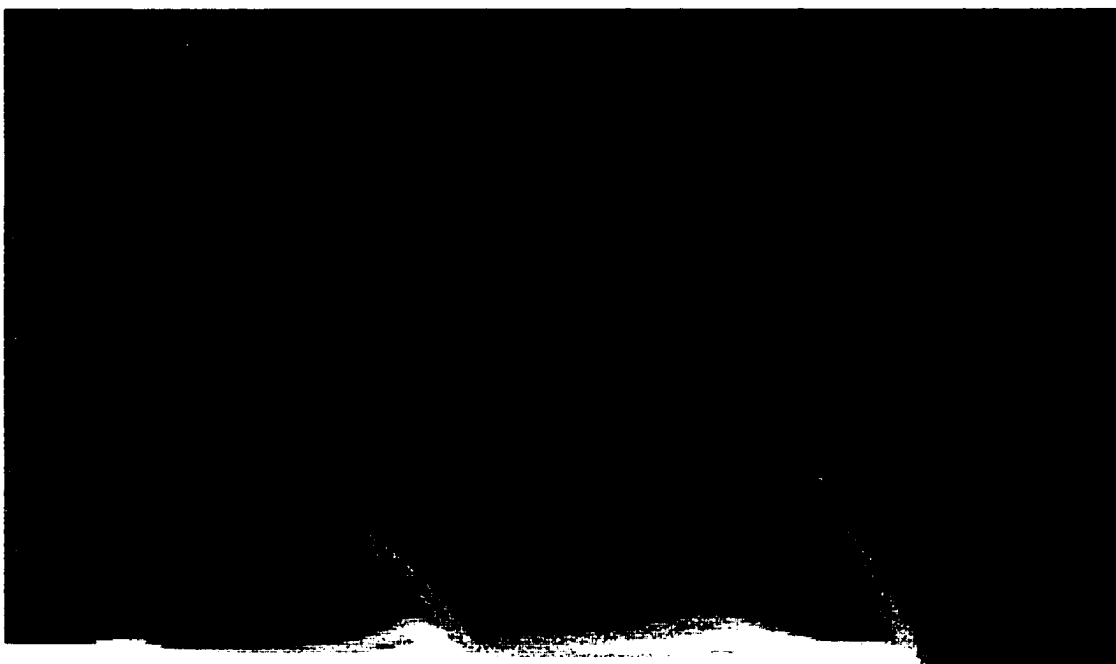
to Figure 3.4, it is seen that the higher- M jets exhibit post-shock regions that are much more evacuated than the lower- M jets. The stronger shocks are more efficient in sweeping up the material through which they have passed.

The density images in this thesis show the total mass density of both the jet and the ambient medium. Ideally, one would prefer to visualise the behaviour of the entrained ambient gas independently from the kinematics of the atomic jet. There are several variables in the ZEUS3D code which specifically trace the ambient fluid, including the pressure and energy density (called $p2$ and $e2$ respectively). An animation of about 50 images of the ambient energy density over the evolution of the jet was found to provide a very useful method of visualising the entrainment process.

In Section 3.1.4 we briefly discussed the kinematic behaviour of the knots in the simulations, finding that some internal working surfaces travel at speeds around 100% of the jet speed, with others around 75%. Eislöffel & Mundt (1998) found a nearly bimodal distribution of knots speeds, some around 50% and others close to 100% of the flow velocity, and the rest around 67%. The small number of knots in DG Tau B suggests this distribution could be vastly different for a more evolved outflow, but the finding that the knot speeds and bulk jet speed are comparable in the simulations as well as in nature gives credence to the simulations.

Images of the velocity divergence term $\nabla \cdot \mathbf{v}$, as illustrated in Figure 3.7b, help us understand the shock structure, both close to the jet and far away from it. The coincidence of negative velocity divergence with the off-axis regions of enhanced density is further evidence of nested bow shocks giving rise to new sites of entrainment in a stellar outflow. The profound influence of working surfaces created by these nested bow shocks on the environment of a stellar jet has been demonstrated, and sets the stage for the model we develop for DG Tau B below.

a) Density (Logarithmic Scale)



b) Velocity Divergence (Linear Scale)



Fig. 3.7.— Density and Velocity Divergence Images For Simulation D5.
Dark regions in 3.7*b* show strong shock activity.

a) O I Emissivity



b) CO Emission

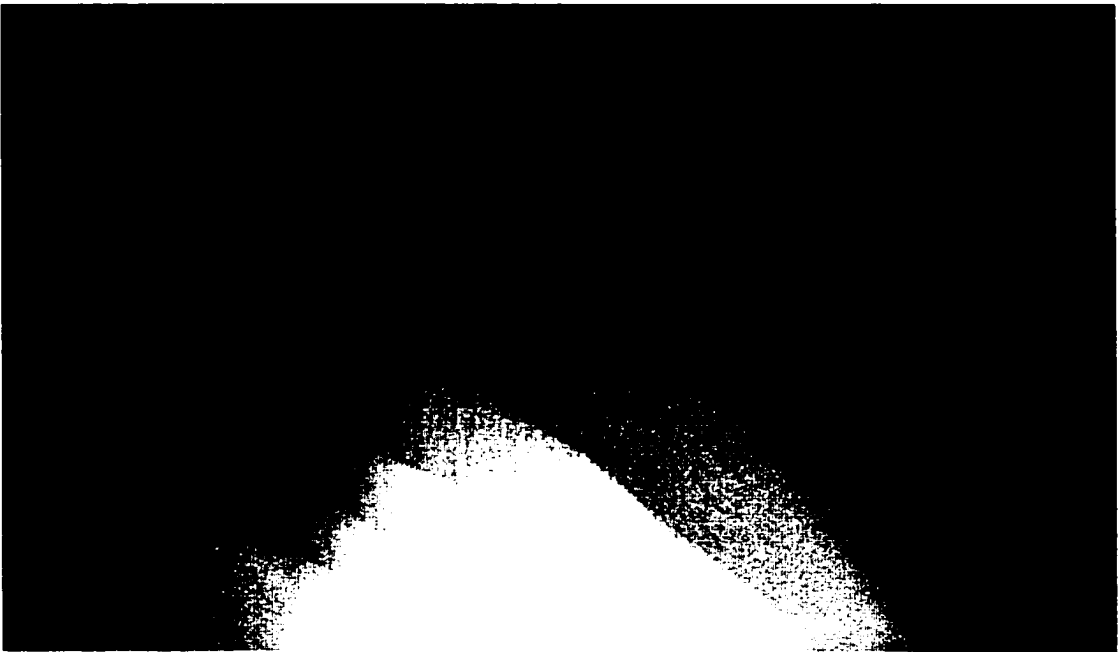


Fig. 3.8.— Logarithmic O I and CO Emissivity Images for Simulation D5.

Observationally, these kinematic features are not the most direct quantities that can be measured. The velocities and densities of the material under investigation can only be inferred by looking at the radiation given off by the astronomical object. For this reason, we must also consider the *emission* from the source. A large portion of the code development for this thesis is related to the simulation of emissivities of the atomic species involved in cooling the jet, as well as the possible molecular emission that is provoked by the stellar jet. A successful model should be able to reproduce the emission features in addition to the kinematic properties we have just described.

3.3.2. *Emission Features in the Outflow*

The [S II] emission seen in DG Tau B from optical observations (see Figures 1.3 and 1.4) is characterised as a linear chain of knots emanating from the protostar. The working surfaces and nested bow shocks are key components in the simulation of observable atomic and molecular emission. In Figure 3.8a we see the simulated [O I] emissivity from Simulation D5, which allows us to infer the [S II] emissivity expected from the outflow, a quantity often of importance in optical spectral studies of outflows. As with the density images described above, maximum emission of these ions occurs at the site of the working surfaces within the jet beam. Since we have coupled the emissivity to the cooling from neutral oxygen atoms, it seems reasonable that the maximum emission would coincide with the regions of high density, since the cooling depends on the number density of the gas that is present. The atomic emission should not stray far from the jet axis, and indeed the emissivity images show that the atomic jet is well-collimated.

The degree of collimation in the jet can be expressed quantitatively as the aspect ratio, the ratio of the jet length to its width. From Table 1 in Chapter 2, the aspect ratio for DG Tau B is about 45. The jet width was taken as the extent of the [S II] emission away from the jet axis, and we shall do the same for our simulated jets. We arrive at a range of values for the aspect ratio of between 30 and 55. The large uncertainty in this number is completely tied to the small values of the jet width, whereas the length of the jet is a much more certain value. The width of the jet is not a well-defined physical parameter, and so the aspect ratio must be considered to be a fairly coarse measurement when characterising a jet with observational data. For example, the deconvolved [S II] image of DG Tau B seen as part of Figure 1.4 is taken from Mundt *et al.* (1991), yet an image that has not been deconvolved appears in Eislöffel and Mundt (1995) which is about twice as wide. The knots in the jet cause the atomic outflow to widen considerably, in both the simulations and the optical images. Regardless, the fact that the aspect ratios of the simulations is comparable to that of DG Tau B is one indication that the simulations have been sufficiently evolved for a meaningful comparison with DG Tau B.

Figure 3.8*b* shows the emissivity from CO gas for Simulation D5 using the method previously described. The broad shocks given by this low-Mach jet provide a very convenient manner in which the CO gas can be entrained along the jet boundary in successive “bursts,” giving the emissivity image its characteristic appearance. The entrained ambient gas emits both close to and away from the jet axis, which is also the behaviour seen with the $J = 1 - 0$ observations. The nested bow shocks readily disturb the molecular gas, and as this ambient material expands, the centre region gradually decreases in (molecular) density. Dissociation of CO may accelerate this evacuation of molecular gas along the jet axis, and thus telescope observations

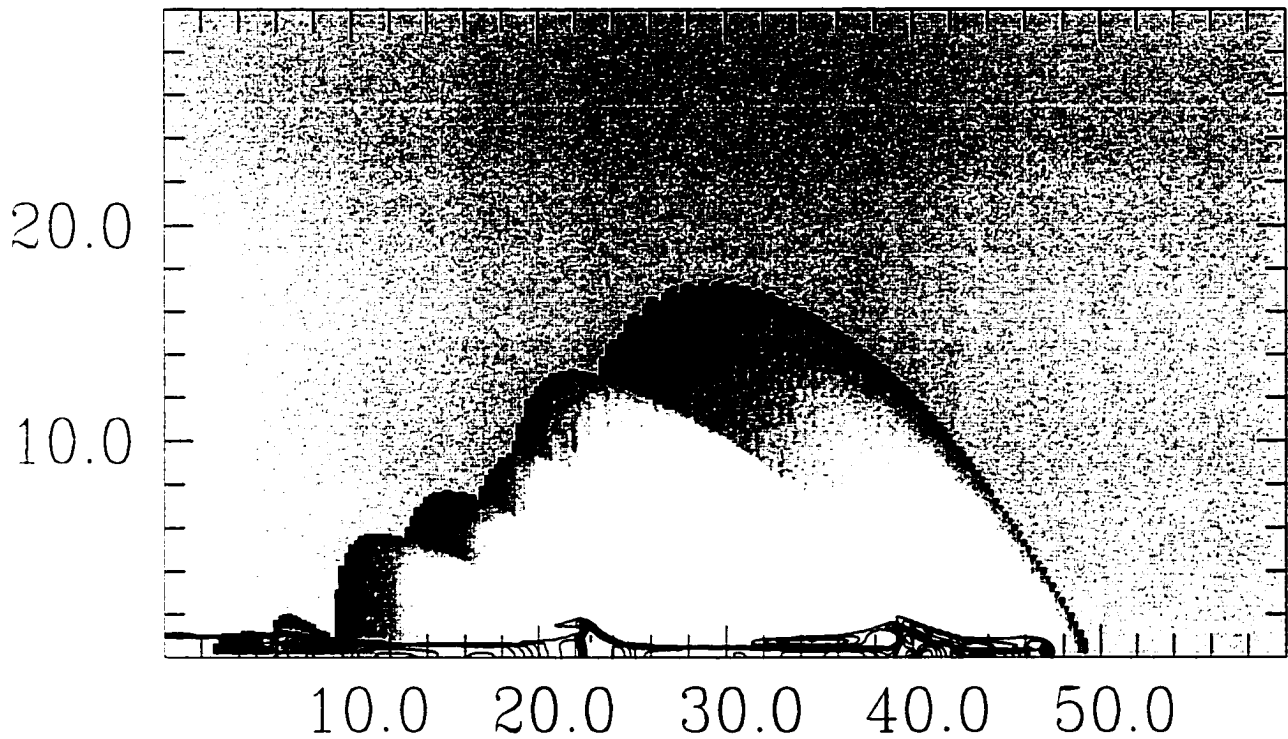


Fig. 3.9.— A Contour Image of Simulated O_I Emissivity Superimposed upon a Greyscale Image of the Ambient Gas for Simulation D5. The unperturbed CO has been artificially brightened.

will see DG Tau B as an edge-brightened source with reduced emission along the jet outlined by the atomic emission. With increased sensitivity one could detect more of this central CO emission, provided any interior extended emission is not resolved out, but the brighter edges give the appearance that the CO emission bifurcates from the axis. The tendency for these simulations to be more centre-brightened than edge-brightened has been discussed, and a challenge for future work will be to resolve this issue.

Figure 3.9 combines the two images seen in Figure 3.8. It shows the direct

correspondence between the atomic jet working surfaces and the broadening of the excited ambient material from the nested bow shocks associated with these working surfaces. In comparison to DG Tau B, we see that in both cases a knot in the jet gives rise to a broadening of the molecular gas in the region behind it and away from the jet beam. The lack of a bow shock in DG Tau B does not pose a serious problem with our model since the effect of the leading bow shock in the simulation is not different from the behaviour seen by later shocks. In fact the lack of short spacings in the interferometric observations of CO in DG Tau B means that larger-scale structure is not seen, so perhaps increased sensitivity in telescopes will be able to delineate a bow shock feature in the future.

These two-dimensional images make an attempt to account for the total integrated intensity that is observed in the radio observations, but the simulation does not consider the obscuration of observations caused by inclination geometries. For these reasons, the emission predictions made here are only the first step towards more realistic “numerical observations.” The CO emissivity estimates are somewhat more physical than the atomic species since we have attempted to simulate an integration through the line of sight rather than calculating the emissivity on the two-dimensional grid.

The aspect ratio of the molecular outflow is largely dependent on the initial values of M and η , and the notable broadening of the outflow as a result of the bow shock and successive internal shocks give ratios in the range of 1 to 3. A visual inspection of Figures 1.3 and 1.4 implies that the length-to-width ratio of DG Tau B is indeed around 2, illustrating the lack of collimation in the molecular flow when compared to the atomic jet. As with the atomic jets, the outflow width is somewhat difficult to define since the region of the ambient medium that is dynamically

important is shaped quite irregularly. As a result of the interaction of the bow shock and internal shocks with the molecular environment, our estimate of the width of the outflow is an average of widths along the jet axis.

This model of DG Tau B, that of a partially ionised atomic stellar jet with episodic outbursts of material that drive a molecular outflow, is considerably successful in outlining main features seen in Figure 1.4. The atomic emission seen in DG Tau B is a linear chain of knots that extend along the jet axis. Figures 3.5 and 3.8*a* show the simulated counterpart to this structure, a cooling jet of atomic gas emanating from the source. The effect of this cooling jet on the surrounding molecular gas is seen in the images of predicted ambient emission, such as in Figure 3.8*b*. Of course, a non-cooling jet can also give rise to a perturbed ambient medium which would have a morphology defined by the structure of the working surfaces in the jet.

Given the simplicity of the code that was developed to simulate these features, it is entirely feasible that further work would enable the modelling of DG Tau B and other young stellar outflows to predict more accurately the physical quantities (*eg.*, η and M) related to these objects.

3.4. Conclusion And Suggestions For Further Refinement

In summary, we have made comparisons of DG Tau B with cooling variable jets whose input parameters (Mach number and density ratio) are generally accepted to characterise stellar jets. However, it has been demonstrated that the input parameters do not necessarily characterise the cooling jets at a later time, since jets with low-Mach number near the source may evolve into the higher-Mach number jets

further out.

The main achievements of this thesis include the incorporation of published cooling rates from several atomic species into the ZEUS3D code, to allow simulations where radiative cooling in the jet can be accurately predicted. In addition, the code was modified to allow investigations of episodic bursts, thought to explain many H-H objects, and the effects of a cooling stellar jet on its environment. The attempt to produce an image of a three-dimensional CO emissivity prediction from a two-dimensional simulation was a significant demonstration of the capabilities and adaptability of the ZEUS3D code. The simulations of a stellar jet with different initial values of M and η gave an insight to the effects of these quantities on the morphology of the resulting outflow. We found that the degree of collimation in both the atomic and molecular components of the simulated jet was similar to that found in the objects themselves, with the aspect ratios in agreement with those observed for DG Tau B.

As D5 is the model which best reproduces the morphological features of DG Tau B, we are led to conclude DG Tau B is characterised by a Mach 6 outflow with a density ratio of approximately 20 (Table 3). However, observational estimates of the Mach number are in excess of 10 (Mundt 1986), and probably closer to 15, suggesting that any one of the other D models may be more appropriate. However, these other models exhibit rather narrow bow shocks and are clearly out of sorts morphologically with what is observed. We are therefore led to the conclusion that the observations and simulations are in conflict. Either observational estimates of the Mach number are too high (seems unlikely), or the numerical simulations are lacking in one or more important physical details (probably). The need for short-spacing information in molecular observations will address whether the CO in DG Tau B is

more centre-filled than it appears in current observations. Possible extensions to the model that may help resolve this discrepancy are described below.

Density Gradients. As reported in Mundt (1986), observations of molecular gas show steep density gradients with respect to the distance from the central object, r , of the form $\rho(r) \sim r^{-\alpha}$, with α ranging from 2 to 3. The environment around DG Tau B seems to be quite non-uniform, with Mitchell *et al.* reporting the discovery of a small clump of gas surrounding the protostar, possibly a source of entrained gas (MSM97). Future models may include the use of a stratified ambient medium, much like that of de Gouveia dal Pino *et al.* (1996). It would be instructive to see the effect of a density gradient on the stellar jet. With an ambient density that decreases away from the source, the apparent separation of the CO gas may be more prominent. Indeed, Hardee *et al.* (1992) find that with a sharp density gradient, high M jets have broader bow shocks, suggesting at least part of the solution to the conflict between observations and the present simulations outlined above.

Magnetic Fields. Magnetic fields play a dynamically important role in many theories concerning the transport of matter in the vicinity of Young Stellar Outflows. It is often assumed that the magnetic pressure is much less than the thermal or ram pressure in the outflow, and can thus be ignored as being insignificant (Draine 1980). However, even in cases where $B^2/8\pi \ll \rho v_s^2$, magnetohydrodynamic simulations can exhibit significantly different properties than pure hydrodynamic outflows (Frank & Mellema 1997, to name just one).

Treatment of Ionisation in Shock Regions. The approximation of a constant ionisation fraction over most of the jet is believed to be quite reasonable (Bacciotti *et al.* 1995), and is thought to be a result of non-equilibrium processes occurring near the protostar. However, in the leading bow shock and in the internal working

surfaces that follow, the increase in energy and pressure for these regions is sure to accelerate the cooling that occurs there. An attempt to trace the ionisation and recombination rates for the coolants in the jet would allow for a more thorough investigation of these working surfaces as the dynamically important structures that they are.

Emissivities. Similar to the ionisation treatment, simple analytic approximations or substitutions for emissivities of important dynamic species can be replaced by full population level calculations that would allow the atomic and molecular emission to be studied in greater detail. The progress being made with “numerical spectroscopy” and similar techniques to create synthetic line profiles from simulations (Smith *et al.* 1997b, for example) can provide additional ways of comparing theoretical models with the observed emission features seen in Young Stellar Outflows.

Added Dimensions. An axisymmetric model is a useful tool in identifying the bulk properties in a simulation and matching them to observational data. However, two-dimensional models are limited in their ability to predict properties that are almost always three-dimensional in nature, such as the atomic and molecular emission measured from these outflows. To approximate the total line-of-sight integrated intensity of the CO emission in our simulations, it was necessary to (virtually) rotate the two-dimensional grid about the axis of the jet, so as to recreate the cylindrical geometry of the Herbig-Haro object and molecular outflow. Intensity maps of the three-dimensional distribution of atomic and molecular gas would very likely have a better chance of recreating the morphologies seen in Young Stellar Outflows. In addition, a fully three-dimensional model could be oriented with different inclination geometries in an effort to simulate the radial and tangential components of outflows with varying degrees of inclination.

In addition to the above, a more thorough study of many of the jet parameters can be performed in order to learn about other Young Stellar Outflows. For example, even though the spacings between knots for this model did not directly correspond to those of DG Tau B, we demonstrated the ability to create knots with different velocities and spacings. Further modifications of the variable velocity subroutine can allow us to perform models which are closer matches to what is observed phenomenologically.

APPENDIX

Herein are the subroutines written to be appended to the ZEUS3D FORTRAN code, with a brief description of what each routine does.

The first subroutine, CKEVINIT, is necessary to declare the variables for both variable and cooling jets. Also the cooling rate tables from Raga *et al.* (1997), ya1 through ya8, are declared. The variables `arr1a` and `arr2a` are the logarithmic values of electron density and temperature, respectively, for which the cooling tables are useful. Lines which begin with an asterisk are precompiler commands which are used in creating the working form of the ZEUS3D FORTRAN code. More detail on this precompilation process is given in the ZEUS3D manual.

```
*insert zeus3d.9999
*deck ckevinit
C=====
C
C           B E G I N   S U B R O U T I N E
C           C K E V I N I T
C=====
C
C           subroutine ckevinit
C
C           kad:zeus3d.ckevinit <----- pressure work plus cooling
C                                   August, 1997
C
C           written by: Kevin Douglas, December 1997
C
C           PURPOSE: This routine declares parameters like abundances and
C           ionisation fractions for the cooling routine performed in kevcool.
C           As well, settings are available for a variable-velocity jet
C           with velocity
C            $v = v_o (1 + \text{ampjet} \cdot \sin(\text{frqjet} \cdot \text{prtime}) \cdot \cos(\text{frqamp} \cdot \text{prtime}))$ 
C           Data tables with cooling rates are also defined.
C
C           INPUT VARIABLES:
C
C           OUTPUT VARIABLES:
```



```

1 , -24.044, -24.044, -24.044, -24.044, -24.044, -24.044
1 , -24.044, -24.044, -24.044, -24.044, -24.044, -24.044, -24.044
1 /
c TABLE ya3 is for CI cooling
  data ((ya3(rowan,hema), rowan=1,13), hema=1,14) /
1 -23.663, -23.672, -23.700, -23.774, -23.932, -24.170
1 , -24.448, -24.780, -25.190, -25.654, -26.142, -26.638, -27.137
1 , -23.560, -23.572, -23.609, -23.705, -23.899, -24.176
1 , -24.473, -24.795, -25.188, -25.643, -26.126, -26.621, -27.119
1 , -23.458, -23.474, -23.521, -23.641, -23.873, -24.189
1 , -24.512, -24.830, -25.200, -25.639, -26.116, -26.609, -27.106
1 , -23.358, -23.379, -23.438, -23.583, -23.851, -24.205
1 , -24.561, -24.884, -25.230, -25.646, -26.112, -26.600, -27.097
1 , -23.261, -23.287, -23.360, -23.532, -23.832, -24.220
1 , -24.611, -24.955, -25.284, -25.668, -26.115, -26.596, -27.090
1 , -23.167, -23.199, -23.287, -23.486, -23.816, -24.229
1 , -24.655, -25.035, -25.364, -25.713, -26.131, -26.597, -27.086
1 , -23.076, -23.116, -23.221, -23.445, -23.800, -24.234
1 , -24.687, -25.109, -25.467, -25.794, -26.168, -26.609, -27.087
1 , -22.990, -23.038, -23.160, -23.411, -23.787, -24.235
1 , -24.706, -25.163, -25.569, -25.909, -26.244, -26.640, -27.095
1 , -22.909, -22.966, -23.107, -23.381, -23.775, -24.234
1 , -24.715, -25.194, -25.645, -26.037, -26.368, -26.712, -27.123
1 , -22.834, -22.900, -23.061, -23.357, -23.765, -24.231
1 , -24.718, -25.208, -25.687, -26.132, -26.514, -26.842, -27.193
1 , -22.765, -22.842, -23.021, -23.337, -23.757, -24.227
1 , -24.712, -25.193, -25.650, -26.071, -26.468, -26.851, -27.215
1 , -22.157, -22.246, -22.427, -22.722, -23.118, -23.571
1 , -24.034, -24.466, -24.831, -25.149, -25.502, -25.926, -26.396
1 , -22.032, -22.142, -22.350, -22.667, -23.059, -23.449
1 , -23.758, -23.952, -24.090, -24.273, -24.575, -24.985, -25.451
1 , -21.904, -22.030, -22.248, -22.541, -22.830, -23.027
1 , -23.128, -23.187, -23.270, -23.443, -23.750, -24.164, -24.632
1 /
  data ((ya3(rowan,hema), rowan=1,13), hema=15, 28) /
1 -21.749, -21.870, -22.052, -22.244, -22.375, -22.438
1 , -22.469, -22.504, -22.584, -22.766, -23.084, -23.503, -23.965
1 , -21.532, -21.622, -21.734, -21.825, -21.873, -21.894
1 , -21.911, -21.943, -22.029, -22.222, -22.549, -22.964, -23.402
1 , -21.259, -21.313, -21.370, -21.409, -21.428, -21.438
1 , -21.451, -21.486, -21.579, -21.783, -22.112, -22.509, -22.887
1 , -20.968, -20.997, -21.026, -21.043, -21.052, -21.059
1 , -21.073, -21.110, -21.210, -21.422, -21.745, -22.098, -22.387
1 , -20.691, -20.707, -20.721, -20.730, -20.735, -20.741
1 , -20.755, -20.797, -20.903, -21.118, -21.419, -21.706, -21.904
1 , -20.438, -20.446, -20.454, -20.459, -20.463, -20.468
1 , -20.484, -20.528, -20.640, -20.851, -21.115, -21.330, -21.458
1 , -20.208, -20.213, -20.217, -20.221, -20.223, -20.229
1 , -20.246, -20.294, -20.409, -20.609, -20.829, -20.982, -21.066
1 , -20.000, -20.003, -20.006, -20.008, -20.010, -20.016
1 , -20.035, -20.085, -20.202, -20.387, -20.566, -20.675, -20.733

```

```

1 , -19.812, -19.814, -19.816, -19.817, -19.820, -19.827
1 , -19.846, -19.900, -20.018, -20.187, -20.333, -20.414, -20.456
1 , -19.645, -19.646, -19.647, -19.649, -19.651, -19.659
1 , -19.680, -19.738, -19.856, -20.013, -20.134, -20.196, -20.230
1 , -19.497, -19.498, -19.499, -19.500, -19.503, -19.511
1 , -19.535, -19.597, -19.718, -19.863, -19.966, -20.017, -20.045
1 , -19.369, -19.369, -19.370, -19.371, -19.374, -19.383
1 , -19.410, -19.477, -19.600, -19.737, -19.828, -19.870, -19.895
1 , -19.257, -19.257, -19.258, -19.259, -19.263, -19.273
1 , -19.302, -19.375, -19.501, -19.632, -19.713, -19.750, -19.773
1 , -19.159, -19.160, -19.160, -19.162, -19.166, -19.177
1 , -19.211, -19.289, -19.419, -19.545, -19.618, -19.652, -19.673
1 /

```

```

data ((ya3(rowan,hema), rowan=1,13), hema=29, 41) /

```

```

1 -19.074, -19.075, -19.076, -19.077, -19.082, -19.095
1 , -19.132, -19.217, -19.350, -19.472, -19.540, -19.570, -19.591
1 , -19.000, -19.000, -19.000, -19.003, -19.008, -19.023
1 , -19.064, -19.157, -19.293, -19.411, -19.474, -19.503, -19.523
1 , -18.934, -18.934, -18.935, -18.937, -18.942, -18.959
1 , -19.005, -19.105, -19.245, -19.360, -19.419, -19.446, -19.466
1 , -18.874, -18.874, -18.875, -18.878, -18.884, -18.903
1 , -18.954, -19.061, -19.205, -19.316, -19.372, -19.397, -19.417
1 , -18.820, -18.820, -18.821, -18.824, -18.831, -18.852
1 , -18.909, -19.024, -19.170, -19.278, -19.331, -19.355, -19.375
1 , -18.769, -18.770, -18.771, -18.774, -18.782, -18.806
1 , -18.869, -18.991, -19.139, -19.245, -19.295, -19.318, -19.339
1 , -18.722, -18.723, -18.724, -18.727, -18.736, -18.763
1 , -18.832, -18.962, -19.113, -19.215, -19.263, -19.286, -19.307
1 , -18.677, -18.678, -18.679, -18.683, -18.693, -18.723
1 , -18.799, -18.936, -19.089, -19.188, -19.234, -19.256, -19.279
1 , -18.634, -18.635, -18.636, -18.640, -18.652, -18.686
1 , -18.769, -18.913, -19.067, -19.164, -19.207, -19.229, -19.253
1 , -18.593, -18.593, -18.595, -18.599, -18.612, -18.650
1 , -18.740, -18.892, -19.046, -19.140, -19.182, -19.204, -19.229
1 , -18.552, -18.553, -18.554, -18.559, -18.574, -18.616
1 , -18.714, -18.873, -19.027, -19.118, -19.159, -19.180, -19.207
1 , -18.512, -18.512, -18.514, -18.520, -18.537, -18.583
1 , -18.689, -18.855, -19.009, -19.097, -19.136, -19.158, -19.186
1 , -18.472, -18.473, -18.475, -18.481, -18.500, -18.551
1 , -18.666, -18.837, -18.991, -19.076, -19.114, -19.136, -19.167
1 /

```

c TABLE ya4 is for CII cooling

```

data ((ya4(rowan,hema), rowan=1,13), hema=1,14) /

```

```

1 -20.565, -20.728, -21.027, -21.438, -21.905, -22.394
1 , -22.891, -23.390, -23.890, -24.389, -24.889, -25.389, -25.889
1 , -20.530, -20.691, -20.987, -21.395, -21.862, -22.351
1 , -22.847, -23.346, -23.846, -24.346, -24.846, -25.345, -25.845
1 , -20.512, -20.668, -20.959, -21.365, -21.830, -22.319
1 , -22.815, -23.314, -23.814, -24.313, -24.813, -25.313, -25.813
1 , -20.505, -20.657, -20.942, -21.344, -21.808, -22.295
1 , -22.792, -23.290, -23.790, -24.290, -24.790, -25.290, -25.790

```

```

1 , -20.509, -20.654, -20.932, -21.329, -21.791, -22.278
1 , -22.774, -23.273, -23.772, -24.272, -24.772, -25.272, -25.772
1 , -20.521, -20.659, -20.928, -21.320, -21.779, -22.265
1 , -22.761, -23.259, -23.759, -24.259, -24.759, -25.259, -25.759
1 , -20.539, -20.670, -20.930, -21.314, -21.770, -22.255
1 , -22.751, -23.249, -23.749, -24.248, -24.748, -25.248, -25.748
1 , -20.563, -20.685, -20.935, -21.312, -21.764, -22.248
1 , -22.743, -23.241, -23.741, -24.240, -24.740, -25.240, -25.740
1 , -20.591, -20.705, -20.943, -21.312, -21.760, -22.243
1 , -22.737, -23.235, -23.735, -24.234, -24.734, -25.234, -25.734
1 , -20.622, -20.728, -20.955, -21.314, -21.758, -22.239
1 , -22.733, -23.231, -23.730, -24.230, -24.730, -25.230, -25.730
1 , -20.656, -20.755, -20.969, -21.319, -21.757, -22.236
1 , -22.729, -23.227, -23.726, -24.226, -24.726, -25.226, -25.726
1 , -20.683, -20.776, -20.981, -21.322, -21.757, -22.234
1 , -22.727, -23.224, -23.723, -24.223, -24.723, -25.223, -25.723
1 , -20.712, -20.799, -20.995, -21.327, -21.757, -22.233
1 , -22.725, -23.222, -23.721, -24.221, -24.721, -25.221, -25.721
1 , -20.743, -20.823, -21.010, -21.334, -21.759, -22.232
1 , -22.723, -23.220, -23.719, -24.219, -24.719, -25.219, -25.719
1 /
data ((ya4(rowan,hema), rowan=1,13), hema=15, 28) /
1 -20.774, -20.850, -21.027, -21.341, -21.760, -22.232
1 , -22.722, -23.219, -23.718, -24.218, -24.718, -25.218, -25.718
1 , -20.807, -20.877, -21.045, -21.349, -21.763, -22.232
1 , -22.721, -23.218, -23.717, -24.215, -24.713, -25.205, -25.680
1 , -20.840, -20.905, -21.064, -21.358, -21.766, -22.232
1 , -22.719, -23.211, -23.697, -24.159, -24.558, -24.838, -24.985
1 , -20.874, -20.934, -21.084, -21.367, -21.765, -22.219
1 , -22.680, -23.101, -23.423, -23.608, -23.689, -23.718, -23.728
1 , -20.902, -20.957, -21.095, -21.358, -21.722, -22.100
1 , -22.396, -22.565, -22.637, -22.662, -22.671, -22.674, -22.675
1 , -20.893, -20.939, -21.052, -21.260, -21.508, -21.694
1 , -21.787, -21.823, -21.835, -21.839, -21.841, -21.841, -21.841
1 , -20.768, -20.797, -20.865, -20.977, -21.083, -21.143
1 , -21.168, -21.176, -21.179, -21.180, -21.180, -21.180, -21.180
1 , -20.492, -20.505, -20.534, -20.578, -20.616, -20.635
1 , -20.642, -20.644, -20.645, -20.646, -20.646, -20.646, -20.646
1 , -20.143, -20.148, -20.159, -20.175, -20.189, -20.196
1 , -20.199, -20.200, -20.200, -20.200, -20.200, -20.200, -20.200
1 , -19.792, -19.794, -19.798, -19.805, -19.810, -19.813
1 , -19.814, -19.814, -19.815, -19.815, -19.815, -19.815, -19.815
1 , -19.464, -19.465, -19.467, -19.469, -19.472, -19.473
1 , -19.474, -19.474, -19.474, -19.474, -19.474, -19.474, -19.474
1 , -19.169, -19.169, -19.170, -19.171, -19.173, -19.173
1 , -19.173, -19.173, -19.174, -19.174, -19.174, -19.174, -19.174
1 , -18.912, -18.912, -18.913, -18.913, -18.914, -18.914
1 , -18.914, -18.914, -18.914, -18.914, -18.914, -18.914, -18.914
1 , -18.696, -18.696, -18.696, -18.696, -18.697, -18.697
1 , -18.697, -18.697, -18.697, -18.697, -18.697, -18.697, -18.697
1 /

```



```

1 , -50.000, -50.000, -50.000, -50.000, -50.000, -50.000, -50.000
1 , -50.000, -50.000, -50.000, -50.000, -50.000, -50.000
1 , -50.000, -50.000, -50.000, -50.000, -50.000, -50.000, -50.000
1 , -50.000, -50.000, -50.000, -50.000, -50.000, -50.000
1 , -50.000, -50.000, -50.000, -50.000, -50.000, -50.000, -50.000
1 , -50.000, -50.000, -50.000, -50.000, -50.000, -50.000
1 , -50.000, -50.000, -50.000, -50.000, -50.000, -50.000, -50.000
1 /
data ((ya5(rowan,hema), rowan=1,13), hema=15, 28) /
1 -50.000, -50.000, -50.000, -50.000, -50.000, -50.000
1 , -50.000, -50.000, -50.000, -50.000, -50.000, -50.000, -50.000
1 , -50.000, -50.000, -50.000, -50.000, -50.000, -50.000
1 , -50.000, -50.000, -50.000, -50.000, -50.000, -50.000, -50.000
1 , -26.012, -26.012, -26.012, -26.012, -26.013, -26.013
1 , -26.013, -26.015, -26.021, -26.033, -26.050, -26.064, -26.071
1 , -24.377, -24.377, -24.377, -24.377, -24.377, -24.377
1 , -24.378, -24.379, -24.384, -24.395, -24.411, -24.425, -24.432
1 , -23.089, -23.089, -23.089, -23.089, -23.089, -23.089
1 , -23.090, -23.091, -23.096, -23.106, -23.121, -23.134, -23.140
1 , -22.078, -22.078, -22.078, -22.078, -22.078, -22.078
1 , -22.078, -22.080, -22.084, -22.093, -22.107, -22.119, -22.126
1 , -21.284, -21.284, -21.284, -21.284, -21.284, -21.285
1 , -21.285, -21.286, -21.289, -21.298, -21.310, -21.322, -21.329
1 , -20.659, -20.659, -20.659, -20.659, -20.659, -20.659
1 , -20.659, -20.660, -20.663, -20.670, -20.682, -20.693, -20.700
1 , -20.155, -20.155, -20.155, -20.155, -20.155, -20.155
1 , -20.155, -20.156, -20.159, -20.165, -20.176, -20.186, -20.192
1 , -19.733, -19.733, -19.733, -19.733, -19.733, -19.733
1 , -19.733, -19.734, -19.736, -19.741, -19.751, -19.760, -19.766
1 , -19.365, -19.365, -19.365, -19.365, -19.365, -19.365
1 , -19.365, -19.366, -19.368, -19.373, -19.382, -19.391, -19.396
1 , -19.043, -19.043, -19.043, -19.043, -19.043, -19.043
1 , -19.043, -19.044, -19.046, -19.051, -19.060, -19.070, -19.076
1 , -18.766, -18.766, -18.766, -18.766, -18.766, -18.766
1 , -18.767, -18.768, -18.770, -18.776, -18.787, -18.798, -18.805
1 , -18.538, -18.538, -18.538, -18.538, -18.538, -18.538
1 , -18.538, -18.539, -18.542, -18.549, -18.562, -18.576, -18.584
1 /
data ((ya5(rowan,hema), rowan=1,13), hema=29, 41) /
1 -18.354, -18.354, -18.354, -18.354, -18.354, -18.354
1 , -18.355, -18.356, -18.359, -18.367, -18.383, -18.399, -18.408
1 , -18.212, -18.212, -18.212, -18.212, -18.212, -18.212
1 , -18.212, -18.213, -18.217, -18.226, -18.243, -18.262, -18.273
1 , -18.104, -18.104, -18.104, -18.104, -18.104, -18.104
1 , -18.104, -18.106, -18.110, -18.119, -18.138, -18.158, -18.171
1 , -18.025, -18.025, -18.025, -18.025, -18.026, -18.026
1 , -18.026, -18.027, -18.031, -18.041, -18.061, -18.083, -18.097
1 , -17.971, -17.971, -17.971, -17.971, -17.971, -17.971
1 , -17.972, -17.973, -17.977, -17.987, -18.007, -18.030, -18.045
1 , -17.937, -17.937, -17.937, -17.937, -17.937, -17.937
1 , -17.937, -17.938, -17.942, -17.952, -17.972, -17.995, -18.011

```

```

1 , -17.918, -17.918, -17.918, -17.918, -17.918, -17.918
1 , -17.918, -17.920, -17.923, -17.933, -17.952, -17.976, -17.992
1 , -17.912, -17.912, -17.912, -17.912, -17.912, -17.912
1 , -17.912, -17.913, -17.917, -17.926, -17.945, -17.969, -17.985
1 , -17.916, -17.916, -17.916, -17.916, -17.916, -17.916
1 , -17.917, -17.918, -17.921, -17.929, -17.947, -17.971, -17.988
1 , -17.929, -17.929, -17.929, -17.929, -17.929, -17.929
1 , -17.929, -17.930, -17.933, -17.941, -17.958, -17.981, -17.998
1 , -17.948, -17.948, -17.948, -17.948, -17.948, -17.948
1 , -17.948, -17.949, -17.952, -17.959, -17.975, -17.997, -18.014
1 , -17.972, -17.972, -17.972, -17.972, -17.972, -17.972
1 , -17.972, -17.973, -17.976, -17.982, -17.997, -18.019, -18.036
1 , -18.000, -18.000, -18.000, -18.000, -18.000, -18.001
1 , -18.001, -18.001, -18.004, -18.010, -18.024, -18.044, -18.061
1 /

```

c TABLE ya6 is for OI cooling

```

data ((ya6(rowan,hema), rowan=1,13), hema=1,14) /
1 -23.932, -23.932, -23.933, -23.933, -23.933, -23.935
1 , -23.939, -23.952, -23.986, -24.062, -24.210, -24.474, -24.857
1 , -23.683, -23.683, -23.683, -23.683, -23.684, -23.685
1 , -23.691, -23.706, -23.745, -23.831, -23.993, -24.271, -24.663
1 , -23.478, -23.478, -23.478, -23.478, -23.479, -23.481
1 , -23.487, -23.504, -23.550, -23.646, -23.821, -24.113, -24.515
1 , -23.309, -23.309, -23.309, -23.309, -23.310, -23.312
1 , -23.319, -23.339, -23.390, -23.496, -23.686, -23.992, -24.402
1 , -23.169, -23.169, -23.169, -23.169, -23.170, -23.172
1 , -23.180, -23.203, -23.260, -23.376, -23.580, -23.899, -24.317
1 , -23.052, -23.052, -23.052, -23.053, -23.053, -23.056
1 , -23.065, -23.090, -23.153, -23.280, -23.496, -23.827, -24.253
1 , -22.954, -22.954, -22.955, -22.955, -22.956, -22.959
1 , -22.969, -22.997, -23.065, -23.201, -23.429, -23.772, -24.204
1 , -22.872, -22.872, -22.872, -22.872, -22.873, -22.877
1 , -22.887, -22.918, -22.992, -23.136, -23.376, -23.729, -24.166
1 , -22.801, -22.801, -22.801, -22.802, -22.803, -22.807
1 , -22.818, -22.851, -22.931, -23.083, -23.333, -23.695, -24.137
1 , -22.740, -22.740, -22.740, -22.741, -22.742, -22.746
1 , -22.759, -22.794, -22.878, -23.038, -23.297, -23.668, -24.115
1 , -22.687, -22.687, -22.687, -22.687, -22.689, -22.693
1 , -22.707, -22.744, -22.833, -23.000, -23.268, -23.646, -24.097
1 , -22.614, -22.614, -22.615, -22.615, -22.617, -22.622
1 , -22.637, -22.678, -22.775, -22.952, -23.235, -23.625, -24.082
1 , -22.547, -22.547, -22.547, -22.548, -22.550, -22.555
1 , -22.572, -22.618, -22.721, -22.910, -23.207, -23.607, -24.069
1 , -22.483, -22.483, -22.483, -22.484, -22.486, -22.492
1 , -22.511, -22.561, -22.672, -22.870, -23.180, -23.589, -24.048
1 /
data ((ya6(rowan,hema), rowan=1,13), hema=15, 28) /
1 -22.419, -22.419, -22.419, -22.420, -22.422, -22.429
1 , -22.450, -22.504, -22.620, -22.827, -23.141, -23.532, -23.932
1 , -22.340, -22.340, -22.341, -22.341, -22.344, -22.351
1 , -22.372, -22.428, -22.543, -22.740, -23.013, -23.294, -23.524

```

```

1 , -22.206, -22.206, -22.206, -22.207, -22.209, -22.216
1 , -22.235, -22.283, -22.378, -22.524, -22.689, -22.822, -22.941
1 , -21.973, -21.973, -21.973, -21.974, -21.975, -21.980
1 , -21.994, -22.026, -22.085, -22.164, -22.240, -22.305, -22.399
1 , -21.664, -21.664, -21.664, -21.664, -21.665, -21.668
1 , -21.676, -21.694, -21.725, -21.764, -21.802, -21.848, -21.944
1 , -21.339, -21.339, -21.339, -21.339, -21.340, -21.342
1 , -21.346, -21.356, -21.373, -21.394, -21.419, -21.463, -21.569
1 , -21.037, -21.037, -21.037, -21.037, -21.037, -21.039
1 , -21.041, -21.047, -21.057, -21.071, -21.092, -21.141, -21.259
1 , -20.768, -20.768, -20.768, -20.768, -20.768, -20.769
1 , -20.771, -20.775, -20.782, -20.793, -20.815, -20.870, -21.002
1 , -20.532, -20.532, -20.532, -20.532, -20.532, -20.533
1 , -20.534, -20.537, -20.543, -20.553, -20.577, -20.641, -20.788
1 , -20.324, -20.324, -20.324, -20.324, -20.324, -20.325
1 , -20.326, -20.329, -20.334, -20.345, -20.373, -20.447, -20.608
1 , -20.140, -20.140, -20.140, -20.140, -20.140, -20.141
1 , -20.142, -20.145, -20.150, -20.162, -20.195, -20.281, -20.458
1 , -19.977, -19.977, -19.977, -19.977, -19.977, -19.977
1 , -19.979, -19.981, -19.987, -20.001, -20.040, -20.140, -20.332
1 , -19.830, -19.830, -19.830, -19.830, -19.830, -19.831
1 , -19.832, -19.834, -19.841, -19.858, -19.905, -20.019, -20.226
1 , -19.697, -19.697, -19.697, -19.697, -19.697, -19.698
1 , -19.699, -19.702, -19.709, -19.730, -19.785, -19.916, -20.135
1 /
data ((ya6(rowan,hema), rowan=1,13), hema=29, 41) /
1 -19.575, -19.575, -19.575, -19.575, -19.575, -19.576
1 , -19.577, -19.581, -19.589, -19.614, -19.679, -19.827, -20.058
1 , -19.462, -19.462, -19.462, -19.462, -19.463, -19.463
1 , -19.465, -19.469, -19.479, -19.508, -19.585, -19.750, -19.990
1 , -19.357, -19.357, -19.357, -19.357, -19.358, -19.358
1 , -19.360, -19.365, -19.377, -19.411, -19.501, -19.683, -19.931
1 , -19.258, -19.258, -19.258, -19.258, -19.259, -19.259
1 , -19.261, -19.267, -19.281, -19.322, -19.426, -19.624, -19.877
1 , -19.164, -19.164, -19.164, -19.164, -19.165, -19.165
1 , -19.168, -19.174, -19.191, -19.239, -19.358, -19.572, -19.827
1 , -19.074, -19.074, -19.074, -19.074, -19.074, -19.075
1 , -19.078, -19.085, -19.106, -19.162, -19.296, -19.524, -19.780
1 , -18.987, -18.987, -18.987, -18.987, -18.987, -18.989
1 , -18.992, -19.000, -19.024, -19.090, -19.240, -19.481, -19.734
1 , -18.902, -18.902, -18.902, -18.903, -18.903, -18.904
1 , -18.908, -18.918, -18.946, -19.023, -19.189, -19.441, -19.690
1 , -18.820, -18.820, -18.820, -18.820, -18.821, -18.822
1 , -18.826, -18.838, -18.872, -18.960, -19.143, -19.402, -19.645
1 , -18.739, -18.739, -18.739, -18.739, -18.740, -18.742
1 , -18.747, -18.760, -18.800, -18.901, -19.100, -19.365, -19.600
1 , -18.659, -18.659, -18.660, -18.660, -18.660, -18.663
1 , -18.668, -18.685, -18.730, -18.845, -19.060, -19.329, -19.555
1 , -18.581, -18.581, -18.581, -18.581, -18.582, -18.584
1 , -18.591, -18.610, -18.664, -18.793, -19.022, -19.292, -19.508
1 , -18.503, -18.503, -18.503, -18.504, -18.505, -18.507

```



```

1 , -19.951, -20.022, -20.141, -20.281, -20.382, -20.441, -20.497
1 , -19.707, -19.707, -19.708, -19.709, -19.714, -19.728
1 , -19.761, -19.828, -19.937, -20.060, -20.146, -20.195, -20.245
1 , -19.557, -19.557, -19.557, -19.559, -19.563, -19.577
1 , -19.609, -19.674, -19.776, -19.886, -19.960, -20.002, -20.046
1 , -19.427, -19.427, -19.428, -19.429, -19.434, -19.447
1 , -19.478, -19.539, -19.632, -19.728, -19.789, -19.824, -19.859
1 , -19.304, -19.304, -19.304, -19.305, -19.310, -19.321
1 , -19.350, -19.405, -19.484, -19.561, -19.609, -19.635, -19.661
1 , -19.177, -19.177, -19.177, -19.178, -19.182, -19.192
1 , -19.216, -19.262, -19.325, -19.383, -19.418, -19.436, -19.454
1 /

```

```

data ((ya7(rowan,hema), rowan=1,13), hema=29, 41) /
1 -19.049, -19.049, -19.050, -19.050, -19.053, -19.061
1 -19.081, -19.117, -19.164, -19.207, -19.232, -19.245, -19.257
1 -18.928, -18.928, -18.929, -18.929, -18.931, -18.938
1 -18.953, -18.981, -19.016, -19.048, -19.066, -19.075, -19.083
1 -18.821, -18.821, -18.821, -18.822, -18.824, -18.828
1 -18.840, -18.861, -18.889, -18.912, -18.926, -18.933, -18.938
1 -18.731, -18.731, -18.731, -18.732, -18.733, -18.737
1 -18.746, -18.762, -18.784, -18.802, -18.813, -18.818, -18.822
1 -18.658, -18.658, -18.659, -18.659, -18.660, -18.663
1 -18.670, -18.683, -18.700, -18.715, -18.724, -18.728, -18.732
1 -18.602, -18.602, -18.602, -18.603, -18.603, -18.606
1 -18.612, -18.622, -18.636, -18.649, -18.656, -18.660, -18.663
1 -18.560, -18.560, -18.561, -18.561, -18.561, -18.563
1 -18.568, -18.577, -18.589, -18.600, -18.606, -18.609, -18.611
1 -18.531, -18.531, -18.531, -18.531, -18.531, -18.533
1 -18.537, -18.544, -18.555, -18.564, -18.570, -18.573, -18.575
1 -18.511, -18.511, -18.511, -18.511, -18.512, -18.513
1 -18.516, -18.523, -18.532, -18.540, -18.545, -18.548, -18.550
1 -18.500, -18.500, -18.500, -18.500, -18.500, -18.501
1 -18.504, -18.510, -18.517, -18.525, -18.530, -18.532, -18.534
1 -18.495, -18.495, -18.495, -18.495, -18.496, -18.496
1 -18.499, -18.504, -18.510, -18.517, -18.522, -18.524, -18.526
1 -18.496, -18.496, -18.496, -18.496, -18.496, -18.497
1 -18.499, -18.503, -18.509, -18.516, -18.520, -18.522, -18.524
1 -18.501, -18.501, -18.501, -18.501, -18.501, -18.502
1 -18.504, -18.507, -18.513, -18.519, -18.523, -18.525, -18.526
1 /

```

c TABLE ya8 is for OIII cooling

```

data ((ya8(rowan,hema), rowan=1,13), hema=1,14) /
1 -20.660, -20.668, -20.691, -20.757, -20.909, -21.178
1 -21.549, -21.991, -22.469, -22.961, -23.459, -23.958, -24.458
1 -20.543, -20.551, -20.573, -20.635, -20.779, -21.031
1 -21.384, -21.814, -22.288, -22.779, -23.276, -23.775, -24.275
1 -20.450, -20.457, -20.479, -20.538, -20.673, -20.910
1 -21.248, -21.669, -22.139, -22.629, -23.125, -23.624, -24.124
1 -20.378, -20.384, -20.405, -20.461, -20.589, -20.814
1 -21.140, -21.555, -22.022, -22.511, -23.008, -23.506, -24.006
1 -20.323, -20.329, -20.349, -20.403, -20.525, -20.740

```

```

1 , -21.058, -21.468, -21.934, -22.422, -22.918, -23.417, -23.917
1 , -20.284, -20.290, -20.309, -20.360, -20.477, -20.685
1 , -20.997, -21.404, -21.868, -22.356, -22.852, -23.350, -23.850
1 , -20.259, -20.265, -20.283, -20.332, -20.444, -20.646
1 , -20.953, -21.356, -21.819, -22.306, -22.802, -23.301, -23.800
1 , -20.246, -20.252, -20.269, -20.316, -20.424, -20.621
1 , -20.921, -21.322, -21.783, -22.270, -22.765, -23.264, -23.763
1 , -20.245, -20.250, -20.266, -20.310, -20.414, -20.605
1 , -20.900, -21.297, -21.756, -22.242, -22.738, -23.236, -23.736
1 , -20.252, -20.257, -20.272, -20.314, -20.413, -20.598
1 , -20.887, -21.279, -21.736, -22.222, -22.717, -23.215, -23.715
1 , -20.266, -20.271, -20.285, -20.325, -20.419, -20.598
1 , -20.880, -21.267, -21.722, -22.206, -22.701, -23.199, -23.699
1 , -20.287, -20.292, -20.305, -20.342, -20.431, -20.603
1 , -20.878, -21.260, -21.711, -22.195, -22.689, -23.187, -23.687
1 , -20.314, -20.317, -20.329, -20.364, -20.448, -20.613
1 , -20.881, -21.255, -21.704, -22.186, -22.680, -23.178, -23.677
1 , -20.344, -20.347, -20.358, -20.390, -20.469, -20.627
1 , -20.886, -21.254, -21.698, -22.179, -22.671, -23.167, -23.665
1 /
data ((ya8(rowan,hema), rowan=1,13), hema=15, 28) /
1 -20.377, -20.381, -20.391, -20.419, -20.493, -20.643
1 , -20.894, -21.253, -21.692, -22.164, -22.640, -23.108, -23.577
1 , -20.412, -20.415, -20.424, -20.450, -20.519, -20.660
1 , -20.900, -21.245, -21.661, -22.083, -22.458, -22.791, -23.154
1 , -20.442, -20.444, -20.452, -20.476, -20.537, -20.667
1 , -20.887, -21.195, -21.533, -21.811, -22.007, -22.203, -22.494
1 , -20.448, -20.450, -20.457, -20.476, -20.528, -20.637
1 , -20.817, -21.046, -21.252, -21.384, -21.482, -21.628, -21.891
1 , -20.402, -20.404, -20.409, -20.423, -20.461, -20.540
1 , -20.661, -20.798, -20.901, -20.964, -21.028, -21.153, -21.401
1 , -20.294, -20.295, -20.298, -20.307, -20.330, -20.379
1 , -20.451, -20.524, -20.576, -20.611, -20.661, -20.776, -21.010
1 , -20.145, -20.146, -20.148, -20.153, -20.166, -20.194
1 , -20.235, -20.275, -20.304, -20.328, -20.371, -20.477, -20.697
1 , -19.990, -19.990, -19.991, -19.994, -20.002, -20.018
1 , -20.042, -20.065, -20.084, -20.102, -20.141, -20.238, -20.442
1 , -19.844, -19.845, -19.845, -19.847, -19.852, -19.861
1 , -19.876, -19.891, -19.904, -19.919, -19.954, -20.042, -20.226
1 , -19.711, -19.711, -19.712, -19.713, -19.716, -19.722
1 , -19.732, -19.742, -19.751, -19.764, -19.794, -19.872, -20.033
1 , -19.579, -19.579, -19.579, -19.580, -19.582, -19.586
1 , -19.592, -19.599, -19.606, -19.616, -19.642, -19.707, -19.838
1 , -19.427, -19.427, -19.427, -19.428, -19.429, -19.432
1 , -19.436, -19.441, -19.445, -19.453, -19.473, -19.522, -19.618
1 , -19.244, -19.244, -19.244, -19.244, -19.245, -19.247
1 , -19.249, -19.252, -19.255, -19.261, -19.274, -19.307, -19.370
1 , -19.040, -19.040, -19.040, -19.040, -19.040, -19.041
1 , -19.042, -19.044, -19.046, -19.050, -19.058, -19.079, -19.117
1 /
data ((ya8(rowan,hema), rowan=1,13), hema=29, 41) /

```

```

1  -18.837, -18.837, -18.837, -18.837, -18.837, -18.838
1  , -18.839, -18.840, -18.841, -18.843, -18.848, -18.861, -18.884
1  , -18.654, -18.654, -18.654, -18.654, -18.654, -18.654
1  , -18.655, -18.655, -18.656, -18.657, -18.661, -18.669, -18.683
1  , -18.497, -18.497, -18.497, -18.497, -18.497, -18.498
1  , -18.498, -18.498, -18.499, -18.500, -18.502, -18.507, -18.516
1  , -18.368, -18.368, -18.368, -18.368, -18.368, -18.368
1  , -18.368, -18.369, -18.369, -18.369, -18.371, -18.374, -18.381
1  , -18.264, -18.264, -18.264, -18.264, -18.264, -18.264
1  , -18.264, -18.264, -18.264, -18.265, -18.265, -18.268, -18.272
1  , -18.181, -18.181, -18.181, -18.181, -18.181, -18.182
1  , -18.182, -18.182, -18.182, -18.182, -18.183, -18.184, -18.187
1  , -18.117, -18.117, -18.117, -18.117, -18.117, -18.117
1  , -18.117, -18.117, -18.117, -18.118, -18.118, -18.119, -18.121
1  , -18.069, -18.069, -18.069, -18.069, -18.069, -18.069
1  , -18.069, -18.070, -18.070, -18.070, -18.070, -18.071, -18.073
1  , -18.036, -18.036, -18.036, -18.036, -18.036, -18.036
1  , -18.036, -18.036, -18.036, -18.037, -18.037, -18.037, -18.039
1  , -18.015, -18.015, -18.015, -18.015, -18.015, -18.015
1  , -18.015, -18.015, -18.015, -18.016, -18.016, -18.016, -18.017
1  , -18.005, -18.005, -18.005, -18.005, -18.005, -18.005
1  , -18.005, -18.005, -18.005, -18.005, -18.005, -18.005, -18.006
1  , -18.002, -18.002, -18.002, -18.002, -18.002, -18.002
1  , -18.002, -18.002, -18.003, -18.003, -18.003, -18.003, -18.004
1  , -18.007, -18.007, -18.007, -18.007, -18.007, -18.007
1  , -18.007, -18.007, -18.007, -18.007, -18.008, -18.008, -18.009
1  /

```

c-----

```

c
c      common / kevcocom /
1     fnh, fih, fnc, fic1, fic2, fno, fio1, fio2, Lscale, Tscale, n_ophys
c      common / vjtcom /
1     ampjet, frqjet, frqamp
c      common / kcoolcom /
1     arr1a, arr2a, ya
c      common / speccom /
1     cl_spec
c      common / cointcom /
1     vpm, vpmax
c  Input parameters for problem generator kevcgen:
c     fnh  fraction of n that is neutral hydrogen (=x_h*fn_h)
c     fih  fraction of n that is ionised hydrogen
c     fnc  fraction of n that is neutral carbon
c     fic1 fraction of n that is singly ionised carbon
c     fic2 fraction of n that is doubly ionised carbon
c     fno  fraction of n that is neutral oxygen
c     fio1 fraction of n that is singly ionised oxygen
c     fio2 fraction of n that is doubly ionised oxygen
c     ampjet amplitude of sine term in variable jet
c     frqjet frequency of sine term (=2*pi/period)
c     frqamp frequency to allow amplitude to vary also

```

```

c   Lscale Cooling scale factor
c   Tscale Temperaute scale factor
c
c   namelist / kevcgen /
1  fnh,fih,fnc,fi1,fi2,fno,fio1,fio2,ampjet,frqjet,frqamp
2  , vjphys, n_ophys, machjet, vpmi, vpmx
c
c   Default values (give a nonvariable jet)
c
c   fnh   = 0.8991
c   fih   = 0.0999
c   fnc   = 3.069e-4
c   fi1   = 2.3077e-5
c   fi2   = 2.3077e-8
c   fno   = 6.534e-4
c   fio1  = 6.5934e-6
c   fio2  = 6.5934e-9
c   ampjet = 0.0
c   frqjet = 0.0
c   frqamp = 0.0
c   vpmi  = 0.0
c   vpmx  = 1.0
c   machjet = 6.0
c   USEFUL DG TAU B VALUES
c   vjphys is in km/s , n_ophys is in cm-3
c   vjphys = 190.0
c   n_ophys = 10000.0
c
c   read ( ioin , kevcgen )
c   write ( iolog, kevcgen )
c
c   etajet   = djet / damb
c   Tscale = 87.856 * vjphys**2 / machjet**2
c   Lscale = 7.01035e-20 * n_ophys**2 *(sqrt(etajet)+etajet)/ vjphys
c
c   do 400 k = 1, kn
c     do 500 j = 1, jn
c       do 600 i = 1, in
c         do 700 ii = 1, 8
c           cl_spec (i, j, k, ii) = 0.0
c         continue
c       continue
c     continue
c   continue
c-----
c   write (iotty, 2010)
c   write (iolog, 2010)
2010 format('KEVCINIT : Initialisation complete.')
c
c   return
c   end

```

```

=====
C
C
C           E N D       S U B R O U T I N E
C           C K E V I N I T
C
=====

```

The next subroutine, VARJET2, causes the velocity of the jet to vary sinusoidally at its inlet according to the values of `ampjet` and `frqjet`.

```

*deck varjet2
=====
C
C
C           B E G I N   S U B R O U T I N E
C           V A R J E T 2
C
=====
C
C       subroutine varjet2
C
C       kad:zeus3d.varjet2 <----- uses parameters from
C                               varjet1 to pulse jet.
C                               June 1997
C       written by: Kevin A. Douglas
C       modified 1:
C
C       PURPOSE:  allows parameters for amplitude and frequency of jet
C       to be used to pulse jet at inner boundary
C
C       LOCAL VARIABLES:
C
C       EXTERNALS:  BNDYFLGS, BNDYALL, BSETMAG
C
-----
C
C
C       *call comvar
C           real      ampjet, frqjet, frqamp
C           integer   i, j, k
C
C
C       common / vjtcom / ampjet, frqjet, frqamp
C
C       external bndyflgs, bndyall, bsetmag
C
C

```

```

*if -def,ISYM
C
C   Set inflow boundary values.
C
  do 50 k=ksmn,kemx
    do 40 j=jsmn,jemx
      vliib1(j,k) = v1jet*(1.0 + ampjet*cos(frqamp*prtime)
1          *sin(frqjet*prtime))
      vliib2(j,k) = v1jet*(1.0 + ampjet*cos(frqamp*prtime)
1          *sin(frqjet*prtime - 2.0*pi*dx1a(ism1)/rjet))
40    continue
50    continue
*endif -ISYM
C
C   Set all boundary values
C
  call bndyflgs
  call bndyall
*if def,MHD
  call bsetmag
*endif MHD
C
C
  return
  end

C
C=====
C
C           E N D   S U B R O U T I N E
C           V A R J E T 2
C
C=====

```

The next subroutine, KEVCOOL, attempts to subtract the proper amount of cooling from the energy equation and update the energy for the next timestep.

```

*deck kevcool
C=====
C
C           B E G I N       S U B R O U T I N E
C           K E V C O O L
C
C=====
  subroutine kevcool ( p )
C
C   kad:zeus3d.kevcool <----- pressure work plus cooling

```

August, 1997

```
c
c
c   written by: Kevin Douglas, adapted from pdvcool
c
c   PURPOSE:  This routine uses an iterative secant procedure to find
c   the new energy in the source step by solving the implicit eqn:
c
c        $de / dt = -p(e) * DIV(v) - L(T, n_e)$ 
c
c   where L is an empirical cooling function of T (energy) and n_e,
c
c
c   INPUT VARIABLES:
c   p           pressure at old e (stored in "wa3d")
c
c   OUTPUT VARIABLES:
c
c   LOCAL VARIABLES:
c
c   EXTERNALS:
c   ISMAX
c   DIVERG
c
c *call comvar
c   FIRST DECLARE VARIABLES AND PARAMETERS
c
c       integer      itmax
c       real         accerr
c       parameter    (accerr = 1.0e-4)
c       parameter    ( itmax = 40)
c       real         swap, feold(in), fenew(in), errmax
c       real         accerr, root(in), eold(in), enew(in), exold(in)
c
c
c       integer      i          , j          , k          , imax      , jmax
c       1            , iter      , itdex     , itmaxx   , indix
c       real         fofe(in)   , dfde     , de(in)
c       real         gamm, q1
c
c
c       integer      indx      (ijkn), itmaxi   (ijkn)
c       real         ftmp      (ijkn), en       (ijkn), err      (ijkn)
c       1            , errmxi  (ijkn)
c
c
c       real         cool_a   ( in,  jn,  kn)
c       real         p        ( in,  jn,  kn)
c       real         divv     ( in,  jn,  kn)
c
c
c       common      / clratcom / cool_a
c
c
c       equivalence  ( indx      , wald      ), ( itmaxi   , wb1d      )
c       1            , ( ftmp      , wc1d      ), ( en       , wd1d      )
```

```

1          , ( err      , weld      ), ( errmxi  , wf1d      )
c
c    Careful! "wa3d", "wb3d", and "wc3d" used by SRCSTEP.
c
c    equivalence ( divv      , wd3d      )
c
c    External statements
c
c    integer      ismax
c    external     ismax      , diverg
c
c-----
c    Compute divergence of velocity field
c
c    call diverg ( v1, v2, v3, 0, 0, divv, q1 )
c
c    Constants.
c    gamm = gam(1)
c
c
c    k = ks
c    j = js
c    i = is
c  *if -def, KSYM
c    do 70 k=ks, ke
c  *endif -def, KSYM
c  *if -def, JSYM
c    do 60 j=js,je
c  ccc    call cooltab(e(1,j,k), e2(1,j,k), d(1,j,k), cool_a, is, ie)
c  *endif -def, JSYM
c  *if -def, ISYM
c    do 10 i=is,ie
c  *if def, TWOFLUID
c    call cooltab(e(i,j,k), e2(i,j,k), d(i,j,k), cool_a(i,j,k)
c      1      , i , j , k )
c  *endif def, TWOFLUID
c  *if -def, TWOFLUID
c    cool_a(i,j,k) = 0.0
c  *endif -def, TWOFLUID
c
c    Initial guesses.
c
c
c    eold (i) = e(i,j,k) - dt * p(i,j,k) * divv(i,j,k)
c    enew (i) = e(i,j,k)
c      1      - dt * ( cool_a(i,j,k) )
c
c
c    feold(i) = dt * (0.5 * (gamm * eold(i) + p(i,j,k))
c      1      * divv(i,j,k) + cool_a(i,j,k) )
c      2      - dt * (p(i,j,k) * divv(i,j,k))
c    fenew(i)=dt*(0.5*(gamm*enew(i) + p(i,j,k))*divv(i,j,k))
c

```

```

c   Pick the bound with the smaller function value as the most
c   recent guess.
c
c       if (abs(fenew(i)).lt.abs(feold(i))) then
c           root(i) = eold(i)
c           exold(i) = enew(i)
c           swap    = feold(i)
c           feold(i) = fenew(i)
c           fenew(i) = swap
c       else
c           exold(i) = eold(i)
c           root(i) = enew(i)
c       endif
c   10      continue
c
c -----
c   PERFORM COOLING STEP
c
c       Secant iteration.
c
c       do 20 i=is, ie
c           CHECK IF THE JET ENERGY IS NON-ZERO,
c           OTHERWISE NO COOLING IS PERFORMED
c           if ( e(i, j, k) .le. accerr) then
c               enew(i) = max1(e(i,j,k), 0.0)
c               goto 20
c           endif
c       do 30 iter=1,itmax
c
c   cfofe (fenew) is the FUNCTION we want to be zero:
c   cfofe(edummy) = ( edummy(i) - e(i,j,k) )
c   1              + dt * ( 0.5 * ( gamm * edummy(i) + p(i,j,k) )
c   2                  * divv(i,j,k)
c   3                  + cool_a(i,j,k) )
c
c   Secant Method root-finder, p. 350 of Numerical Recipes
c
c   use FUNCTION root to get value of en
c   implement secant method to find value of en
c -----
c           de(i) = (exold(i) - root(i)) * fenew(i)
c   1              / (fenew(i) - feold(i))
c           exold(i) = root(i)
c           feold(i) = fenew(i)
c           root(i) = root(i) + de(i)
c   *if def, TWOFLUID
c           call cooltab(root(i), e2(i,j,k), d(i,j,k), cool_a(i,j,k)
c   1              , i, j, k)
c   *endif def, TWOFLUID
c   *if -def, TWOFLUID
c           cool_a(i,j,k) = 0.0

```

```

*endif -def, TWOFLUID
      fenew(i) = ( root(i) - e(i,j,k) )
1          + dt * ( 0.5 * ( gamm * root(i) + p(i,j,k) )
1          * divv(i,j,k)
1          + cool_a(i,j,k) )
c      write (6, *) e(i, j, k), cool_a(i,j,k), i, j, iter
      enew(i) = root(i)
      err (i) = abs ( de(i) / enew(i) )
      if (err(i).lt.accerr.or.fenew(i).eq.0) goto 20
c Convergence.
c-----
c
c
30      continue
      if (e(i,j,k) .lt. 1.0e-10) then
          enew(i) = 0.0
          go to 20
      endif
      pause 'maximum iterations exceeded in KEVCOOL'
20      continue
c
c
      do 50 i=is,ie
          e(i,j,k) = enew(i)
50      continue
*endif -def, ISYM
c
*if -def, JSYM
60      continue
*endif -def, JSYM
*if -def, KSYM
70      continue
*endif -def, KSYM
c
c
c-----
c
      return
      end
c=====
c
c          E N D   S U B R O U T I N E
c          K E V C O O L
c=====

```

The next subroutine, COOLTAB, does the actual calculation of the cooling rates by interpolating the cooling tables declared at the beginning using the current

values of temperature and electron densities. It also stores the cooling rates into a four-dimensional array in case emission maps are desired for the coolants.

```

*deck cooltab
C=====
C
C           B E G I N           S U B R O U T I N E
C                   C O O L T A B
C=====
C           subroutine cooltab ( enrg, enrg2, dens, Lcool, i, j, k)
C
C           kad:zeus3d.cooltab <----- pressure work plus cooling
C                                   October, 1997
C
C           written by: Kevin Douglas, adapted from pdvcool
C
C           PURPOSE: This routine calculates the amount of cooling to subtract
C           in the energy equation:
C
C                $de / dt = -p(e) * DIV(v) - n_e * N * L(T, n_e)$ 
C
C           where L is an empirical cooling function of T and n_e, interpolated
C           from tables in this very subroutine.
C
C           INPUT VARIABLES:
C           e, e2, d           energy of jet, e of ambient, density of cell
C
C           OUTPUT VARIABLES:
C
C           Lcool             amount of cooling to subtract in energy eqn.
C
C           LOCAL VARIABLES:
C
C           EXTERNALS:
C           ISMAX
C
C
C           *ca imp
C           *ca par
C           FIRST DECLARE VARIABLES AND PARAMETERS
C
C           Number Densities, etc.
C           real             maxlog
C           parameter        (maxlog = 6.0)
C           integer          ii, i, j, k
C           real             fnh, fih, fnc, fic1, fic2, fno, fio1, fio2
C           real             enrg, enrg2, dens, Lcool, Lscale, Tscale
C           real             t_phys, frac_a, lmcool(8), cool_a

```

```

real          n_a, n_e, n_h, n_c, n_o, n_s(8)
real          t_physlog, n_eolog, n_ophys
real          n_h0, n_h1, n_c0, n_c1, n_c2, n_o0, n_o1, n_o2
equivalence  (n_h0, n_s(1)), (n_h1, n_s(2))
equivalence  (n_c0, n_s(3)), (n_c1, n_s(4)), (n_c2, n_s(5))
equivalence  (n_o0, n_s(6)), (n_o1, n_s(7)), (n_o2, n_s(8))
common       / kevccom /
1 fnh, fih, fnc, fic1, fic2, fno, fio1, fio2, Lscale, Tscale, n_ophys
integer      ine, jtm, inum, jnum
real         nplus, nminus, tplus, tminus, yinterp
c  DECLARE TABLES AND ARRAYS STORED IN KCOOLCOM
real        arr2a(41), arr1a(13)
real        ya(13,41,8)
common     / kcoolcom / arr1a, arr2a, ya
c  DECLARE ARRAY TO KEEP TRACK OF COOLING
real        cl_spec(in, jn, kn, 8)
common     / speccom / cl_spec

c
c
c  CHANGE THINGS TO DEAL WITH PHYSICAL UNITS
c -----
c  FIND TEMPERATURE, ELECTRON DENSITY, ETC.
c -----
c
c
c        cool_a      = 0.0
c        Lcool = 0.0
c        if (enrg .le. 0.0001) return
c
c        t_phys      = Tscale * enrg / dens
c        frac_a      = enrg / (enrg + 0.6 * enrg2)
c        n_a         = frac_a * dens * (n_ophys)
c        n_h         = n_a * 0.999
c        n_c         = n_a * 0.00033
c        n_o         = n_a * 0.00066
c        n_h0        = n_a * fnh
c        n_h1        = n_a * fih
c        n_c0        = n_a * fnc
c        n_c1        = n_a * fic1
c        n_c2        = n_a * fic2
c        n_o0        = n_a * fno
c        n_o1        = n_a * fio1
c        n_o2        = n_a * fio2
c        n_e         = n_h1 + n_c1 + 2.0 * n_c2 + n_o1 + 2.0 * n_o2
c        n_eolog     = log10(n_e)
c        t_physlog   = log10(t_phys)
c
c        if ( ( (n_eolog .ge. 1) .and. (n_eolog .le. 6) ) .and.
1      ( (t_physlog .ge. 2) .and. (t_physlog .le. 6) ) ) then
c
c  MUST INTERPOLATE VALUE OF COOLING GIVEN n_e AND t_phys
c

```

```

c    CALCULATE GRID POINTS CLOSEST TO THE CO-ORDINATE
      do 50 inum = 1, 13
          ine = inum
          if (arr1a(inum) .gt. n_elog) go to 40
50    continue
40    continue
      nplus      = arr1a(ine) - n_elog
      nminus     = n_elog      - arr1a(ine - 1)
      do 60 jnum = 1, 41
          jtm = jnum
          if (arr2a(jnum) .gt. t_physlog) go to 20
60    continue
20    continue
      tplus      = arr2a(jtm) - t_physlog
      tminus     = t_physlog   - arr2a(jtm - 1)
      do 15 ii = 1, 8
c
c          yinterp = ( nplus * tplus * ya(ine - 1, jtm - 1, ii)
1          + nminus * tplus * ya(ine, jtm - 1, ii)
2          + nplus * tminus * ya(ine - 1, jtm, ii)
3          + nminus * tminus * ya(ine, jtm, ii))
4          / ((nplus + nminus) * (tplus + tminus))
c
c
c          lmcool(ii) = n_e * n_s(ii) * 10.0**(yinterp)
          cool_a = cool_a + lmcool(ii)
c    MULTIPLY COOLING RATES BY A LARGE NUMBER AND STORE THEM
          cl_spec(i, j, k, ii) = lmcool(ii) * 1.0e20
15    continue
c
c    endif
c    SCALE COOLING TO ZEUS UNITS
          Lcool = cool_a / Lscale
c
c    return
      end
c=====
c
c          E N D          S U B R O U T I N E
c          C O O L T A B
c=====

```

The next subroutine, COOLSPEC, creates a three-dimensional array of the cooling rates calculated in COOLTAB for the species that the user wishes to create emission maps.

```

*deck coolspec
C=====
C
C          B E G I N      S U B R O U T I N E
C                    C O O L S P E C
C=====
C          subroutine coolspec ( clspecs, ii, iall)
C
C          kad:zeus3d.coolspec<----- writes cooling rates to 3d
C                    arrays                    march, 1998
C
C          written by: Kevin Douglas, adapted from pres
C
C          PURPOSE: Take 4-d array cl_spec and make 3d array for contour plots
C                    or pixel dumps of cooling, ie. cooling rate due to
C                    species ii.
C
C          INPUT VARIABLES:
C          ii          =1 => HI
C                    =2 => HII
C                    =3 => CI
C                    =4 => CII
C                    =5 => CIII
C                    =6 => OI
C                    =7 => OII
C                    =8 => OIII
C                    =9 => SII (emission)
C          iall       =0 => compute block bounded by "ism2" to "iep2" ,
C                    "jsm2" to "jep2" ,
C                    "ksm2" to "kep2"
C                    =1 => compute block bounded by "ismnm2" to "iemxp2",
C                    "jsmnm2" to "jemxp2",
C                    "ksmnm2" to "kemxp2"
C
C          OUTPUT VARIABLES:
C          clspecs      array of cooling.
C
C          LOCAL VARIABLES:
C
C          EXTERNALS: [NONE]
C-----
C
*ca comvar
C
integer      ii, iall
integer      i, j, k
integer      kmin, kmax, jmin, jmax, imin, imax
real         cl_spec(in, jn, kn, 8)

```

```

common / speccom / cl_spec
real      clspecs (in, jn, kn)
c
c-----
c
      if (iall .eq. 1) then
        kmin = ksmnm2
        kmax = kemxp2
        jmin = jsnm2
        jmax = jemxp2
        imin = isnm2
        imax = iemxp2
      else
        kmin = ksm2
        kmax = kep2
        jmin = js2
        jmax = jep2
        imin = is2
        imax = iep2
      endif
      k = ks
      j = js
      i = is
c
c
*if -def, KSYM
      do 30 k=kmin, kmax
*endif -KSYM
*if -def, JSYM
      do 20 j=jmin, jmax
*endif -JSYM
*if -def, ISYM
      do 10 i=imin, imax
*endif -ISYM
          if (icool .eq. 2) then
            if (ii .le. 8) then
              clspecs(i, j, k) = cl_spec(i, j, k, ii)
            else
c      SII emission can be well approximated by the OI cooling
c      (see Cabrit et al. 1990 ApJ 354, 687)
c      The 1.5 factor comes from Edwards et al. 87ApJ321,473 and
c      is to illustrate that the SII emission is generally 1.5
c      stronger in HH objects than the OI emission.
              if (ii.eq.9) clspecs(i, j, k) = 1.5*cl_spec(i, j, k, 6)
            endif
          else
            clspecs(i, j, k) = 0.0
          endif
*if -def, ISYM
      10      continue
*endif -ISYM

```

```

*if -def,JSYM
  20   continue
*endif -JSYM
*if -def,KSYM
  30   continue
*endif -KSYM
C
C-----
C
      return
      end
C=====
C
C           E N D   S U B R O U T I N E
C           C O O L S P E C
C
C=====

```

The next subroutine, COOLMOL, calculates a three-dimensional array of emission estimates for molecules in the ambient medium.

```

*deck coolmol
C=====
C
C           B E G I N   S U B R O U T I N E
C           C O O L M O L
C
C=====
      subroutine coolmol ( xb, yb, clmol )
C
C   kad:zeus3d.coolmol<----- writes molecular emission to 3d
C   arrays                               july, 1998
C
C   written by: Kevin Douglas, adapted from pres
C
C   PURPOSE: Calculate emission estimate of molecular CO and store
C             into 3d array for contour plots or pixel dumps.
C             This is set up to find the column density from a 2-D grid.
C
C
C   INPUT VARIABLES
C
C   OUTPUT VARIABLES:
C     clmol          array of molecular emission (arbitrary units)
C
C   LOCAL VARIABLES:

```

```

C
C  EXTERNALS:
C
C-----
C
C  *ca comvar
C
C      integer      i, j, k, bigi, bigj, iii, jjj
C      real         clmol(npx, npx), vpll, emit, xb(*), yb(*)
C      real         ray1, ray2, sintheta1, sintheta2, path1, errors
C      real         qdrnt1, qdrnt2, qdrnt3, vpmi, vpmx
C      real         theta, sintheta, costheta, theta1, theta2
C
C      common / cointcom /      vpmi, vpmx
C-----
C
C      k = ks
C      j = js
C      i = is
C
C
C      do 20 bigi = 1, npx
C        do i = is, ie
C          if ( xb(bigi) .gt. x1a(i) ) iii=i
C        end do
C
C      do 18 bigj = 1, npx
C      Launch a ray.
C      clmol(bigi, bigj) = 0.0
C      do j = js, je
C        if ( yb(bigj) .gt. x2a(j) ) jjj=j
C      end do
C      do 10 j = je, jjj, -1
C
C        ray1 = x2a(j)
C        ray2 = x2a(j + 1)
C      Test what the ray intersects.
C      qdrnt2 = 1.0 - (yb(bigj)/ray2)**2
C      sintheta2 = sqrt (amax1(qdrnt2, 0.0) )
C      theta2 = asin(amax1(-1.0, amin1(1.0, sintheta2) ) )
C      if ( yb(bigj) .lt. ray1 ) then
C      CASE1
C        qdrnt1 = 1.0 - (yb(bigj)/ray1)**2
C        sintheta1 = sqrt ( amax1(qdrnt1, 0.0))
C        theta1 = asin(amax1(-1.0, amin1(1.0, sintheta1) ) )
C        path1 = ray2 * sintheta2 - ray1 * sintheta1
C      else
C      CASE 2
C        path1 = ray2 * sintheta2
C        theta1 = 0.0
C      endif

```

```

c   Find the proper amount of emission to include.
      sintheta = sin ( 0.5 * ( theta1 + theta2 ) )
      costheta = cos ( 0.5 * ( theta1 + theta2 ) )
      qdrnt3 = v2(iii,j,k)**2 * sintheta**2 +
1      v3(iii,j,k)**2 * costheta**2
      vp11 = sqrt ( amax1( qdrnt3, 0.0) )
      if ((vp11 .ge. vpmin) .and. (vp11 .le. vpmax)) then
cc      emit = e2(iii,j,k) * pathl * d(iii,j,k)
      emit = e2(iii,j,k) * pathl
      else
      emit = 0.0
      endif
      clmol (bigi, bigj) = clmol(bigi, bigj) + emit
10      continue
18      continue
20      continue
c
c-----
c
      return
      end
c=====
c
c           E N D       S U B R O U T I N E
c                   C O O L M O L
c=====

```

The next subroutine, COOLVPDV, calculates the ratio of atomic cooling done in COOLTAB to the amount of work done by expansion ($P \cdot dV$ work).

```

*deck coolvpdv
c=====
c
c           B E G I N       S U B R O U T I N E
c                   C O O L V P D V
c=====
      subroutine coolvpdv ( clvpdv, ii , iall)
c
c   kad:zeus3d.coolvpdv<----- writes energy loss ratios to
c       arrays                    april, 1998
c
c   written by: Kevin Douglas, adapted from pres
c
c   PURPOSE: Divide pdv work (total pressure) by cooling rate.

```

```

C
C
C INPUT VARIABLES:
C   ii          =1 => pdv work / cooling rate
C              =2 => nothing yet
C
C   iall        =0 => compute block bounded by "ism2"   to "iep2"   ,
C                                                    "jsm2"   to "jep2"   ,
C                                                    "ksm2"   to "kep2"   ,
C              =1 => compute block bounded by "ismnm2" to "iemxp2",
C                                                    "jsnm2" to "jemxp2",
C                                                    "ksnm2" to "kemxp2"
C
C OUTPUT VARIABLES:
C   clvpdv      array of ratio of energy loss.
C
C LOCAL VARIABLES:
C
C EXTERNALS: [NONE]
C
C-----
C
C *ca comvar
C
C   integer      ii, iall, i, j, k
C   integer      kmin, kmax, jmin, jmax, imin, imax
C   real          clvpdv (in, jn, kn), cool_a(in,jn,kn), q1
C   real          p(in, jn, kn) , divv(in, jn, kn)
C   common       / clratcom / cool_a
C
C-----
C
C   if (iall .eq. 1) then
C     kmin = ksmnm2
C     kmax = kemxp2
C     jmin = jsnm2
C     jmax = jemxp2
C     imin = isnm2
C     imax = iemxp2
C   else
C     kmin = ksm2
C     kmax = kep2
C     jmin = js2
C     jmax = jep2
C     imin = ism2
C     imax = iep2
C   endif
C   k = ks
C   j = js
C   i = is
C

```

```

C
*if -def, KSYM
    do 30 k=kmin,kmax
*endif -KSYM
*if -def, JSYM
    do 20 j=jmin,jmax
*endif -JSYM
*if -def, ISYM
    do 10 i=imin,imax
*endif -ISYM
        if (ii .eq. 1 .and. cool_a(i,j,k) .ge. 1.e-3) then
            call pres ( p, 1, 1)
            call diverg ( v1, v2, v3, 0, 0, divv, q1 )
            clvpdv(i,j,k) =abs(cool_a(i,j,k)/p(i,j,k)*divv(i,j,k))
        else
            clvpdv(i,j,k)=0.0
        endif
*if -def, ISYM
    10      continue
*endif -ISYM
*if -def, JSYM
    20      continue
*endif -JSYM
*if -def, KSYM
    30      continue
*endif -KSYM
C
C-----
C
        return
        end
C=====
C
C          E N D      S U B R O U T I N E
C          C O O L V P D V
C
C=====

```

The next lines consist of microsurgical changes to existing subroutines within the ZEUS3D code. These changes are necessary to allow the above subroutines to function properly. An `insert` command will include the new FORTRAN lines into the subroutine at the line number following the name of the routine.

```
*insert srcstep.146
```

```

c      Option to call KEVCOOL, which uses cooling tables
      if (icool .eq. 2) then
          call pres    ( p, 1, 0 )
          call kevcool ( p )
      endif
*insert plot2d.62
c 32.  h1      - cooling due to HI          (contour)
c 33.  h2      - cooling due to HII         (contour)
c 34.  c1      - cooling due to CI          (contour)
c 35.  c2      - cooling due to CII         (contour)
c 36.  c3      - cooling due to CIII        (contour)
c 37.  o1      - cooling due to OI          (contour)
c 38.  o2      - cooling due to OII         (contour)
c 39.  o3      - cooling due to OIII        (contour)
c 40.  sf      - emission due to SII       (contour)
c 41.  co      - emission due to CO        (contour)
c 42.  wk      - work divided by cooling rate (contour)
*insert plot2d.838
c---- plot 32 : cooling due to HI -----
c
      if (plt2var(n) .eq. 'h1') then
          phdr = 'HI Cooling (:F10:h:B:1:NFO:)'
          call coolspec ( wa3d, 1, 1)
          call slice2d ( wa3d, ibtm, jbtm, kbtm, itop, jtop, ktop
1              , wa2d )
      endif
c
c---- plot 33 : cooling due to HII -----
c
      if (plt2var(n) .eq. 'h2') then
          phdr = 'HII Cooling (:F10:h:B:2:NFO:)'
          call coolspec ( wa3d, 2, 1)
          call slice2d ( wa3d, ibtm, jbtm, kbtm, itop, jtop, ktop
1              , wa2d )
      endif
c
c---- plot 34 : cooling due to CI -----
c
      if (plt2var(n) .eq. 'c1') then
          phdr = 'CI Cooling (:F10:c:B:1:NFO:)'
          call coolspec ( wa3d, 3, 1)
          call slice2d ( wa3d, ibtm, jbtm, kbtm, itop, jtop, ktop
1              , wa2d )
      endif
c
c---- plot 35 : cooling due to CII -----
c
      if (plt2var(n) .eq. 'c2') then
          phdr = 'CII Cooling (:F10:c:B:2:NFO:)'
          call coolspec ( wa3d, 4, 1)
          call slice2d ( wa3d, ibtm, jbtm, kbtm, itop, jtop, ktop

```

```

1          , wa2d )
endif
c
c---- plot 36 : cooling due to CIII -----
c
      if (plt2var(n) .eq. 'c3') then
        phdr = 'CIII Cooling (:F10:c:B:3:NFO:)'
        call coolspec ( wa3d, 5, 1)
        call slice2d ( wa3d, ibtm, jbtm, kbtm, itop, jtop, ktop
1          , wa2d )
      endif
c
c---- plot 37 : cooling due to OI -----
c
      if (plt2var(n) .eq. 'o1') then
        phdr = 'OI Cooling (:F10:o:B:1:NFO:)'
        call coolspec ( wa3d, 6, 1)
        call slice2d ( wa3d, ibtm, jbtm, kbtm, itop, jtop, ktop
1          , wa2d )
      endif
c
c---- plot 38 : cooling due to OII -----
c
      if (plt2var(n) .eq. 'o2') then
        phdr = 'OII Cooling (:F10:o:B:2:NFO:)'
        call coolspec ( wa3d, 7, 1)
        call slice2d ( wa3d, ibtm, jbtm, kbtm, itop, jtop, ktop
1          , wa2d )
      endif
c
c---- plot 39 : cooling due to OIII -----
c
      if (plt2var(n) .eq. 'o3') then
        phdr = 'OIII Cooling (:F10:o:B:3:NFO:)'
        call coolspec ( wa3d, 8, 1)
        call slice2d ( wa3d, ibtm, jbtm, kbtm, itop, jtop, ktop
1          , wa2d )
      endif
c
c---- plot 40 : emission due to SII -----
c
      if (plt2var(n) .eq. 'sf') then
        phdr = 'SII Emission (:F10:S:B:II:NFO:)'
        call coolspec ( wa3d, 9, 1)
        call slice2d ( wa3d, ibtm, jbtm, kbtm, itop, jtop, ktop
1          , wa2d )
      endif
c
c---- plot 41 : emission due to CO -----
c
      if (plt2var(n) .eq. 'co') then

```

```

        phdr = 'CO Emission (:F10:CO:NFO:)'
c      call coolmol ( wa2d, 1)
        call coolmol ( wa3d, 1)
        call slice2d ( wa3d, ibtm, jbtm, kbtm, itop, jtop, ktop
1          , wa2d )
        endif
c
c----- plot 42 : PDV Work divided by Cooling -----
c
        if (plt2var(n) .eq. 'wk') then
        phdr = 'Work vs. Cooling (:F10:wk:NFO:)'
        call coolvpdv ( wa3d, 1, 1)
        call slice2d ( wa3d, ibtm, jbtm, kbtm, itop, jtop, ktop
1          , wa2d )
        endif
c
*insert pixdmp.65
c 34. h1      - cooling due to HI          zih1NNNXX.MM
c 35. h2      - cooling due to HII         zih2NNNXX.MM
c 36. c1      - cooling due to CI          zic1NNNXX.MM
c 37. c2      - cooling due to CII         zic2NNNXX.MM
c 38. c3      - cooling due to CIII        zic3NNNXX.MM
c 39. o1      - cooling due to OI          zio1NNNXX.MM
c 40. o2      - cooling due to OII         zio2NNNXX.MM
c 41. o3      - cooling due to OIII        zio3NNNXX.MM
c 42. sf      - emission due to SII       zisfNNNXX.MM
c 43. co      - emission due to CO        zicoNNNXX.MM
c 44. wk      - work divided by cooling rate ziwkNNNXX.MM
*insert pixdmp.611
c----- pixel 34 : cooling due to HI -----
c
        if (pixvar(n) .eq. 'h1') then
        call coolspec ( wa3d, 1, 1)
        call slice2d ( wa3d, ibeg, jbeg, kbeg, iend, jend, kend
1          , wa2d )
        vrble = 'HI cooling          '
        endif
c
c----- pixel 35 : cooling due to HII -----
c
        if (pixvar(n) .eq. 'h2') then
        call coolspec ( wa3d, 2, 1)
        call slice2d ( wa3d, ibeg, jbeg, kbeg, iend, jend, kend
1          , wa2d )
        vrble = 'HII cooling          '
        endif
c
c----- pixel 36 : cooling due to CI -----
c
        if (pixvar(n) .eq. 'c1') then
        call coolspec ( wa3d, 3, 1)

```

```

        call slice2d ( wa3d, ibeg, jbeg, kbeg, iend, jend, kend
1          , wa2d )
        vrble = 'CI cooling      '
    endif

c
c----- pixel 37 : cooling due to CII -----
c
        if (pixvar(n) .eq. 'c2') then
            call coolspec ( wa3d, 4, 1)
            call slice2d ( wa3d, ibeg, jbeg, kbeg, iend, jend, kend
1          , wa2d )
            vrble = 'CII cooling      '
        endif

c
c----- pixel 38 : cooling due to CIII -----
c
        if (pixvar(n) .eq. 'c3') then
            call coolspec ( wa3d, 5, 1)
            call slice2d ( wa3d, ibeg, jbeg, kbeg, iend, jend, kend
1          , wa2d )
            vrble = 'CIII cooling     '
        endif

c
c----- pixel 39 : cooling due to OI -----
c
        if (pixvar(n) .eq. 'o1') then
            call coolspec ( wa3d, 6, 1)
            call slice2d ( wa3d, ibeg, jbeg, kbeg, iend, jend, kend
1          , wa2d )
            vrble = 'OI cooling      '
        endif

c
c----- pixel 40 : cooling due to OII -----
c
        if (pixvar(n) .eq. 'o2') then
            call coolspec ( wa3d, 7, 1)
            call slice2d ( wa3d, ibeg, jbeg, kbeg, iend, jend, kend
1          , wa2d )
            vrble = 'OII cooling     '
        endif

c
c----- pixel 41 : cooling due to OIII -----
c
        if (pixvar(n) .eq. 'o3') then
            call coolspec ( wa3d, 8, 1)
            call slice2d ( wa3d, ibeg, jbeg, kbeg, iend, jend, kend
1          , wa2d )
            vrble = 'OIII cooling    '
        endif

c
c----- pixel 42 : emission due to SII -----

```

```

c
      if (pixvar(n) .eq. 'sf') then
        call coolspec ( wa3d, 9, 1)
        call slice2d ( wa3d, ibeg, jbeg, kbeg, iend, jend, kend
1          , wa2d )
        vrble = 'SII emission      '
      endif

c
c----- pixel 43 : emission due to CO -----
c
      if (pixvar(n) .eq. 'co') then
        call coolmol ( xb, yb, qty )
        vrble = 'CO emission      '
        go to 1000
      endif

c
c----- pixel 44 : PDV Work divided by Cooling -----
c
      if (pixvar(n) .eq. 'wk') then
        call coolvpdv ( wa3d, 1, 1)
        call slice2d ( wa3d, ibeg, jbeg, kbeg, iend, jend, kend
1          , wa2d )
        vrble = 'enrg loss pdv_c '
      endif

c
*i pixdmp.636
1000  continue

```

REFERENCES

- Achterberg, A., Blandford, R. D., & Goldreich, P. 1983, *Nature*, **304**, 607
- André, P. 1997, in IAU Symp. 182, *Herbig-Haro Flows and the Birth of Low Mass Stars*, eds. B. Reipurth & C. Bertout (Kluwer,Dordecht), 483
- Anglada, G. 1995, *RMxAA*, **1**, 67
- Ambartsumian, V. A. 1954, Comm. Byuarakan Obs. No. 13
- Arnaud, M & Rothenflug, R. 1985 *A&AS*, **60**, 425
- Bacciotti, F. 1997, in IAU Symp. 182, *Herbig-Haro Flows and the Birth of Low Mass Stars*, eds. B. Reipurth & C. Bertout (Kluwer,Dordecht), 73
- Bacciotti, F., Chiuderi, C., & Oliva, E. 1995, *A&A*, **296**, 185
- Blandford, R. D. & Rees, M. J. 1974, *MNRAS*, **169**, 395
- Blondin, J. M., Fryxell, B. A., & Königl, A. 1990, *ApJ*, **360**, 370
- Böhm, K.-H. 1978, *A&A*, **64**, 115
- Cabrit, S., Edwards, S., Strom, S. E., & Strom, K. M. 1990 *ApJ*, **354**, 687
- Casey, M. P. 1996, M.Sc. Thesis, Saint Mary's U.
- Chandler, C. J., Terebey, S., Barsony, M., Moore, T. J. T., & Gautier, T. N. 1996. *ApJ*. **471**, 308
- Chan, K. L. & Henriksen, R. N. 1980, *ApJ*. **241**, 534
- Chernin, L. M. & Masson, C. R. 1995, *ApJ*, **455**, 182
- Chernin, L. M., Masson, C. R., Gouveia Dal Pino, E. M., Benz, W. 1994, *ApJ*, **426**, 204
- Clarke, D. A. 1996, *ApJ*, **457**, 291
- Clarke, D. A., Norman, M. L., & Burns, J. O. 1986, *ApJ*, **311**, L63
- Clarke, D. A., Harris, D. E., & Carilli, C. L. 1997, *MNRAS*, **284**, 981
- Cliffe, J. A., Frank, A., & Jones, T. W. 1996 *MNRAS*, **282**, 1114
- Cliffe, J. A., Frank, A., Livio, M., & Jones, T. W. 1995, *ApJ*, **447**, L49
- Cohen, M., Harvey, P. M., & Schwartz, R. D. 1985, *ApJ*, **296**, 633
- Davis, C. J., Eislöffel, J., Ray, T. P., & Jenness, T. 1997, *A&A*, **324**, 1013
- Davis, C. J., Mundt, R., & Eislöffel, J. 1994, *ApJ*, **437**, L55
- Davis, C. J. & Smith, M. D. 1995, *ApJ*, **443**, L41

- Draine, B. T. 1980 *ApJ*, **241**, 1021
- Edwards, S., Cabrit, S., Strom, S. E., Heyer, I., Strom, K. M., & Anderson, E. 1987 *ApJ*, **321**, 473
- Eisloffel, J. & Mundt, R. 1995, *Ap&SS*, **233**, 55
- Eisloffel, J. & Mundt, R. 1998, *A&A*, in press
- Elias, J. H. 1980, *ApJ*, **241**, 728
- Falle, S. A. E. G., & Raga, A. C. 1993, *MNRAS*, **261**, 571
- Frank, A. & Mellema, G. 1994, *A&A*, **289**, 937
- . 1996a, *ApJ*, **472**, 684
- . 1997, in IAU Symp. 182, *Herbig-Haro Flows and the Birth of Low Mass Stars*, eds. B. Reipurth & C. Bertout (Kluwer, Dordrecht), 291
- Frank, A., Ryu, D., Jones, T., & Noriega-Crespo, A. 1997, *BAAS*, **190**, 2410
- Gouveia Dal Pino, E. M. & Benz, W. 1994, *ApJ*, **435**, 261
- Gouveia Dal Pino, E. M., Birkinshaw, M., & Benz, W. 1996, *ApJ*, **460**, L111
- Gueth, F., Guilloteau, S., & Bachiller, R. 1996, *A&A*, **307**, 891
- Hardee, P.E., White, R.E., Norman, M.L., Cooper, M.A., & Clarke, D.A., 1992, *ApJ*, **387**, 460
- Hartigan, P., Carpenter, J. M., Dougados, C., & Skrutskie, M. F. 1996, *AJ*, **111**, 1278
- Hartigan, P. & Raymond, J. 1993, *ApJ*, **409**, 705
- Herbig, G. H. 1950, *ApJ*, **111**, 11
- Herbig, G. H. 1957, in IAU Symp. No. 3 ed. G. H. Herbig, Cambridge Univ. Press, p.3
- Jones, B. F. & Cohen, M. 1986, *ApJ*, **311**, L23
- Knapp, G. R., Kuiper, T. B. H., Knapp, S. L., & Brown, R. L. 1976. *ApJ*, **206**, 443
- Kofman, L. & Raga, A. C. 1992, *ApJ*, **390**, 359
- Königl, A. 1982, *ApJ*, **261**, 115
- Krist, J. E. 1998, private communication
- McGregor, P. J., Harrison, T. E., Hough, J. H., & Bailey, J. A. 1994, *MNRAS*, **267**, 755
- McKee, C. F., Storey, J. W. V., & Watson, D. M. 1982 *ApJ*, **259**, 647

- Masson, C. R. & Chernin, L. M. 1993, *A&A*, **414**, 230
- Martin, S. C. 1996, *ApJ*, **473**, 1051
- Mellema, G. & Frank, A. 1997, *MNRAS*, **292**, 795
- Mitchell, G. F., Hasegawa, T. I., Dent, W. R. F., & Matthews, H. E. 1994, *ApJ*, **436**, L177
- Mitchell, G. F., Sargent, A. I., & Mannings, V. 1997, *ApJ*, **483**, L127 [Paper I]
- Mundt, R. 1986, *Can. J. Phys.*, **64**, 407
- Mundt, R., Brugel, E. W., & Bürkhe, T. 1987, *ApJ*, **319**, 275
- Mundt, R. & Fried, J. W. 1983, *ApJ*, **274**, L83
- Mundt, R., Ray, T. P., & Raga, A. C. 1991, *A&A*, **252**, 740
- Neufeld, D. A. & Kaufman, M. J. 1993 *ApJ*, **418**, 263
- Neufeld, D. A., Lepp, S., & Melnick, G. J. 1995 *ApJS*, **100**, 132
- Norman, M. L., Winkler, K. H., & Smarr, L. 1983, in *Astrophysical Jets: Proceedings of the International Workshop*, (Reidel, Dordrecht), 227
- Ouyed, R. & Pudritz, R. E. 1997, *ApJ*, **482**, 712
- Plambeck, R. L. & Snell, R. L. 1995, *ApJ*, **446**, 234
- Press, W. H., Teukolsky, S. A., Vetterling, W. T., & Flannery, B. P. 1992, in *Numerical Recipes in FORTRAN The Art of Scientific Computing*, 2nd ed. Cambridge University Press. pp.103,104,118
- Poetzel, R., Mundt, R., & Ray, T. P. 1992, *A&A*, **262**, 229
- Pudritz, R. E. & Norman, C. A. 1986, *Can. J. Phys.*, **64**, 501
- Raga, A. C. 1995, *RMxAA*, **1**, 103
- . 1997, private communication
- Raga, A. C. & Cabrit, S. 1993, *A&A*, **278**, 267
- Raga, A. C., Cantö, J., Calvet, N., Rodriguez, L. F., & Torrelles, J. M. 1993, *A&A*, **276**, 539
- Raga, A. C. & Kofman, L. 1992, *ApJ*, **386**, 222
- Raga, A. C., Mellema, G., & Lundqvist, P. 1997 *ApJS*, **109**, 517
- Raga, A. C., Taylor, S. D., Cabrit, S., & Biro, S. 1995, *A&A*, **296**, 833
- Reipurth, B. 1994, *A general catalogue of Herbig-Haro objects*, electronically published via anon. ftp to ftp.hq.eso.org, directory /pub/Catalogs/Herbig-Haro.

- Reipurth, B. & Heathcote, S. 1992, *A&A*, **257**, 693
- . 1997, in IAU Symp. 182, *Herbig-Haro Flows and the Birth of Low Mass Stars*, eds. B. Reipurth & C. Bertout (Kluwer,Dordecht), 3
- Rodriguez, L. F., Anglada, G., & Raga, A. C. 1995, *ApJ*, **454**, L149
- Sanders, R. H. 1983, *ApJ*, **266**, 73
- Schwartz, R. D. 1978, *ApJ*, **223**, 884
- Schwartz, R. D., Schultz, A. S. B., Cohen, M., & Williams, P. M. 1995, *ApJ*, **446**, 318
- Shu, F. H., Ruden, S. P., Lada, C. J., & Lizano, S. 1991, *ApJ*, **370**, L31
- Smith, M. D., Suttner, G., Yorke, H. W. 1997a, *A&A*, **323**, 223
- Smith, M. D., Völker, R., Suttner, G., & Yorke, H. W. 1997b, in IAU Symp. 182, *Herbig-Haro Flows and the Birth of Low Mass Stars*, eds. B. Reipurth & C. Bertout (Kluwer,Dordecht), 303
- Snell, R. L., Loren, R. B., & Plambeck, R. L. 1980, *ApJ*, **239**, L17
- Stapelfeldt, K., Burrows, C. J., Krist, J. E., & the WFPC2 Science Team 1997, in IAU Symp. 182, *Herbig-Haro Flows and the Birth of Low Mass Stars*, eds. B. Reipurth & C. Bertout (Kluwer,Dordecht), 355
- Stone, J. M., & Norman, M. L. 1993a, *ApJ*, **413**, 198
- . 1993b, *ApJ*, **413**, 210
- . 1994, *ApJ*, **420**, 237
- Suttner, G., Smith, M. D., Yorke, H. W., & Zinnecker, H. 1997 *A&A*, **318**, 595
- Todo, Y., Uchida, Y., Sato, T., & Rosner, R. 1992, *PASP*, **44**, 245
- Vrba, F. J., Rydgren, A. E., & Zak, D. S. 1985, *AJ*, **90**, 2074
- Ward-Thompson, D., Eiroa, C., & Casali, M. M. 1995 *MNRAS*, **273**, L25

Mail for reinhard mundt Thu, 18 Mar 1999 10:10:07 -0800 (PST)

Page

1

From: Kevin.Douglas@hia.nrc.ca Thu Mar 18 19:10 MET 1999
From: Kevin Douglas <Kevin.Douglas@hia.nrc.ca>
To: Reinhard Mundt <mundt@mpia-hd.mpg.de>
Subject: DG Tau B image
Date: Thu, 18 Mar 1999 10:10:07 -0800 (PST)

Greetings Dr. Mundt.

My name is Kevin Douglas and I am a Master's student in Canada. I have been working on a thesis with George Mitchell, in a project related to his observations of the molecular outflow associated with DG Tau B, an object you discovered with J. W. Fried in 1983. I would like to include the discovery image of DG Tau B in my thesis, since I feel it is important to show the full historical significance of the object. The university regulations say that I must have your written approval to use this image, so I would ask that you send me a letter stating that I may use your image in my thesis. This would be your Figure 4 from the 1983 article in ApJ Letters, vol. 274. I would greatly appreciate it if you could send this letter to me at the following address:

Kevin Douglas
Dominion Radio Astrophysical Observatory
Box 149, Station Main
Penticton B. C.
CANADA V2A 6P3

Thank you for your time, Dr. Mundt.

Kevin Douglas, SVLBI Data Distribution Specialist
Dominion Radio Astrophysical Observatory, Penticton B. C.
Phone: (250) 493-2877 Fax: (250) 493-7767
Now Playing: Motor Totemist Guild - City of Mirrors

*I herewith agree that
Mr. Kevin Douglas can use
the above mentioned DG Tau B image
for his thesis.*

*Reinhard Mundt
April 8, 1999*

DG Tau B image